# Noise Injection Radiometer Test Specifications and Requirements

**Andreas Colliander**

Thesis for the Degree of Master of Science

Helsinki University of Technology
Laboratory of Space Technology
PL3000, FIN-02015 HUT

# PREFACE

The work presented in this Master's Thesis has been carried out in the Laboratory of Space Technology at Helsinki University of Technology. The work is conducted in the frame of European Space Agency (ESA) project MDPP-2 (MIRAS Demonstrator Pilot Project 2).

I thank Professor Martti Hallikainen for being my supervisor. I would also like to thank Mr. Simo Tauriainen and Mr. Kimmo Rautiainen for instructing me on the work and all the personnel of the Laboratory of the Space Technology for their support. Special thanks also to Mr. Joan Capdevila from EADS-CASA and Mr. Manuel Martín-Neira from ESA for valuable comments.

Otaniemi, September 10, 2002

Andreas Colliander

Author: Andreas Colliander

Name of the Thesis: Noise Injection Radiometer Test Specifications and Requirements

Date: 10.9.2002

Number of Pages: 115

Department: Department of Electrical and Communications Engineering

Professorship: Space Technology

Supervisor: Martti Hallikainen

Instructors: Simo Tauriainen and Kimmo Rautiainen

Abstract:

The test plan of a fully polarimetric noise injection radiometer (NIR) of MIRAS (Microwave Imaging Radiometer Using Aperture Synthesis) Demonstrator Pilot Project 2 is presented.

Measurements required for extensive radiometric testing are described in detail. The analysis for solving the vital properties of the NIR is carried out to the point in which it can be applied to the measurement data in a straightforward manner. The uncertainties of the measurements and analysis are discussed thoroughly.

Keywords:

Noise injection radiometer, remote sensing, polarimetric radiometry, Stokes parameters

Tekijä: Andreas Colliander

Työn nimi: Noise Injection Radiometer Test Specifications and Requirements

Päivämäärä: 10.9.2002

Sivuja: 115

Osasto: Sähkö- ja tietoliikennetekniikan osasto

Professuuri: Avaruustekniikka

Työn valvoja: Martti Hallikainen

Työn ohjaajat: Simo Tauriainen ja Kimmo Rautiainen

Tiivistelmä:

Tässä tekstissä esitetään MIRAS (Microwave Imaging Radiometer Using Aperture Synthesis) Demonstrator Pilot Project 2 -projektin täyspolarimetrisen kohinainjektioradiometrin (NIR) testisuunnitelma.

Täydelliseen radiometriseen testaukseen vaadittavat mittaukset kuvataan yksityiskohtaisesti. Mittausjärjestelyt analysoidaan niin, että tarvittavat ominaisuudet voidaan ratkaista suoraviivaisesti mittaustuloksia soveltamalla. Mittausten ja analyysin epävarmuudet selvitetään perusteellisesti.

Avainsanat:

Kohinainjektioradiometri, kaukokartoitus, polarimetrinen radiometria, Stokesin parametrit

# TABLE OF CONTENTS

# LIST OF ACRONYMS AND SYMBOLS

| | |
|---|---|
| CAS | Calibration System |
| CNS | Calibration Network Simulator |
| DICOS | Digital Correlator System |
| ENR | Excess Noise Ratio |
| ESA | European Space Agency |
| HUT | Helsinki University of Technology |
| HUT LST | HUT Laboratory of Space Technology |
| IF | Intermediate frequency |
| LICEF | Light Weight Cost Effective Front-end |
| MDPP-2 | MIRAS Demonstrator Pilot Project 2 |
| MIRAS | Microwave Imaging Radiometer Using Aperture Synthesis |
| NI | Noise Injection |
| NIR | Noise Injection Radiometer (in this document the MDPP-2 NIR) |
| NS | Noise Source |
| PMS | Power Measurement Signal |
| PMU | Power Measurement Unit |
| RF | Radio Frequency |
| rms | Root Mean Square |
| SMOS | Soil Moisture and Ocean Salinity |
| TB | Brightness Temperature |
| TP | Total Power |
| VNA | Vector Network Analyser |
| TI | Test output of I-channel |
| TQ | Test output of Q-channel |

| | |
|---|---|
| $\alpha_H$ | Maximum modulus of the voltage gains of the H-channel receiver |
| $\alpha_V$ | Maximum modulus of the voltage gains of the V-channel receiver |
| $\beta$ | Propagation coefficient |
| $\Delta$ | Generally indicates the uncertainty of the succeeding variable |
| $\Delta G$ | rms change of the system gain |
| $\Delta T_{H,V}^{NI}$ | Antenna measurement accuracy in noise-injection mode |
| $\Delta T_{H,V}^{TP}$ | Antenna measurement accuracy in total power mode |
| $\Delta T_{NI}$ | Theoretically calculated sensitivity in noise-injection mode |
| $\Delta T_{TP}$ | Theoretically calculated sensitivity in total power mode |
| $\Delta T_{\sigma}$ | Sensitivity of a radiometer calculated from the measured data |
| $\Delta T_{lin}$ | Deviation from linear detection |
| $\Delta T_{lin}^{error}$ | Error in calculation of deviation from linear detection |
| $\Delta T_G$ | Error of radiometer caused by gain variations |
| $\Delta T_N$ | Error of radiometer caused by noise i.e. sensitivity |
| $\eta$ | Wave impedance |
| $\eta$ | Noise-injection pulse duty-cycle |
| $\lambda$ | Wavelength |
| $\mu_0$ | Ideal correlation coefficient |
| $\mu_{0,appr}$ | Correlation coefficient determined using an approximation |

| | |
|---|---|
| $\mu_0\|_{i,i}$ | Ideal correlation coefficient between the I-output of the H-channel and I-output of the V-channel |
| $\mu_0\|_{q,i}$ | Ideal correlation coefficient between the Q-output of the H-channel and I-output of the V-channel |
| $\mu$ | The measured correlation coefficient |
| $\mu$ | Mean of variable *x* |
| $\mu\|_{ii}$ | Measured correlation coefficient between the I-output of the H-channel and I-output of the V-channel |
| $\mu\|_{qi}$ | Measured correlation coefficient between the Q-output of the H-channel and I-output of the V-channel |
| $\mu_k$ | In NI-mode measured correlation coefficient |
| $\mu_{ViVq}$ | Correlation coefficient measured between I- and Q-output of V-channel |
| $\mu_{HiHq}$ | Correlation coefficient measured between I- and Q-output of H-channel |
| $\mu_{TP}$ | Correlation coefficient measured in total power mode |
| $\mu_B$ | Correlation coefficient measured in noise-injection mode using the blind mode |
| $\omega$ | Angular velocity |
| $\sigma$ | Standard deviation |
| $\sigma_i$ | Standard deviation of the signal |
| $\sigma_y^2$ | Allan variance |
| $\theta$ | Phase difference |
| $\theta_V^{inph}$ | In-phase error of the V-channel |
| $\theta_H^{inph}$ | In-phase error of the H-channel |
| $\theta_V^{quad}$ | Quadrature error of the V-channel |
| $\theta_H^{quad}$ | Quadrature error of the H-channel |
| $\tau$ | Integration time |
| $\tau$ | Time of delay |
| $\Gamma_{nHnV}$ | Cross correlation of the noise at the input of the receivers |
| $\Gamma_s$ | Autocorrelation function of the analogue signals |
| $\phi_{Hi}$ | Phase response of the I-output of the H-channel |
| $\phi_{Hq}$ | Phase response of the Q-output of the H-channel |
| $\phi_{Vi}$ | Phase response of the I-output of the V-channel |
| $\phi_{Vq}$ | Phase response of the Q-output of the V-channel |
| $a$ | Calibration coefficient |
| $a_i$ | Offset voltage for quantizer |
| $A$ | Calibration coefficient |
| $B$ | Calibration coefficient |
| $b$ | Calibration coefficient |
| $B$ | Bandwidth |
| $B$ | Brightness |
| $B_f$ | Spectral Brightness |
| $B_H$ | Bandwidth of the H-channel |
| $B_V$ | Bandwidth of the V-channel |
| $c$ | Speed of light |
| $e$ | Emissivity |

| | |
|---|---|
| $e$ | Neper's constant |
| $\mathbf{E}$ | Electric field vector |
| $E_1$ | Electric field component |
| $E_2$ | Electric field component |
| $E_v$ | Electric fields of the vertical polarisation |
| $E_h$ | Electric fields of the horizontal polarisation |
| $E_x$ | Electric field component along the x-axis |
| $E_{x0}$ | Magnitude of the electric field component along the x-axis |
| $E_y$ | Electric field component along the y-axis |
| $E_{y0}$ | Magnitude of the electric field component along the y-axis |
| $f$ | Frequency |
| $f$ | General function |
| $f_0$ | Centre frequency |
| $f_D$ | Dicke frequency |
| $F_{NC}$ | Coupling of the noise-injection coupler of the antenna branch |
| $g_{FW}$ | Fringe-washing factor |
| $g_{FW}$ | Fringe-washing function |
| $\tilde{g}$ | Modulus term of TP-mode |
| $\tilde{g}_2$ | Second modulus term of NI-mode |
| $\tilde{g}_3$ | Third modulus term of NI-mode |
| $\tilde{g}_4$ | Fourth modulus term of NI-mode |
| $\tilde{g}_{diff}$ | Difference of two differently determined modulus terms |
| $\tilde{g}_{meas}$ | Modulus term calculated from measured correlation coefficient |
| $G$ | Gain of a radiometer |
| $G_H$ | Gain of H-channel, when using antenna |
| $G_H$' | Gain of H-channel, when calibration port as input |
| $G_V$ | Gain of V-channel, when using antenna |
| $G_V$' | Gain of V-channel, when calibration port as input |
| $h$ | Planck's constant |
| $H_H$ | Frequency response of the H-channel |
| $H_{n,H}$ | Normalised frequency response of the H-channel |
| $H_V$ | Frequency response of the V-channel |
| $H_{n,V}$ | Normalised frequency response of the V-channel |
| $k$ | Boltzmann's constant |
| $L$ | Attenuation |
| $L_{chain}^{H/V,1/2}$ | Attenuation of a connecting chain (from hot (1) or cold (2) load to the H or V channel receiver) |
| $L_{chain,therm}^{H/V,1/2}$ | Attenuation of a connecting chain causing thermal noise (from hot (1) or cold (2) load to the H or V channel receiver) |
| $L(x_{sw})_{change}^{H/V,1/2}$ | Attenuation of the controllable noise source coming from hot (1) or cold load (2) to H or V channel at switch position $x_{sw}$ |
| $L_{NA}$ | Attenuation of the attenuator of antenna noise-injection channel |
| $L_{Nref}$ | Attenuation of the attenuator of reference noise-injection channel |
| $n$ | Number of samples in one averaged period |
| $N$ | Number of samples |
| $N_{2,3,4}$ | Number of samples correlated at each step (2,3,4) of noise injection cycle |

| | |
|---|---|
| $m$ | Number of averaged samples |
| $P$ | A figure proportional to measured power |
| $P_1$ | A figure proportional to measured power from a hot load |
| $P_2$ | A figure proportional to measured power from a cold load |
| $P_A$ | Power of the antenna temperature |
| $P^{cold}$ | A figure proportional to measured power of a cold load |
| $P^{hot}$ | A figure proportional to measured power of a hot load |
| $P_H$ | A figure proportional to measured power from H channel |
| $P_R$ | Power of the receiver noise |
| $P_V$ | A figure proportional to measured power from V channel |
| $P_x$ | A figure proportional to a measured power |
| $P_{detect}$ | A figure proportional to the detected power |
| $r$ | linear-correlation coefficient |
| $R_{hHhV}$ | Cross correlation between the frequency responses |
| $s$ | Standard deviation for discrete data |
| $\mathbf{S}$ | S-matrix |
| $S_{11}$ | Input reflection coefficient |
| $S_{12}$ | Backward transmission coefficient |
| $S_{21}$ | Forward transmission coefficient |
| $S_{22}$ | Output reflection coefficient |
| $S_3$ | Third Stokes parameter |
| $S_4$ | Fourth Stokes parameter |
| $S_H$ | First Stokes parameter |
| $S_V$ | Second Stokes parameter |
| $t$ | Variable indicating time |
| $t_N$ | Noise-injection pulse length |
| $\mathbf{T}$ | Modified Stokes parameters vector |
| $\overline{T}$ | Average of measured brightness temperature |
| $T_1$ | Noise temperature of a hot load |
| $T_1$’ | Noise temperature of a hot load seen through the connecting chain |
| $T_2$ | Noise temperature of a cold load |
| $T_2$’ | Noise temperature of a cold load seen through the connecting chain |
| $T_3$ | Third modified Stokes parameter |
| $T_4$ | Fourth modified Stokes parameter |
| $T_{amb}$ | Ambient physical temperature |
| $T_{ant}$ | Antenna temperature |
| $T_{ant}^{calib}$ | Antenna temperature during calibration |
| $T_{bb}$ | Physical temperature of a blackbody |
| $T_B$ | Brightness temperature |
| $T_C$ | Calibration network noise temperature |
| $T_{cal}^{c}$ | Radiometer input noise temperature when cold load measured |
| $T_{cal}^{h}$ | Radiometer input noise temperature when hot load measured |
| $T_{chain}^{H/V,1/2}$ | Noise temperature of a connecting chain |
| $T_{chain}^{phys}$ | Physical temperature of a connecting chain |
| $T_{cold}$ | Noise temperature of the cold load |
| $T_{hot}$ | Noise temperature of the hot load |
| $T_e$ | Noise temperature of the system after antenna connection |
| $T_H$ | First modified Stokes parameter |

| | |
|---|---|
| $T_{Hant}$ | Antenna temperature of the H-channel |
| $T_{Hant,Vant}^{calib}$ | Antenna temperature during calibration in H- or V-channel |
| $T_{Hrec}$ | Noise temperature of H-channel receiver |
| $T_{HN}$ | Noise injected into the H-channel |
| $T_{in}$ | Input noise temperature |
| $T_{in,meas}$ | Measured TB coming to a receiver |
| $T_{in,calc}$ | Calculated TB coming to a receiver from a known load |
| $T_{inj}$ | Noise temperature coming to the noise-injection coupler of antenna |
| $T_k$ | One measurement sample ($k$) of brightness temperature |
| $T_{leak}$ | Through the noise-injection switch leaked noise temperature |
| $T_{load}$ | Noise temperature of a load |
| $T_{L_{NA}}^{phys}$ | Physical temperature of the $L_{NA}$ |
| $T_{L_{Nref}}^{phys}$ | Physical temperature of the $L_{Nref}$ |
| $T_N$ | Noise injected into the receivers |
| $T_{noise}$ | Noise temperature of a noise source |
| $T_{out}$ | Output noise temperature |
| $T_{phys}$ | Physical temperature |
| $T_{rec}$ | Receiver noise temperature |
| $T_{ref}$ | Reference noise temperature |
| $T_{ref,inj}$ | Reference noise temperature during noise injection |
| $T_{sys}$ | System noise temperature |
| $T_V$ | Second modified Stokes parameter |
| $T_{Vant}$ | Antenna temperature of the V-channel |
| $T_{Vrec}$ | Noise temperature of V-channel receiver |
| $T_{VN}$ | Noise injected into the V-channel |
| $T_x$ | Brightness temperature of a measurement |
| $V_{out}$ | Radiometer output voltage |
| $V_{out}^{c}$ | Radiometer output voltage when connected to the cold load |
| $V_{out}^{h}$ | Radiometer output voltage when connected to the hot load |
| $x$ | General variable |
| y | General variable |
| $x(t)$ | Input signal of one channel being correlated |
| $y(t)$ | Input signal of the other channel being correlated |
| $Y$ | Y-factor |
| $z$ | General variable indicating place |
| $Z$ | The sum used in correlation |

# 1 INTRODUCTION

In this work the test plan of a noise injection radiometer is presented. The motivation of building the noise injection radiometer lies on European Space Agency's (ESA) Soil Moisture and Ocean Salinity (SMOS) mission. Figure 1-1 presents an artist's view of the SMOS satellite. SMOS mission has been selected as one of ESA's Earth Explorer Opportunity Missions. Measurements of L-band brightness temperature over ocean enable the determination of sea surface salinity and over land areas the retrieval of soil moisture.

The SMOS mission requires an L-band radiometer and, therefore, the design of MIRAS (Microwave Imaging Radiometer Using Aperture Synthesis) has been initialised. MIRAS uses, as the name reveals, aperture synthesis as the means of brightness temperature measurements. The benefit is small size and weight compared with a traditional antenna. The cost is complexity and challenging technology.

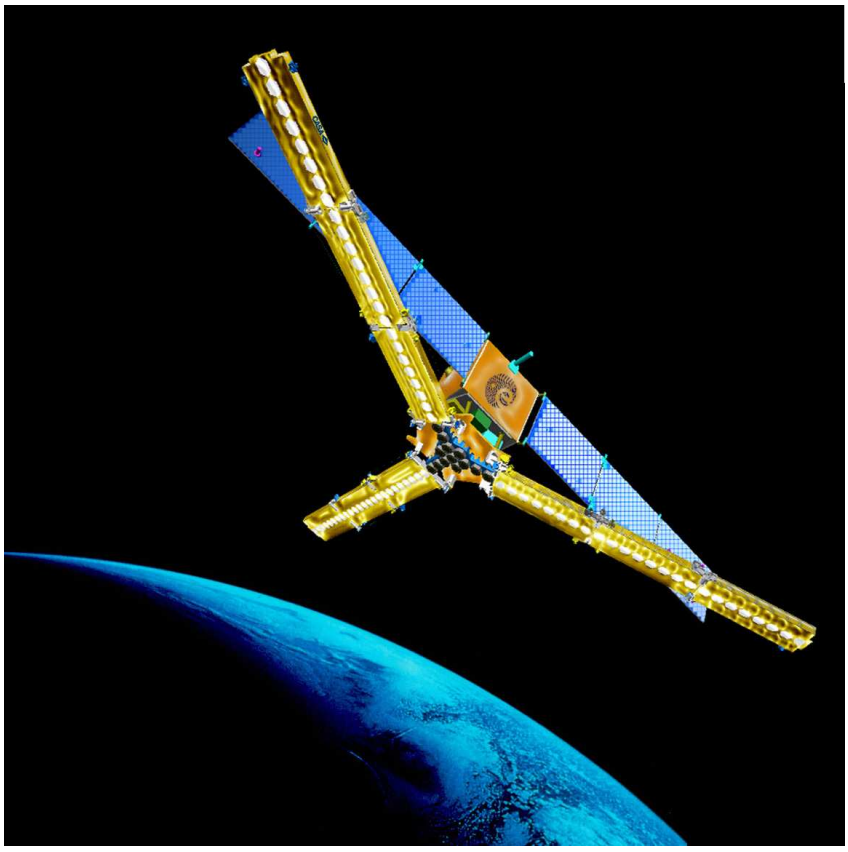

*Figure 1-1. Artist's view of SMOS satellite. The three arms and the hub in the middle forms MIRAS instrument. NIRs are installed in the hub section.*

MIRAS is formed by three arms in a Y-shaped geometry and a central hub section (Figure 1-1). Each arm has three segments and each segment contains 6 LICEF (Light-weight Cost Effective Front-end) receivers. The LICEF is an L-band receiver with a very narrow bandwidth. The hub contains 18 receivers, which are split in three virtual segments. The receivers are calibrated by measuring known noise source. In order to know the noise temperature of the noise source it has to

be measured and this is done by a noise injection radiometer (NIR). Thus the two main functions of NIR are:

1. Antenna measurement with fully polarimetric capability during the measurement phase of MIRAS for retrieval of the brightness temperature map.
2. Measurement of the centralized noise source during the calibration phase of MIRAS to enable calibration of the modulus terms of the LICEF-2 receivers.

A breadboard of this radiometer will be designed by Helsinki University of Technology (HUT) Laboratory of Space Technology (LST) and Toikka Ltd in cooperation and constructed by Ylinen Ltd. The work is being performed under a subcontract for a Spanish company EADS-CASA. HUT LST (meaning the author of this document) has prepared the test plan of NIR (see [9] for the original report) and Ylinen Ltd will carry out the tests in cooperation with HUT LST.

The plan is divided as follows: in Chapter 3 the measurement configurations are described and in Chapter 4 the analysis for the evaluation of NIR parameters is introduced.

# 2 THEORETICAL BACKGROUND

In this chapter the theoretical background of radiometry, radiometers and radiometer testing is covered. Also general aspects of testing are considered.

## 2.1 Microwave Radiometry

This section introduces the basic concepts of radiometry, a field of science and engineering, concerning measurements of electromagnetic radiation. The electromagnetic emission of the objects and the properties of the fields of the electromagnetic radiation are discussed.

### 2.1.1 Passive Microwave Remote Sensing

Every object in our universe radiates electromagnetic radiation. The energy comes from the heat of the object, absorbed radiation of other objects or scattered radiation of other objects. Passive microwave remote sensing is about receiving the radiation of objects and thus making conclusions about the properties of the objects [1].

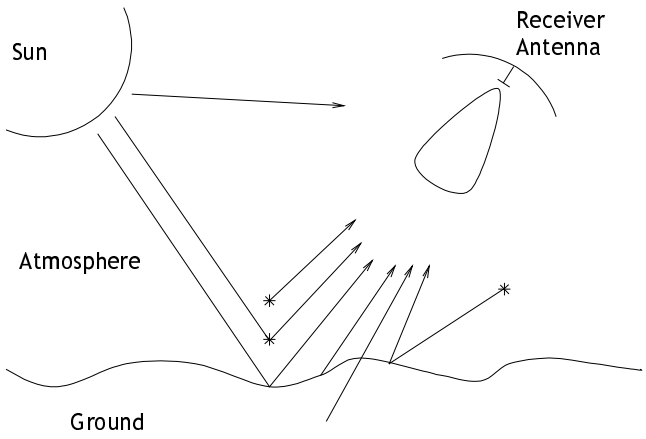


*Figure 2-1. A typical passive remote sensing situation [1]. The measured radiation comes from multiple sources and the detection of the wanted radiation is the main challenge.*

In Figure 2-1 typical circumstances of passive remote sensing situation are presented. The radiation to the sensor antenna, when directed towards earth, comes from multiple sources and normally only one or few of them are desired; the others are distraction. The goal is to receive the wanted radiation with a good enough signal-to-noise ratio in such a manner that the distractive signals can be eliminated.

### 2.1.2 Planck's Blackbody Radiation Law

A blackbody is defined as an idealized, perfectly opaque material that absorbs all the incident radiation at all frequencies [1]. Basically this means that while being

a perfect absorber it is also a perfect emitter, because energy absorbed by an object would increase its temperature if none of the energy were emitted, as stated also in [1].

Radiation of a blackbody is described by the Planck's radiation law, which declares that a blackbody radiates uniformly in all directions with a spectral brightness $B_f$ given by [1]

$$B_f = \frac{2hf^3}{c^2}\left(\frac{1}{e^{\frac{hf}{kT_{bb}}}-1}\right). \tag{2-1}$$

The Planck's law can be approximated by the Wien Radiation law when high frequencies are used, and by the Rayleigh-Jeans law when low frequencies are used [1]. In microwave radiometry the Rayleigh-Jeans law is relevant. Because [1]

$$e^x - 1 = \left(1 + x + \frac{x^2}{2} + \ldots\right) - 1 \cong x \tag{2-2}$$

for $x << 1$, Equation (2-1) can be simplified to

$$B_f = \frac{2f^2 kT_{bb}}{c^2} = \frac{2kT_{bb}}{\lambda^2}, \tag{2-3}$$

which is called Rayleigh-Jeans law. In Figure 2-2 the Planck's law and Rayleigh-Jeans law are compared.

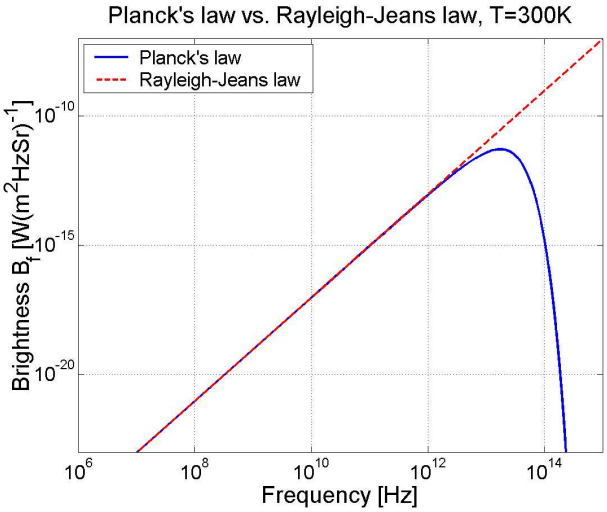


*Figure 2-2. Rayleigh-Jeans law plotted against Planck's blackbody radiation law as function of frequency, when the physical temperature of the object is 300 K.*

The deviation of the Rayleigh-Jeans law from the Planck's law is less than 1 percent if [1]

$$\frac{f}{T_{bb}} < 3.9 \cdot 10^{8}\, Hz / K. \tag{2-4}$$

If the physical temperature of the blackbody is $T_{bb}$ = 300 K the equation above holds for all $f$ < 117 GHz [1].

### 2.1.3 Brightness Temperature

Real materials do not have the ideal properties of the blackbody: they emit less and do not absorb the entire energy incident upon them. The quantity used in radiometry to describe the emitted power is called brightness temperature, often denoted by $T_B$. Brightness temperature of an object is the product of the emissivity and the physical temperature of the object [1]. Emissivity is defined as [1]

$$e(\theta,\phi) = \frac{B(\theta,\phi)}{B_{bb}} = \frac{T_B(\theta,\phi)}{T_{phys}}, \tag{2-5}$$

which is the ratio of the brightness emitted by the object to the brightness emitted by a blackbody at the same temperature and in the same frequency band. Thus [1]

$$T_B(\theta,\phi) = e(\theta,\phi) T_{phys}, \tag{2-6}$$

which is the brightness temperature of an object. It is always smaller than or equal to the physical temperature of the object.

### 2.1.4 Polarisation

The above considered electromagnetic radiation is commonly described with propagating plane waves. For a uniform plane wave propagating in the direction of the positive *z*-axis in a Cartesian coordinate system, the electric field must lie in the *xy*-plane [1]. The electric field vector, **E**, is function of time in any fixed point in space. The tip of the **E** vector draws a curve in the *xy*-plane as time changes. The form of the resulting curve can be divided in three categories: linear, circular or elliptical. The name of the polarisation of the wave comes from this form. Linear and circular polarisations are in fact special cases of elliptical polarisation.

In the circular and elliptical polarisation the tip may move either clockwise or counter clockwise. If it moves clockwise, when looked in the direction of the propagation, it is said to be right-hand polarized and in the case of the counter clockwise movement, it is said to be left-hand polarised [1].

The electromagnetic waves emitted by natural objects consist of a superposition of many statistically independent waves of different polarisations. This kind of a wave is said to be incoherent or unpolarized [1].

A plane wave can be written as a sum of the x- and y-components of the wave. This is, however, same as the sum of two linearly polarized waves, which are equal to the mentioned components [1], that is

$$\begin{aligned}\mathbf{E}=(z,t)&=E_x(z,t)\hat{\mathbf{x}}+E_y(z,t)\hat{\mathbf{y}}\\&=E_{x0}\cos(\omega t-\beta z)\hat{\mathbf{x}}+E_{y0}\cos(\omega t-\beta z+\theta)\hat{\mathbf{y}}\,.\end{aligned}\tag{2-7}$$

The resulting polarisation of the whole wave can be mathematically identified by the phase difference, $\theta$, and the magnitude, $E_{x0}$ and $E_{y0}$, of the components.

### 2.1.5 Stokes Parameters

The Stokes parameters provide a very useful way of describing the polarisation state of an electromagnetic wave [7]. If

$$\begin{aligned}E_x&=\mathrm{Re}\left\{E_1e^{-j\omega t}\right\}=E_1\cos(\omega t+\theta_1)\\E_y&=\mathrm{Re}\left\{E_2e^{-j\omega t}\right\}=E_2\cos(\omega t+\theta_2)\end{aligned}\tag{2-8}$$

then the Stokes parameters can be defined as

$$\begin{aligned}S_H&=E_1^2+E_2^2\\S_V&=E_1^2-E_2^2\\S_3&=2E_1E_2\cos(\theta)\\S_4&=2E_1E_2\sin(\theta)\end{aligned}\tag{2-9}$$

where $S_H$ stands for the total power in the wave, $S_V$ and $S_3$ represent the linearly polarised component and $S_4$ represents the circularly polarized component.

In radiative transfer theory so-called modified Stokes parameters are often used. They are given by [7]

$$\mathbf{T}=\begin{bmatrix}T_H\\T_V\\T_3\\T_4\end{bmatrix}=\frac{\lambda^2}{k\eta}\begin{bmatrix}|E_1|\\|E_2|\\2\,\mathrm{Re}\left\{E_1E_2^{\,*}\right\}\\2\,\mathrm{Im}\left\{E_1E_2^{\,*}\right\}\end{bmatrix}\tag{2-10}$$

where the notation is the one commonly used in radiometry. In the next chapter we take a look at an application of Stokes parameters.

## 2.2 Microwave Radiometers

Radiometer is the most important piece of equipment in radiometry. It is an instrument for receiving electromagnetic radiation in a certain frequency band. In this section we take a look at the basic radiometer principles and the noise injection radiometer of the MDPP-2 project.

### 2.2.1 Total Power Radiometer

A radiometer is a very sensitive microwave receiver to measure the power of the electromagnetic radiation of an object. This radiation is a noise-like signal with very low power and thus the basic problem in radiometers is to distinguish the noise of the receiver from the received noise signal [1].

Figure 2-3 shows a block diagram of a normal total power superheterodyne receiver. It consists of a low-noise amplifier, a mixer mixing the incoming signal to IF frequency $f_{IF}$, IF filter, whose bandwidth $B$ determines the bandwidth of the receiver, IF amplifier, a square law detector, whose output voltage is proportional to its input power, and an integrator.

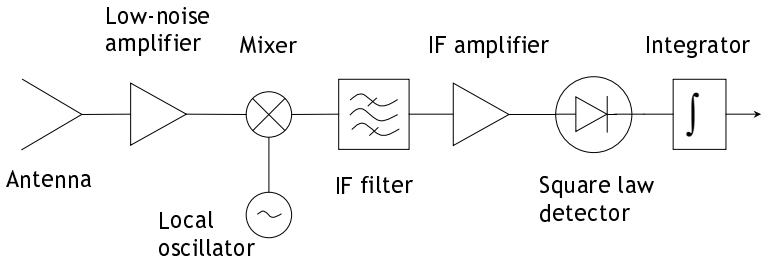


*Figure 2-3. Principle of a total power radiometer realised with a superheterodyne receiver, meaning that the input signal is mixed down to a lower frequency using a mixer [1].*

If the antenna is pointed to a scene with a brightness temperature $T_{ant}$, the antenna power will be $P_A = kT_{ant}B$. The noise power of the receiver is $P_R = kT_{rec}B$, where $T_{rec}$ is the noise temperature (see e.g. [1]) of the receiver. Thus the output voltage of the radiometer is [1]

$$V_0 = G(T_{ant} + T_{rec})kB, \tag{2-11}$$

where $G$ is the gain of the receiver. Two major errors occur with this radiometer. Due to the random nature of noise the noise power varies from one integration period to the next. The standard deviation of the noise level, denoted $\Delta T_N$, has a value of [1]

$$\Delta T_N = \frac{T_{ant} + T_{rec}}{\sqrt{B\tau}}, \tag{2-12}$$

where $\tau$ is the integration time. Obviously when $\tau$ is increased to infinity the error becomes negligible. (2-12) is also called sensitivity or radiometric resolution of a radiometer and its measurement is presented in Section 2.4.

The second error comes from the random gain fluctuations of the receiver, due to instability of the amplifiers, filter and mixer. These variations happen over a period of one second or longer [1]. So if the radiometer is calibrated (see Section 2.7) with a certain value of $G$, which will change by the time a measurement is made, the error will be [1]

$$\Delta T_G = \left(T_{ant} + T_{ref}\right)\frac{\Delta G}{G}, \tag{2-13}$$

where $\Delta G$ is the rms change in the system gain $G$.

### 2.2.2 Dicke Radiometer

A Dicke radiometer is a total power radiometer, which is switched to measure the antenna temperature and a known reference load, often 50 Ω matched load, at a certain frequency (Figure 2-4). The switching frequency has to be high enough to compensate the varying gain of the radiometer. Also the effective bandwidth of the low-pass filter i.e. the integration time and the switching time of the switch have to be taken into account. This means typically a Dicke frequency somewhere between 10 Hz and 1000 Hz [1].

When the radiometer sees the reference load the $T_{ant}$ of equation (2-11) becomes $T_{ref}$ and thus when the measurements of the antenna and reference are subtracted (demodulator in Figure 2-4), the output voltage becomes [1]

$$V_{out} = G\left(T_{ant} + T_{rec}\right)kB - G\left(T_{ref} + T_{rec}\right)kB = G\left(T_{ant} - T_{ref}\right)kB, \tag{2-14}$$

and the receiver noise temperature $T_{rec}$ is eliminated. Now, because the antenna is seen only half the time, the sensitivity $\Delta T_N$ becomes twice as big as in the case of total power radiometer [1]:

$$\Delta T_N = \frac{2\left(T_{ant} + T_{rec}\right)}{\sqrt{B\tau}}. \tag{2-15}$$

However, as shown in [1] Equation (2-14) holds completely only when $T_{ant} = T_{ref}$, since then the gain fluctuations are completely cancelled. A method for acquiring this has to be utilised.

It is said that a Dicke radiometer is balanced when the reference load noise temperature is equal to that of the antenna. This balancing can be made with four methods [1]:

A. Reference-channel control method
B. Antenna-channel noise-injection method
C. Pulsed noise-injection method
D. Gain-modulation method

The radiometer discussed in the following text is of type C and thus the radiometer is called noise injection radiometer (NIR).

### 2.2.3 Noise Injection Radiometer

Equation (2-16) shows the basic principle of a noise injection radiometer. The time average of the reference load equals that of the signal from the antenna branch.

$$\langle T_{ref} \rangle = \langle T_{ant} \rangle + \langle T_N \rangle \tag{2-16}$$

where $T_{ref}$ is the noise temperature of the reference load, $T_{ant}$ is the antenna temperature and $T_N$ is the noise temperature of the injected noise. Brackets represent the infinite time average.

The amount of the injected noise is regulated by adjusting the number or the frequency of the noise pulses so that Equation (2-16) is fulfilled. The sensitivity of a noise injection radiometer is almost the same as that of a Dicke radiometer [1]:

$$\Delta T_N = \frac{2(T_{ref} + T_{rec})}{\sqrt{B\tau}}. \tag{2-17}$$

As can be seen the antenna temperature is effectively all the time the same as that of the reference and thus the sensitivity is slightly worse.

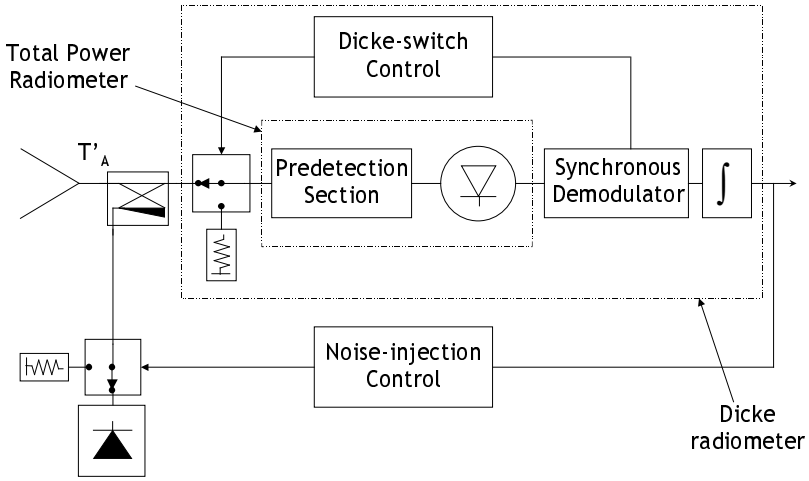


*Figure 2-4. Principle of a total power, Dicke and noise-injection radiometer [1]. Note that the noise injection functionality is just an extension of a Dicke radiometer.*

Figure 2-4 presents the basic structure of a noise-injection radiometer. Notice how the noise-injection part is in a way just an extension of a Dicke radiometer.

## 2.3 System Noise Temperature

The system noise temperature of a radiometer is defined as [1]

$$T_{sys} = T_{ant} + T_{rec}, \tag{2-18}$$

where $T_{sys}$ is the system noise temperature, $T_{ant}$ is the antenna temperature and $T_{rec}$ is the noise temperature of the receiver. $T_{rec}$ is determined here using the total power mode of the NIR and for the noise-injection operation $T_{ant}$ is always (approximately) constant (296K-299K for MDPP-2 NIR [9]).

The system noise temperature plays a key role in any microwave system and especially in radiometers. In this section we take a look at the Y-factor method, explained e.g. in [3], for measuring the system noise temperature of a radiometer.

The Y-factor method is based on power measurements of two known loads, which are at significantly different temperatures. For example, the noise temperature of an amplifier can be determined this way by connecting its other end to the loads and the other to a power meter. Of course, in the case of a radiometer the radiometer itself measures the power from the loads.

Let $T_1$ be the temperature of the hot load and $T_2$ temperature of the cold load. Powers emitted by the loads are now

$$P_1 = GkT_1B + GkT_{rec}B = GkB(T_1 + T_{rec}) \tag{2-19}$$

$$P_2 = GkT_2B + GkT_{rec}B = GkB(T_2 + T_{rec}) \tag{2-20}$$

where $G$ is the gain of the receiver, $k$ is the Boltzmann's constant and $B$ is the bandwidth of the receiver. Note that the receiver gain has to be maintained constant between the measurements. Y-factor is now defined as

$$Y = \frac{P_1}{P_2} = \frac{T_1 + T_{rec}}{T_2 + T_{rec}} \tag{2-21}$$

and it can be determined using the power measurements. By solving $T_{rec}$ from (2-21) yields

$$T_{rec} = \frac{T_1 - YT_2}{Y - 1}. \tag{2-22}$$

The system temperature of a total power radiometer can be defined easily as described above and in the case of Dicke radiometer the Dicke operation should be turned off to measure the system noise temperature.

## 2.4 Measurement of Sensitivity

The sensitivity of a radiometer can be calculated theoretically based on the noise temperature of a radiometer, as introduced in Section 2.2, or it can be calculated from measurements using the standard deviation of measurement results of a stable target [1] as presented in this section.

In practice the sensitivity of a radiometer is the standard deviation of measurement results of a stable target [1]. Thus it can be calculated as presented

in Equation (2-23), which is based on Equation (2-67) of standard deviation. When the target of a measurement is stable all the variations of the noise temperature in the output of a radiometer are due to the noise temperature of the radiometer itself and random variations of the noise-like signal of the target. For example consider Figure 2-5: when there was no variation in the target brightness temperature the sensitivity, pointed out in the figure, could be observed all the time. The smallest observable change in a target can be determined.

$$\Delta T_\sigma = \sqrt{\frac{1}{N-1}\sum_{k=1}^{N}\left(T_k - \overline{T}\right)^2} \tag{2-23}$$

where $N$ is the amount of the samples, $T_k$ is one sample of brightness temperature and $\overline{T}$ is the mean of the samples.

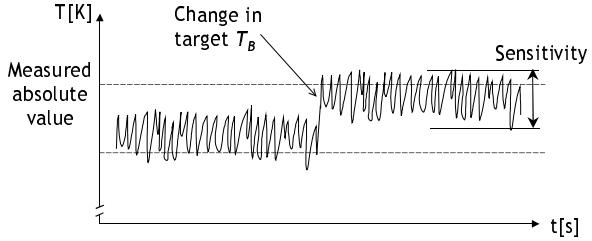


*Figure 2-5. Clarification of the sensitivity. Sensitivity of a radiometer is by definition the smallest observable change in the measured brightness temperature.*

# 2.5 Measurement of RF Connections

In this section we take a look at some methods for modelling RF connections between some device and a receiver. These methods will be used in the following chapters for analysing the effects of the connections on the NIR measurements.

## 2.5.1 Connecting Network

The connection between two ports in a RF system can be described with a lossy two-port network **S**. The network **S** may be any passive, linear, time-invariant network. It is characterised by a scattering matrix **S** given by [3]

$$\mathbf{S} = \begin{bmatrix} S_{11} & S_{12} \\ S_{21} & S_{22} \end{bmatrix} \tag{2-24}$$

where $S_{11}$ and $S_{22}$ are related to the reflection properties of the network and $S_{21}$ and $S_{12}$ are related to the transmission properties of the network. The network $S$ is assumed to have physical temperature of $T_0$. It has also reflection coefficients $R_{01}$ and $R_{02}$ as seen looking out from the network. The network is represented in Figure 2-6.

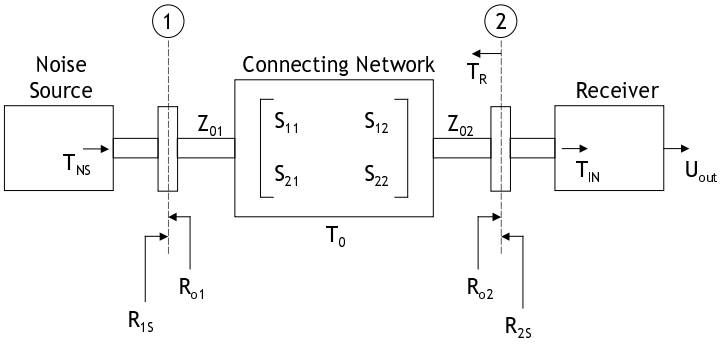


*Figure 2-6. Connecting network representation. Signal passes through the ports 1 and 2 and is affected by the reflection and transmission coefficients characterised by the S-parameters.*

### 2.5.2 Passive Components Inside Connecting Network

The most important component to be analysed in the tests is an attenuator. An attenuator attenuates the incoming signal but it also produces thermal noise due to attenuation. The connecting cables work the same way. If noise temperature $T_{in}$ is connected to the input of an attenuator or a cable then at the output is [3]

$$T_{out} = \frac{T_{in}}{L} + \left(1 + \frac{1}{L}\right) T_{phys}, \tag{2-25}$$

where $L$ is the attenuation of the attenuating element and $T_{phys}$ is the physical temperature of the attenuating element. Attenuation can be measured by determining the $S_{21}$ parameter of the component.

## 2.6 Stability of Radiometer

There are always gain fluctuations in a receiver, no matter how good RF parts are being used and how well the radiometer is temperature-stabilised. Also if the physical temperature changes not only the gain changes but also the behaviour of the radiometer changes. There are methods for cancelling these effects, as described in section 2.2, but they are never ideal and the degree of stability must be characterised.

Stability can be evaluated by measuring a stable target for a long period of time and examining the changes in the output or a better defined method like the Allan variance described in the following section can be used.

### 2.6.1 Allan Variance

Allan variance is a statistical tool originally developed by David W. Allan [4] to characterize the frequency stability of clocks. However, it can also be applied to

evaluation of the stability of systems [6] (i.e. calculated in time domain instead of frequency domain) and, therefore, it is introduced here.

The idea is to calculate the Allan variance of measurement results of a stable source as a function of integration time. In this way the optimum integration time is determined.

As seen in Equation (2-12) the sensitivity of a radiometer would converge to zero with an infinite integration time if the noise of the radiometer were totally uncorrelated i.e. white noise. However, the noise in a radiometer consists of three components, namely: low-frequency drift (correlated noise), 1/f electronic noise and white noise (uncorrelated). There is an optimal integration time after which observing efficiency is lost due to the drift. In [6] the Allan variance is given as

$$\sigma_y^2(m) \cong \frac{1}{m}\sum_{k=1}^{m}\frac{\left(\bar{y}_{k+1}-\bar{y}_k\right)^2}{2} \tag{2-26}$$

where $y_k$ is one averaged period and $m$ is the number of averaged periods. $\bar{y}_k$ is defined as follows:

$$\bar{y}_k = \frac{1}{n}\sum_{i=(k-1)n+1}^{kn} y_i \tag{2-27}$$

where $k$ is the number of averaged period, $n$ is the number of samples in one averaged period, $i$ is number of a sample and $y$ is a sample. The parameters are clarified in Figure 2-7.

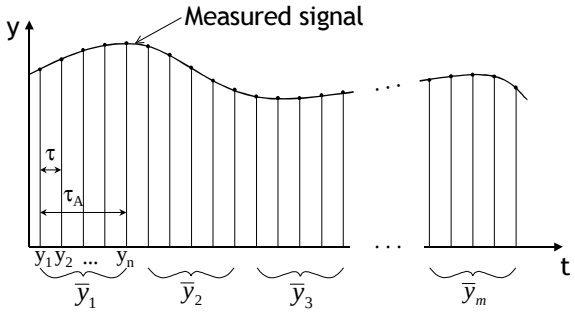


*Figure 2-7. Parameters for Allan variance. The signal is integrated over an interval $\tau$ by the radiometer and then the result is further integrated over an interval $\tau_A$ in order to calculate the Allan variance.*

From the calculation of Equation (2-26) the so-called Allan plot may be drawn (Figure 2-8). The optimal integration time is found at the minimum of the curve.

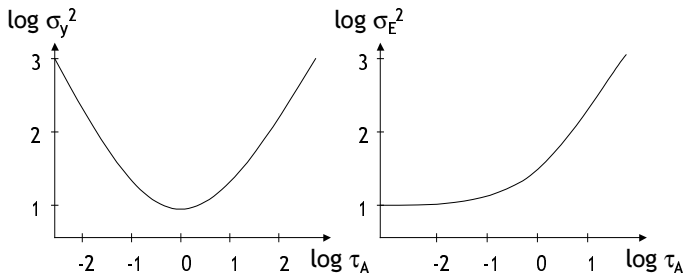


*Figure 2-8. Allan plot (left) and the error for the mean of several individual measurements, $\sigma_E$ (right) [6]. In the Allan plot the optimal integration time is found at the minimum of the curve. The error plot demonstrates that the reliability of the mean severely decreases for longer integration times.*

# 2.7 Radiometer Calibration

## 2.7.1 Total Power Radiometer

Usually the detector of a radiometer is assumed to behave in a liner manner i.e. the output of the radiometer has a straight-line relationship to the received power [1]. In this situation one has to know only two points from the line, that we here call calibration line, to know the brightness temperature of the measured target for every output in a certain range (Figure 2-9).

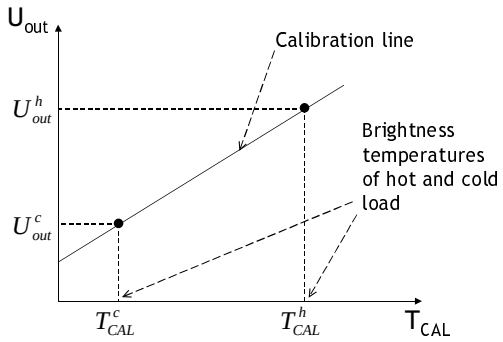


*Figure 2-9. Calibration line of a radiometer in principal. Detection of the radiometer is assumed to behave in a linear manner.*

There has to be at least two targets whose brightness temperatures are known for defining the calibration line. These calibration targets are often called hot and cold load. The response of a linear radiometer is defined as [1]

$$V_{out} = a(T_{in} + b) \tag{2-28}$$

where $a$ and $b$ are the constants for each known value of $V_{out}$ and $T_{in}$. $V_{out}$ is the output of the receiver (often volts) and $T_{in}$ is the noise temperature incident on the radiometer. In principle $b$ is known for balanced Dicke radiometers [1] and only one calibration measurement would be enough to determine the value of $a$ (see

Section 2.7.2). The formulas from [1] can also be written in a more illustrative form

$$V_{out} = aT_{in} + ab = AT_{in} + B \tag{2-29}$$

where $A$ is the rise factor and $B$ is now the offset of the line describing the response of the radiometer. $A$ and $B$ can be calculated from the calibrations in the following manner. If

$$\begin{aligned} V_{out}^{h} &= AT_{cal}^{h} + B \\ V_{out}^{c} &= AT_{cal}^{c} + B \end{aligned} \tag{2-30}$$

then

$$\begin{aligned} A &= \frac{V_{out}^{h} - V_{out}^{c}}{T_{cal}^{h} - T_{cal}^{c}} \\ B &= \frac{V_{out}^{c} T_{cal}^{h} - V_{out}^{h} T_{cal}^{c}}{T_{cal}^{h} - T_{cal}^{c}} \end{aligned} \tag{2-31}$$

where $T_{cal}$ is the noise temperature coming into the radiometer during calibration procedure. Superscripts $h$ and $c$ denote the hot and cold load, respectively.

### 2.7.2 Noise Injection Radiometer

Calibration of a noise injection radiometer is much simpler than that of a total power radiometer. The calibration requires only one known target with which the noise temperature coupled to the antenna channel, through the directional coupler, can be accurately determined [1]:

$$T_N = \frac{T_{ref} - T_A}{\eta}, \tag{2-32}$$

where $T_{ref}$ is the reference load noise temperature, $T_A$ is the antenna temperature and $\eta$ is the length of the antenna injection pulse determined as:

$$\eta = 2t_N f_D, \tag{2-33}$$

where $f_D$ is the Dicke frequency and $t_N$ is the length of the noise injection pulse, which is the output of the noise injection radiometer.

## 2.8 MDPP-2 NIR

The noise injection radiometer is required for the MIRAS aperture synthesis radiometer for two reasons [9]

1. To measure the antenna temperature with fully polarimetric capability during the measurement phase of the whole MIRAS instrument.

2. To measure the output of the first correlated noise source i.e. the centralized noise source during the calibration phase of the whole MIRAS instrument.

The radiometers of MIRAS are composed of LICEF receivers and horizontally and vertically polarised antenna. The noise injection radiometer of the MDPP-2 is built around two LICEF units, so that one is for receiving the horizontal polarisation and the other is for receiving the vertical polarisation. LICEF receivers measure at a frequency of 1.4 GHz with a down-converted Intermediate Frequency (IF) of 8-27 MHz. The IF signal is taken for four actual outputs and for two test outputs. The outputs are:

- PMS1, which is the detector output for total power measurement
- PMS2, which is the detector output for noise-injection control circuitry
- DI, which is the one-bit digitised in-phase signal for correlator
- DQ, which is the one-bit digitised quadrature phase signal for correlator
- TI, which is the in-phase IF signal
- TQ, which is the quadrature phase IF signal

One-bit digitising means that the signal is sampled either as zero or as one depending on the level of the signal. This is effectively the phase information of the signal and it is used by the Digital Correlator System (DICOS), resulting as one-bit two-level correlation (1b2L), in order to calculate the Stokes parameters as introduced below. The in-phase signal means a signal that is not phase shifted and the quadrature phase signal means a signal that is phase shifted 90 degrees from the original. These properties are also needed for Stokes parameter retrieval. The outputs can be found in the block diagram of the NIR, which is presented in Figure 2-10.

The goal of the polarimetric measurements is to calculate the third and fourth Stokes parameters (see Section 2.1.5). For ideal noise free horizontally and vertically polarised radiometer measurement the parameters may be written [9]:

$$\begin{aligned} T_3 &= 2\sqrt{T_{Hant}T_{Vant}}\,\mu_0\big|_{i,i} \\ T_4 &= 2\sqrt{T_{Hant}T_{Vant}}\,\mu_0\big|_{q,i} \end{aligned} \tag{2-34}$$

where $\mu_0|_{i,i}$ is the ideal 1b2L correlation coefficient of the I-output of the H-channel and I-output of the V-channel and $\mu_0|_{q,i}$ is the 1b2L ideal correlation coefficient of the Q-output the H-channel and I-output of the V-channel.

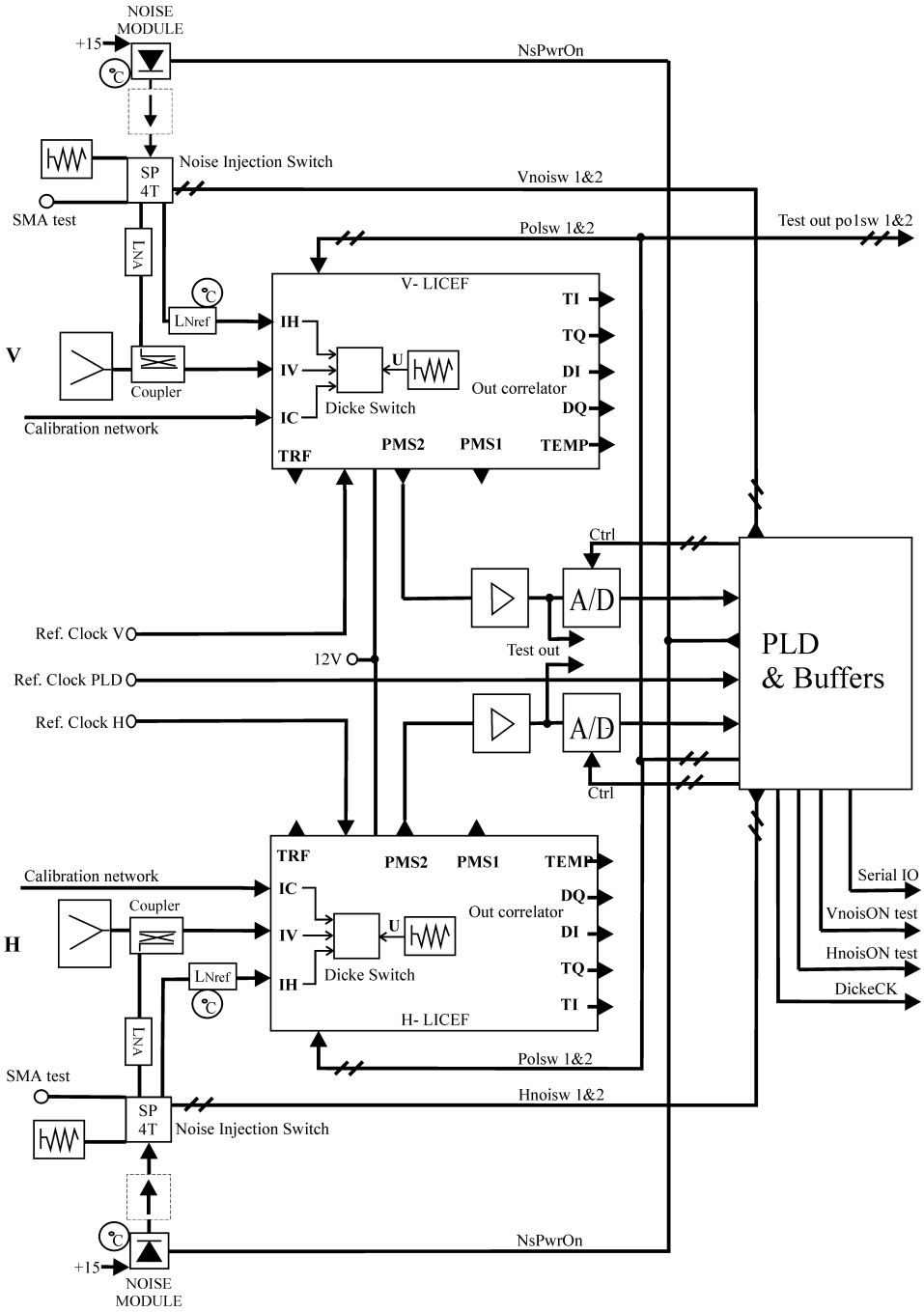


*Figure 2-10. Block diagram of NIR, in which the horizontal and vertical channels are depicted. The noise-injection measurement output of both channels of NIR is taken from the Serial IO line on the right and total power measurement of NIR is taken from the PMS1 outputs of horizontal and vertical channel. Notice the switches Dicke Switch inside the LICEF units and Noise Injection Switch after the noise modules.*

### 2.8.1 Stokes Parameters in MDPP-2 NIR Total Power Mode

MDPP-2 NIR can also operate in total power mode, in which Dicke and noise injection operation is not in use. For the total power measurement of NIR the ideal correlation coefficient $\mu_0$ of Equation (2-34) is defined from the following relation [9]:

$$\mu = \tilde{g}\mu_0, \tag{2-35}$$

where $\mu$ is the real measured correlation coefficient and the modulus term $\tilde{g}$ is defined as [9]

$$\tilde{g} = g_{FW}\sqrt{\frac{T_{Vant}}{T_{Vant}+T_{Vrec}}}\sqrt{\frac{T_{Hant}}{T_{Hant}+T_{Hrec}}}, \tag{2-36}$$

in which $g_{FW}$ is the so-called fringe-washing factor (see Sections 2.8.3 and 2.8.4). When the above equations are applied to Equation (2-34) the following result is derived:

$$\begin{aligned} T_3 &= \frac{2}{g_{FW}}\sqrt{T_{Hant}+T_{Hrec}}\sqrt{T_{Vant}+T_{Vrec}}\,\mu\big|_{i,i} \\ T_4 &= \frac{2}{g_{FW}}\sqrt{T_{Hant}+T_{Hrec}}\sqrt{T_{Vant}+T_{Vrec}}\,\mu\big|_{q,i} \end{aligned}, \tag{2-37}$$

from which the Stokes parameters may be determined when the horizontal and vertical brightness temperatures and correlation coefficient are measured and the noise temperatures of the two channels are known. In total power mode the quantizer and the correlator operate on the basis of the following equations:

$$\mu = \sin\left(\frac{\pi}{2}Z\right) \tag{2-38}$$

where

$$Z = \frac{1}{N}\sum_{i=1}^{N} sign(x(t_i))sign(y(t_i)) \tag{2-39}$$

in which $x(t)$ and $y(t)$ are the input signals being digitised and correlated and $N$ is the number of samples being correlated.

### 2.8.2 Stokes Parameters in MDPP-2 NIR Noise-Injection Mode

Normally MDPP-2 NIR operates in noise-injection mode. The equations above hold for total power mode but for noise-injection mode the correlation coefficient are not defined equally because the Dicke reference load is measured and additional noise is injected. For the noise-injection measurement of NIR the ideal correlation coefficient $\mu_0$ of Equation (2-34) is defined using the following relation [9]

$$\mu_k = \tilde{g}_k\mu_0, \quad k=1,2,3,4 \tag{2-40}$$

in which indices 1 through 4 are time steps in Dicke cycle and are defined here as follows:

1. Measurement of Dicke load
2. Antenna measurement with noise injection to both channels (horizontal and vertical)
3. Antenna measurement with noise injection to one channel (only horizontal or vertical)
4. Antenna measurement without noise injection

and the so-called modulus terms are defined as follows for the case the noise injection pulse is longer in channel V:

$$\tilde{g}_2 = g_{FW}\sqrt{\frac{T_{Vant}}{T_{Vant}+T_{Vrec}+T_{VN}}}\sqrt{\frac{T_{Hant}}{T_{Hant}+T_{Hrec}+T_{HN}}} \tag{2-41}$$

$$\tilde{g}_3 = g_{FW}\sqrt{\frac{T_{Vant}}{T_{Vant}+T_{Vrec}+T_{VN}}}\sqrt{\frac{T_{Hant}}{T_{Hant}+T_{Hrec}}} \tag{2-42}$$

$$\tilde{g}_4 = g_{FW}\sqrt{\frac{T_{Vant}}{T_{Vant}+T_{Vrec}}}\sqrt{\frac{T_{Hant}}{T_{Hant}+T_{Hrec}}} \tag{2-43}$$

where $g_{FW}$ is the fringe-washing factor (see Equation (2-47)). In the case when the noise injection pulse is longer in channel H it is just needed to exchange 'V' and 'H' in Equation (2-42).

$\mu_0$ is here the real correlation coefficient that would be measured if an ideal and completely noise-free version of the NIR was operated in total power mode and can be solved from the following equation, which is the real-valued correlation measured with the real NIR:

$$\mu_k = \sin\left(\sin^{-1}(\tilde{g}_2\mu_0)\frac{N_2}{N}+\sin^{-1}(\tilde{g}_3\mu_0)\frac{N_3}{N}+\sin^{-1}(\tilde{g}_4\mu_0)\frac{N_4}{N}\right), \tag{2-44}$$

where $N$ is the number of samples during the whole Dicke cycle and $N_2$, $N_3$ and $N_4$ are the number of samples during the respective step.

In the noise-injection mode the correlator is assumed to operate on the basis of the following equations:

$$\mu_k = \sin\left(\frac{\pi}{2}Z_k\right) \tag{2-45}$$

where

$$Z_k = \frac{1}{N_k}\sum_{i=1}^{N_k} sign(x(t_i))sign(y(t_i)) \tag{2-46}$$

in which $k$ represents the Dicke cycle step. The Stokes parameters of Equation (2-34) can now be solved when $\mu|_{i,i}$, $\mu|_{q,i}$, $N$, $N_2$, $N_3$, $N_4$, $\tilde{g}_2$, $\tilde{g}_3$ and $\tilde{g}_4$ are known.

### 2.8.3 Calculation of Fringe-Washing Function

The fringe-washing function is defined for two non-identical receivers as the equivalent low-pass signal, with respect to the reference centre frequency $f_0$, of the cross correlation between the analytic frequency responses of the two receivers, normalised to its maximum value [10]. The fringe-washing function can be determined with two methods: in this Section the method based on the frequency responses of the receivers is presented and in the next the method based on the correlation coefficient measurement is discussed.

An analytical formula for the fringe-washing function [10] applied for the H- and V-channels can be written as:

$$g_{FW}(\tau) = \frac{1}{\sqrt{B_H B_V}} \int_{-f_0}^{\infty} H_{n,H}(f + f_0) H_{n,V}^{*}(f + f_0) e^{j2\pi f\tau} df \tag{2-47}$$

where $B_H$ and $B_V$ are the bandwidths of the H- and V-channels, respectively; $H_{n,H}$ and $H_{n,V}$ are the normalised frequency responses of the H- and V-receivers, respectively and $\tau$ is the time delay between the receivers. The bandwidths and the frequency responses are measured e.g. with a vector network analyser (VNA).

### 2.8.4 Measurement of Fringe-Washing Function

In this section the fringe-washing function $g_{FW}$ is determined using a method introduced for aperture synthesis radiometry [14]. Correlated noise is injected to the receivers and the receiver output cross-correlations at different time delays are measured.

The complex cross correlation between the analogue outputs of H- and V-channel is [14]

$$\Gamma_{sHsV}(\tau) = [\Gamma_{nHnV}(\tau) * R_{hHhV}(\tau)] e^{-j2\pi f_0 \tau} \tag{2-48}$$

where $R_{hHhV}(\tau)$ is the cross correlation between the frequency responses and $\Gamma_{nHnV}$ is the cross correlation of the noise at the input of the receivers. It is shown [14] that

$$\Gamma_{sHsV}(\tau) = 2k_B T_N \sqrt{B_H B_V}\, \alpha_H \alpha_V g_{FW}(\tau) \tag{2-49}$$

where $k_B$ is the Boltzmann's constant; $T_N$ is the noise injected into the receivers; $B_H$ and $B_V$ are the bandwidths of the H- and V-channel receivers, respectively; $\alpha_H$ and $\alpha_V$ are the maximum modulus of the voltage gains of the H- and V-channel receivers, respectively and $g_{FW}(\tau)$ is the fringe-washing function.

The cross correlation of the 1-bit digitised version of the receiver outputs is a function of the normalised cross correlation of the corresponding analogue signals

$$\Gamma^{p}_{dHdV}(\tau) = \frac{2}{\pi}\arcsin\frac{\Gamma^{p}_{sHsV}(\tau)}{\sqrt{\Gamma_{sH}(0)\Gamma_{sV}(0)}}, \tag{2-50}$$

in which superscript $p$ denotes the real or imaginary part, $\Gamma_s(\tau)$ is the autocorrelation function of the analogue signals and

$$\Gamma_{sH/V}(0) = 2k_B(T_N + T_{H/Vrec})B_{H/V}\alpha_{H/V}, \tag{2-51}$$

where $T_{rec}$ is the receiver noise temperature. Now $\Gamma^{p}_{dHdV}(\tau)$ can be written as

$$\Gamma^{p}_{dHdV}(\tau) = \frac{2}{\pi}\arcsin\left(\frac{T_N}{\sqrt{(T_N + T_{Hrec})(T_N + T_{Vrec})}}g^{p}_{FW}(\tau)\right), \tag{2-52}$$

from which the fringe-washing function can be solved yielding

$$g^{p}_{FW}(\tau) = \frac{1}{T_N}\sqrt{(T_N + T_{Hrec})(T_N + T_{Vrec})}\sin\left(\frac{\pi}{2}\Gamma^{p}_{dHdV}(\tau)\right). \tag{2-53}$$

The above equation shows that the fringe-washing function can be determined when the noise $T_N$ injected into the receivers and their noise temperatures $T_{rec}$ are known and the cross correlation of the output is measured for all values of the delay $\tau$.

In a so-called 3-delay method [14] the cross correlation is measured only with three different delays, namely early ($\tau$=-$T$), punctual ($\tau$=0) and late ($\tau$=+$T$). The method relies on the fact that the frequency responses of the two receivers (H and V) are fairly close to a nominal one (rectangular).

If the frequency responses of the receivers were ideal i.e. rectangular shaped, the corresponding ideal fringe-washing function would be the well-known *sinc* function. However the actual receiver frequency responses are not perfectly rectangular and they also differ from each other in the cut-off frequencies, noise equivalent bandwidths, bandpass shapes and group delays. This results in a fringe-washing function that is not a pure *sinc* function, but since the frequency responses are close to the nominal one also the fringe-washing function is close to the nominal *sinc* function. With the measurements of three different delays a *sinc* can be fit in amplitude as a good approximation to the actual fringe-washing function.

The following equations are used in the approximation of the real fringe-washing function [14] (second order polynomial is used in phase fitting):

$$\left|g_{FW}(\tau_{1,2,3})\right| \approx A\,\mathrm{sinc}\left(B(\tau_{1,2,3} - C)\right) \tag{2-54}$$

$$\arg g_{FW}(\tau_{1,2,3}) \approx D\tau^2_{1,2,3} + E\tau_{1,2,3} + F \tag{2-55}$$

where $\tau_{1,2,3}$ corresponds to the delay values of -*T*, 0, +*T*. With DICOS-3 it is convenient to use $T = 17.9$ *ns*, which is the sampling frequency of its channels. Coefficients *A*, *B* and *C* can be found numerically and coefficients *D*, *E* and *F* require solving the following linear system:

$$\begin{aligned} D &= \left( \frac{\Phi_T + \Phi_{-T}}{2} - \Phi_0 \right) \frac{1}{T^2} \\ E &= \left( \frac{\Phi_T + \Phi_{-T}}{2} \right) \frac{1}{T} \\ F &= \Phi_0 \end{aligned} \tag{2-56}$$

where $\Phi$ is the measured phase arg $g_{FW}$ at the given delay. The real cross correlation must be regarded as noisy due to the finite integration time of the correlator. This adds uncertainty to the above approximation.

### 2.8.5 MDPP-2 NIR Calibration

The calibration procedure of MDPP-2 NIR will consist of the following steps [18]:

A. First the normal noise-injection measurement of NIR is calibrated by obtaining the injection noise temperatures as introduced in Section 2.7.2.

B. The I- and Q-signals of both channels are digitized with quantizers that have offsets. Thus the normalized quantizer offset voltages have to be solved.

   Both channels are set to measure the reference loads and each of the four digital outputs are correlated with a signal that is continuously 1 or 0 (property of DICOS). The normalized quantizer voltage offsets are now obtained from:

$$\frac{a_i}{\sigma_i} = \pm \mu_i \sqrt{\frac{2}{\pi}}, \quad i = 1,2,3,4 \tag{2-57}$$

   where $a_i$ is the offset voltage for quantizer *i*, $\sigma_i$ is the standard deviation of the signal at the quantizer and $\mu_i$ is the measured correlation coefficient. The signal levels in both channels are taken from the power detector outputs.

C. The receivers' I- and Q-signals have phase errors. The in-phase error is the phase difference between the receivers' I-signals and the quadrature error is the phase difference deviation from 90 degrees of the I- and Q-signals of a receiver.

   Both channels are set to measure continuously the calibration network noise and the correlations and the detector output voltages in the both

channels are measured. Now the offsets $a_i/\sigma_i$ that were obtained in step B are corrected to account for the new power level. The offset correction is done by solving the following kind of equations:

$$\sin^{-1}\left(\mu_{ij}^{raw}\right)=\sin^{-1}\left(\mu_{ij}\right)-\frac{1}{2\sqrt{1-\mu_{ij}^2}}\left(\frac{\mu_{ij}a_i^2}{\sigma_i^2}+\frac{\mu_{ij}a_j^2}{\sigma_j^2}+\frac{2a_ia_j}{\sigma_i\,\sigma_j}\right), \tag{2-58}$$

where $\mu_{ij}^{raw}$ is the measured correlation and $\mu_{ij}$ is the true correlation of quantizer outputs $i$ and $j$. Then the quadrature errors of both channels are solved:

$$\begin{aligned}\theta_V^{quad} &= -\sin^{-1}\left(\mu_{Vi,Vq}\right)\\ \theta_H^{quad} &= -\sin^{-1}\left(\mu_{Hi,Hq}\right)\end{aligned} \tag{2-59}$$

and the in-phase error between the channels is obtained from the phase of the complex correlation, after removing the quadrature errors as follows:

$$\begin{bmatrix}\mu_{ii}\\ \mu_{qi}\end{bmatrix}_{new}=\mathbf{Q}^{-1}\begin{bmatrix}\mu_{ii}\\ \mu_{qi}\end{bmatrix}_{old}\quad\text{and}\quad\begin{bmatrix}\mu_{qq}\\ \mu_{iq}\end{bmatrix}_{new}=\mathbf{Q}^{-1}\begin{bmatrix}\mu_{qq}\\ \mu_{iq}\end{bmatrix}_{old} \tag{2-60}$$

in which

$$\mathbf{Q}=\begin{bmatrix}\cos\left(\frac{1}{2}\theta_H^{quad}-\frac{1}{2}\theta_V^{quad}\right) & \sin\left(\frac{1}{2}\theta_H^{quad}-\frac{1}{2}\theta_V^{quad}\right)\\ -\sin\left(\frac{1}{2}\theta_H^{quad}+\frac{1}{2}\theta_V^{quad}\right) & \cos\left(\frac{1}{2}\theta_H^{quad}+\frac{1}{2}\theta_V^{quad}\right)\end{bmatrix}. \tag{2-61}$$

$\mathbf{Q}^{-1}$ is calculated in Section 4.4.3.

D. The receiver noise temperatures have to be solved in order to solve the modulus terms of NIR.

The measurement results from steps B and C are applied to the Y-factor method introduced in Section 2.3 in order to calculate the receiver noise temperatures of the both channels, that is $T'_{Vrec,Hrec}$. Then the noise temperatures that describes the whole antenna-receiver system for both channels are solved using the following equation

$$T_{Vrec,Hrec}=\frac{G'_{V,H}}{G_{V,H}}\left(T'_{Vrec,Hrec}+T_{phys}\right)-T_{phys}, \tag{2-62}$$

where the $G_{V,H}$'/$G_{V,H}$ are ratios describing the gain difference between using the calibration port and using the antenna as the input port for V-

and H-channels, respectively and $T_{phys}$ is the physical temperature of the antenna and the calibration network connection.

E. The fringe-washing factor has to be solved in order to find the modulus terms of NIR. It is determined by using the 3-delay method introduced in Section 2.8.4.

F. Finally the 3rd and 4th Stokes parameters can be calibrated and measured. They are solved from the following equation:

$$T_3 + jT_4 = \frac{2\sqrt{T_{Vant}T_{Hant}}\,\mu N}{\tilde{g}_2 N_2 + \tilde{g}_3 N_3 + \tilde{g}_4 N_4}, \tag{2-63}$$

in which $\mu$ is the measured offset (step B), in-phase and quadrature (step C) corrected correlation coefficient of the target, $T_{Vant}$ and $T_{Hant}$ are the measured brightness temperatures at both polarisations (step A) and $\tilde{g}_2$, $\tilde{g}_3$ and $\tilde{g}_4$ are the calculated modulus terms (steps D and E, see Equations (2-41) to (2-43)). The values of $N$, $N_2$, $N_3$ and $N_4$ are determined from the NIR output.

# 2.9 Data and Error Analysis

In this section a closer look is taken at the theory of measurement results analysis and error estimation.

## 2.9.1 Basic Statistical Tools

### Standard Deviation

According to [8] the standard deviation can be defined as

$$\sigma \equiv \sqrt{\left\langle (x_i - \mu)^2 \right\rangle} \tag{2-64}$$

where $x_i$ is one sample, $i$ is the number of a sample and $\mu$ is mean of $x$ that is

$$\mu \equiv \langle x \rangle \tag{2-65}$$

In the above equations the brackets denote infinite time average and they can be approximated with a finite sum. Thus $\mu$ can be written as the sample mean $\bar{x}$, which is [8]

$$\bar{x} = \frac{1}{N}\sum x_i \tag{2-66}$$

and the standard deviation for discrete finite data set can be written as [8]

$$s = \sqrt{\frac{1}{N-1}\sum\left(x_i - \bar{x}\right)^2} \tag{2-67}$$

where the factor *N*-1, rather than *N*, is required in the denominator to account for the fact that the parameter $\bar{x}$ has been determined from the data not independently.

**Linear-correlation Coefficient**

A measure for overall linearity of a combined data set can be found. In other words, for data set y, dependency (in linear manner) on another data set, say x, can be calculated. The dependency is called linear-correlation coefficient [8] and is defined as

$$r = \frac{N\sum x_i y_i - \sum x_i \sum y_i}{\sqrt{N\sum {x_i}^2 - \left(\sum x_i\right)^2}\sqrt{N\sum {y_i}^2 - \left(\sum y_i\right)^2}} \tag{2-68}$$

where *r* is linear-correlation coefficient, *y* is the dependent variable, *x* affecting variable and *N* is the number of samples.

## 2.9.2 Error of Measurement

In the error analysis the standard propagation of error will mainly be used. It is defined as [8]

$$\Delta f\left(x_1, x_2, ...x_n\right) = \sqrt{\sum_{i=1}^{n}\left(\Delta x_i \frac{\partial f}{\partial x_i}\right)^2_{x_1^0, x_2^0, ..x_n^0}} \tag{2-69}$$

where the superscript 0 denotes the value of the variable at the point in which the uncertainty of *f* is evaluated.

# 3 DESCRIPTION OF MEASUREMENTS

In this chapter the required measurements for solving radiometer properties are described.

## 3.1 Overview of Test Procedure

In the tests the following measurements are needed:

- Measurement of two known loads in controllable ambient temperature:
  With this measurement the system noise temperature can be determined using the Y-factor method. Theoretical sensitivity can be calculated with the system noise temperature and sensitivity based on measurements is solved from measured standard deviation. Stability is determined in constant ambient temperature and in varying ambient temperature.
- Measurement of a changing load:
  The linearity of NIR can be found by measuring known alternating input power.
- Measurement of absorber targets and sky:
  With measurements of the absorber targets the measurements of the system noise temperature, sensitivity and stability may be further evaluated. Sky measurements are also important for NIR calibration accuracy evaluation.
- Measurement of controllable polarimetric loads:
  By measuring controllable polarimetric loads the polarimetric operation of NIR can be determined.
- Measurement of controllable polarimetric antenna load:
  With polarimetric antenna loads final conclusions about the ability of NIR to measure the Stokes parameters can be drawn. Validation of the calibration procedure is also an important application of this measurement.

The following text describes the hardware and methods required for the measurements. These configurations will be referred to as Configuration A, Configuration B and so on up to Configuration G. Table 3-1 below is used as a reference throughout the text indicating which radiometer properties and which measurement configurations are concerned. The left-hand side shows the radiometer properties that are to be solved i.e. the goals of the tests.

*Table 3-1. Description of which measurement configuration is needed for determining certain radiometer property.*

| CONFIGURATION | A | B | C | D | E | F | G |
|---|---|---|---|---|---|---|---|
| System Noise Temperature | | X | | | | | |
| Sensitivity | | X | | | X | | |
| Linearity | | | X | | | | |
| Polarimetric Properties | X | X | | X | | X | |
| Stability | | X | | | X | | |
| Calibration Accuracy | X | X | X | X | X | X | X |
| Absolute Accuracy | X | X | X | X | X | X | X |

## 3.2 Data Formats and Recording

Control and recording equipment of the measurement configurations can consist of variable components and devices but all the measured data, for instance temperatures and radiometer data, have to be accurately synchronised. The data should also be made available for normal PCs (e.g. in standard ASCII format) for universal compatibility and ease of use.

### 3.2.1 Test Setup in General

The NIR test setup from the measurement signal point of view is presented in Figure 3-1 [12]. All the measurements are logged to one PC, which can also control the switches and attenuators in the measurement configurations. The "measurement control and recording" block of the measurement configurations (e.g. Figure 3-4) include all the blocks of Figure 3-1 except the NIR and CNS (Calibration Network Simulator). The equipment of Figure 3-1 consists of the NIR EGSE (Electronic Ground Support Equipment) system [12].

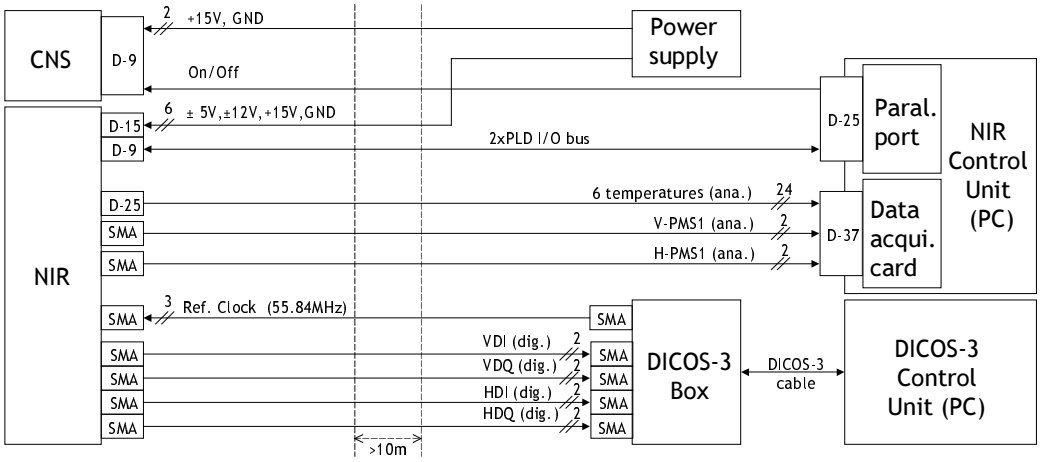


*Figure 3-1. Schematic diagram of NIR test setup [12]. The equipment on the right-hand side in the figure is the EGSE [12]. Note that the cables between NIR and EGSE have to be at least 10 meters long in order to make the measurement possible in different kind of environments with adequate disturbance shielding.*

### 3.2.2 NIR Data Format

MDPP-2 NIR data includes the measured power from H- and V-channel (raw noise injection pulse length ($N_H$ and $N_V$) and calibrated brightness temperature calculated in the NIR Control Unit if the calibration values are available), measured total power (PMS1) from H- and V-channel, temperatures from 6 temperature sensors, measurement mode flag and correlation coefficients from DICOS-3 ($\mu_{HiVi}$, $\mu_{HqVi}$, $\mu_{HiVq}$, $\mu_{HqVq}$, $\mu_{HiHq}$, $\mu_{ViVq}$, $\mu_{Hi0}$, $\mu_{Hq0}$, $\mu_{Vi0}$ and $\mu_{Vq0}$). The last four correlation coefficient values are the correlations with zero signal and they are used in calibration for quantizer offset voltage solving (Section 2.8.5).

The data logging system of the NIR will be such that all the data, except the DICOS-3 output, is saved in one file including date, time and a running sample number. The DICOS-3 data is then applied and the Stokes parameters can be calculated.

### 3.2.3 Test Measurement Data Handling

The test measurement equipment produces data consisting generally of temperatures, switch state and attenuator state information. All these will be logged into the same file for each measurement to simplify the analysis.

The logging program has to be able to run simultaneously with the NIR logging program in order to synchronise all the data easily. Of course, two computers can be used but then extra care has to be taken to synchronise the measurements accurately.

## 3.3 NIR Antenna Branch Measurements

In these measurements the effects of connections between the antenna and the receiver are examined. The antenna branch of the NIR is under focus since its properties play a key role when the antenna temperature is determined [9]. In the measurements a VNA is used to determine the reflection and transport coefficients (see Section 2.5) of the branch as seen from the receiver and to the receiver (Figure 3-2). Both channels are measured. The measurement equipment includes the following:

- NIR (antenna branch cabling detached from the receiver and noise-injection circuit unit)
- Absorber load for antenna termination
- Matched termination
- VNA.

In the first and second measurements (Figure 3-2) the absorber is placed in front of the antenna as in standard antenna impedance measurements (e.g. [3]). In the second measurement the reflections of the connections of the antenna branch are determined. In the third measurement the transmission coefficients of the branch are determined. In the fourth measurement the coupling of the coupler from the noise-injection source to the antenna branch is measured in order to get a reliable value (i.e. not based on specifications) for this, since it is a crucial component when the antenna temperature is evaluated.

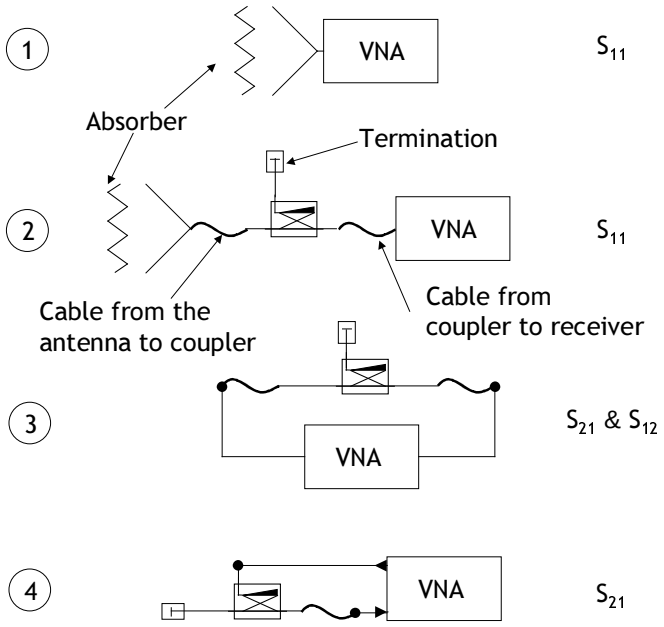


*Figure 3-2. Configurations for antenna branch measurements. Measurement 1 serves as a reference for the measurement 2 where the antenna connection reflection, seen by the receiver, is measured. In measurement 3 the line between the antenna and receiver is investigated and in measurement 4 coupling of the noise-injection coupler is determined.*

Measurements are performed at a temperature around 23-26°C since that is the operational temperature of the NIR [9]. The measurements produce knowledge about the antenna branch reflection coefficient of which may prove to be crucial when tracing possible problems in the NIR operation.

## 3.4 Measurement A: Frequency Response

In this configuration NIR receiver channels are measured end-to-end with a VNA in order to find out the phase and frequency response. Also in-phase error, quadrature error and fringe-washing function (see Section 2.8) of the receivers can be calculated from these measurements. Table 3-2 is summary of NIR properties that can be solved with this setup.

*Table 3-2. Radiometer properties solved using Measurement Configuration A*

| | A | B | C | D | E | F | G |
|---|---|---|---|---|---|---|---|
| System Noise Temperature | | X | | | | | |
| Sensitivity | | X | | | X | | |
| Linearity | | | X | | | | |
| Polarimetric Properties | X | X | | X | | | X |
| Stability | | X | | | X | | |
| Calibration Accuracy | X | X | X | X | X | X | X |
| Absolute Accuracy | X | X | X | X | X | X | X |

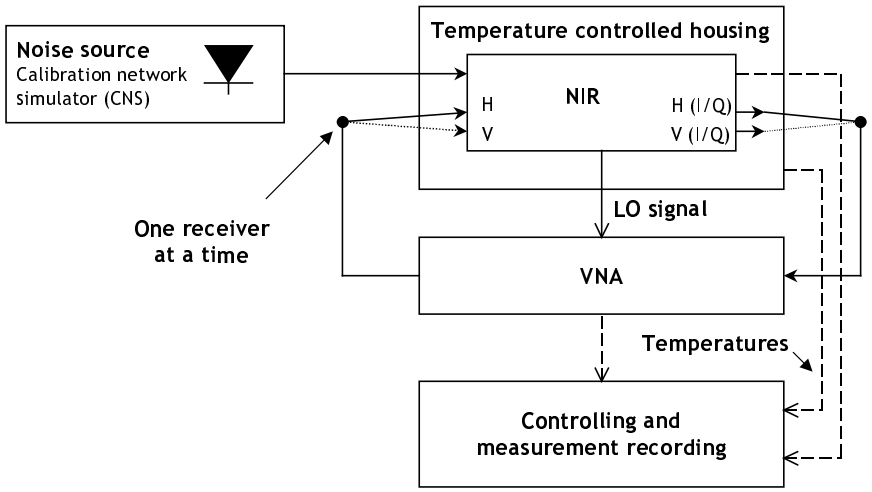


*Figure 3-3. Schematic diagram of the measurements with a VNA. VNA has to be synchronised with the NIR LO signal.*

**Configuration**

In this configuration NIR is connected to the VNA and measurement PC (Figure 3-3). The VNA will be equipped with an internal mixer so that the response of the IF channels can be measured directly. The mixer is synchronised with the local oscillator of the NIR. NIR noise-injection operation is off and the measurement is made with I- and Q-signals of the two channels (see Section 2.8). The temperature information of the NIR and its ambient is recorded. The equipment needed to perform the measurement is listed below:

- NIR in temperature controllable housing
- VNA
- CNS
- Equipment to record the results.

See Appendix D for details on the selection of components and devices. The configuration produces the following data: NIR ambient temperature and standard VNA data. Data handling and storing is considered in more detail in Section 3.2.

**1. S-parameter Measurement Routine without Noise from CNS**

The NIR is turned on and the output is connected to a VNA. Before the measurement the full S-parameter calibration of the VNA is performed. The CNS is off. Full TI- and TQ-output S-parameter measurements are performed for both channels of the NIR. The measurement is repeated at four different temperatures, because connection matching in general is very temperature dependent and it has strong effect on signal phase. The temperatures are 18°C, 23°C, 26°C and 31°C (23-26°C is the NIR operational range [9]).

**2. S-parameter Measurement Routine with Noise from CNS**

This measurement is like the previous, but now the CNS is kept on to see its effect on the measured frequency and phase response.

## 3.5 Measurement B: Basic Configuration

First the radiometer shall be tested without antennas. This allows identification of additional disturbances caused by the antenna.

*Table 3-3. Radiometer properties solved using Measurement Configuration B.*

| | A | B | C | D | E | F | G |
|---|---|---|---|---|---|---|---|
| System Noise Temperature | | X | | | | | |
| Sensitivity | | X | | | X | | |
| Linearity | | | X | | | | |
| Polarimetric Properties | X | X | | X | | | X |
| Stability | | X | | | X | | |
| Calibration Accuracy | X | X | X | X | X | X | X |
| Absolute Accuracy | X | X | X | X | X | X | X |

These measurements require two matched loads at different temperatures: at the room temperature and at the temperature of liquid nitrogen (Figure 3-4).

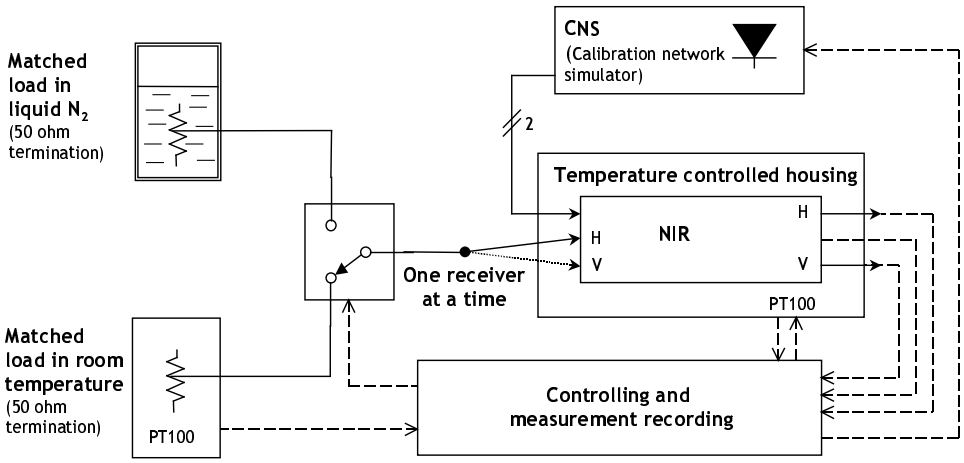


*Figure 3-4. Measurement configuration using matched loads. The cold load is a matched termination sunk in liquid nitrogen (Appendix A) and the hot load is a matched termination in room temperature with temperature measurement sensor. The loads are connected to the NIR using a PC controlled switch. S-parameters of the chain are measured before the actual measurements.*

**Configuration**

The temperature of the hot load has to be accurately known and recorded with a high temporal resolution (at least every 10 seconds). The cooling of the cold load is difficult to realise automatically. When the load is sunk in a container filled with liquid nitrogen, the problem is the filling of the container. That is easily done on regular basis aside other work but automatic operation, e.g. during nights, is

difficult. Considerations about realising a cold load are introduced in Appendix A. The measurement configuration consists of the following items (see Figure 3-4):

- NIR in temperature controllable housing
- Matched load in liquid nitrogen (Appendix A)
- Matched load in room temperature
- Electronically controlled switch
- CNS
- Power meter
- Equipment to control the switch and record the results.

The selection of the components and devices is considered in Appendix D. A rather complicated data set is gathered during the measurements including standard NIR data (Section 3.2.2), temperature of the hot load, NIR ambient temperature and switch status. Data handling and storing is considered in more detail in Section 3.2.

In the following a closer look is taken at each measurement routine made with this configuration. Notice again that the motivation for these different routines is fully revealed in Chapter 4. All the measurements are performed for both channels.

**1. Total Power Mode Measurement at a Constant Ambient Temperature**

This measurement routine is performed in the total power mode in order to find out the total power behaviour and the noise temperature of the receiver. The switch connected to the receivers is turned to the hot and cold load every 20 seconds during a 60-minute measurement period. The measurement is repeated three times. The CNS is off. The NIR ambient temperature NIR is kept stable (within 0.2°C) somewhere between 23°C and 26°C [9].

**2. Varying Temperature Measurement in Total Power Mode**

This measurement routine uses the NIR total power mode. The CNS is turned off all the time. The switch connected to the receivers is turned to the hot and cold load every 20 seconds during each measurement period. Two kinds of measurements are performed:

For the first measurement the ambient temperature is brought up to 50°C and lowered to 5°C 4 times so that the temperature is changed in 5°C steps and every step is measured 5 minutes.

The second time the temperature is varied from 23°C to 26°C 8 times. This is the predicted temperature range for the final NIR [9]. Now the temperature is changed in 1°C steps and every step is measured for a period of 5 minutes.

**3. Long Duration Measurement in Total Power Mode**

This measurement is also made in the total power mode. The switch is removed from the measurement configuration and the hot load is measured for 24 hours. The CNS is off. The ambient temperature is kept stable (within 0.2°C) somewhere

between 23°C and 26°C [9]. Based on this measurement the Allan variance of the receivers can be determined (see Section 2.6.1).

**4. Total Power Mode Measurement of an Active Noise Source**

In this routine the correlated noise of the CNS is measured in total power mode. The cold and hot external sources are also measured from time to time to control the gain fluctuation of the receiver. The following procedure will be performed:

Brief duration measurement of the hot load, brief duration measurement of the cold load followed by long time measurements of the CNS.

This procedure is repeated continuously during a one-hour period, which will be repeated three times. The ambient temperature is kept stable (within 0.2°C) somewhere between 23°C and 26°C [9]. This measurement provides also data for solving the polarimetric properties (Section 4.4).

**5. Noise-injection Mode Measurement at a Constant Ambient Temperature**

Normal noise-injection operation of the radiometer is used in this routine. The switch connected to the receivers is turned to the hot and cold load every 20 seconds during each measurement period. The length of the measurement period is 2 hours and the period is repeated four times. The CNS is turned on for two of the measurements and for the other two off. This is done to observe possible effects of the high power noise at the input of the Dicke switch (Figure 2-10). The absolute ambient temperature should be kept stable (within 0.2°C) somewhere between 23°C and 26°C [9].

**6. Noise-injection Mode Measurement in Varying Ambient Temperature**

The normal noise-injection routine is being used. The CNS is off. The switch connected to the receivers is turned to the hot and cold load every 20 seconds during each measurement period. Two kinds of measurements are performed:

For the first measurement the ambient temperature is brought up to 50°C and reduced to 5°C 4 times (sequence defined as before) so that the temperature is changed in 5°C steps and every step is measured for 5 minutes.

The second time the temperature is varied from 23°C to 26°C [9] 8 times (sequence defined as before). Now the temperature is changed in 1°C steps and every step is measured for 5 minutes

**7. Long Duration Measurement in Noise-injection Mode**

Normal noise-injection operation is being used and the switch is removed from the configuration and the hot load measured 24 hours. The CNS is off all the time. The measurement is done once. The ambient temperature is kept stable i.e. within 0.2°C somewhere between 23°C and 26°C [9]. This measurement provides data for the calculation of the Allan variance in noise-injection mode (Section 2.6.1).

**8. Measurement of Noise Source in Noise-injection Mode**

In this routine the correlated noise of the CNS is measured in noise-injection mode. The cold and hot external sources are also measured to get a reference for the measurement. The following procedure will be performed:

Brief duration measurement of the hot load, brief duration measurement of the cold load following long duration measurements of the CNS.

This procedure is repeated continuously during a one-hour period, which will be repeated three times. The ambient temperature is kept stable (within 0.2°C) somewhere between 23°C and 26°C [9]. This routine provides also data for the polarimetric properties analysis in Section 4.4.

## 3.6 Measurement C: Linearity

In this configuration the main objective is to establish the degree of linearity of the received power detection in the both total power and noise injection mode.

*Table 3-4. Radiometer properties solved using Measurement Configuration C*

| | A | B | C | D | E | F | G |
|---|---|---|---|---|---|---|---|
| System Noise Temperature | | X | | | | | |
| Sensitivity | | X | | | X | | |
| Linearity | | | X | | | | |
| Polarimetric Properties | X | X | | X | | | X |
| Stability | | X | | | X | | |
| Calibration Accuracy | X | X | X | X | X | X | X |
| Absolute Accuracy | X | X | X | X | X | X | X |

The radiometer is connected to a controllable noise source and to a stable matched load. As a result a curve describing the response of the radiometer as function of the incoming power can be defined.

A major source of error is the attenuator. Therefore it is essential to determine the attenuation in every position. Also every route the signal goes in the connecting network (switch, attenuator, power divider) will be measured using a VNA, as explained in Routine 1. This produces a data set that is used for the linearity analysis.

**Configuration**

The controllable noise source is realised by connecting the receivers to a cold load and an active noise source through a switch and a controllable attenuator. When the switch is turned to the cold load and the attenuation is increased the noise temperature seen by the receiver increases and when the switch is turned to the active noise source and the attenuation is increased the noise temperature seen by the receivers decreases.

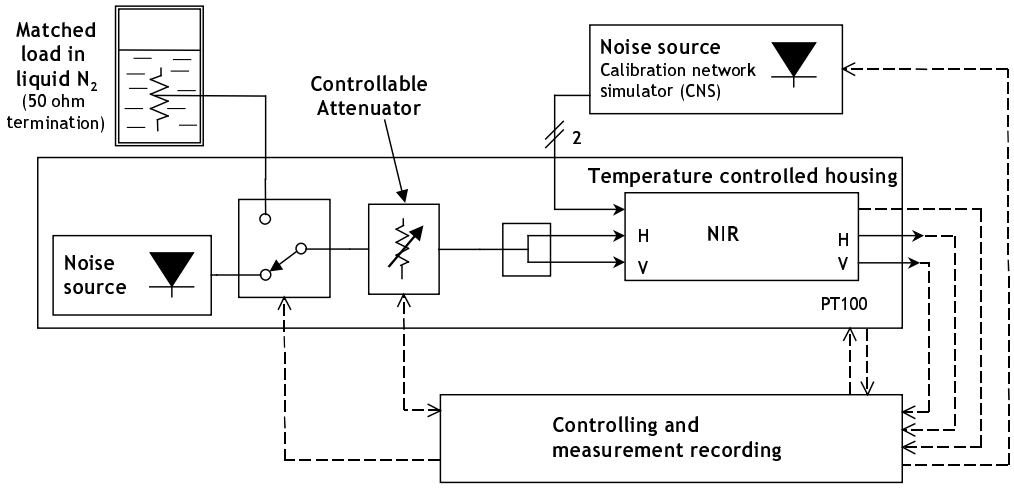


*Figure 3-5. Measurement configuration for linearity measurements. The controllable noise source is realised using an active noise source, a matched termination in liquid nitrogen, a switch and a controllable attenuator. The S-parameters of the connecting chain are measured for every position of the controllable attenuator.*

From time to time the switch is turned to the cold load position and the attenuation is turned to minimum in order to get a reference for the measurements. For another reference the switch is turned to the noise source, which is off, and the attenuation is turned to the maximum. In the latter case the receivers see a noise temperature equal to the physical temperature of the chain.

The amount of attenuation and the physical temperature of the attenuator have to be known accurately because the whole analysis is based on the attenuation and noise temperature figure given by the attenuator. See Appendix A for realising the cold load. The measurement configuration consists of the following parts (Figure 3-5):

- NIR and the measurement chain in a temperature controllable housing
- Matched load in liquid nitrogen (Appendix A)
- Noise source
- Electronically controllable attenuator
- Electronically controllable switch
- Power divider
- CNS
- Equipment to control the switch and the attenuator and to record the results.

See Appendix D for more details about selection of the components and devices. The configuration produces the following data: standard NIR data, status of the switch, amount of attenuation of the attenuator, temperature of the attenuator and ambient temperature of the NIR. Data handling and storing is considered in more detail in Section 3.2.

**1. VNA Measurement of the Connecting Network**

First the connecting network has to be measured using the VNA in order to know the accurate attenuation for every attenuator position. The following measurement procedure is performed:

The VNA is connected to the cold load input and to the active noise source input of the switch and to the H-channel and V-channel output of the power divider. In this way there are four different combinations for the connections. Full S-parameter measurement is performed with every possible attenuator state in every connection combination.

The standard VNA data files produced by the above measurements are stored for analysis. The temperature of the components is kept stable during the measurement (within 0.2°C) somewhere between 23°C and 26°C [9] e.g. using the NIR temperature controlled NIR housing (Appendix D).

**2. Total Power Mode**

This whole measurement procedure is performed twice. On the first time the CNS is turned off and for the second time it is turned on in order to identify any effect it may have on the measurements.

The linearity in total power mode should also be known. Therefore, the controllable noise source is also measured in total power mode. The steps are as follows:

1. A brief measurement of the controllable noise source with the coldest input (cold load with minimum attenuation) for calibration
2. A brief measurement of the controllable noise source so that the noise source is off and the maximum attenuation is selected (the chain works like a matched load) for calibration
3. Measurement of the controllable noise source (noise source turned on)

The steps are repeated four times. The idea is to increase and lower the noise temperature of the controllable noise source during every two measurement cycles i.e. 1 minute calibration (step 1 and 2), 30 minutes controllable noise source going up (step 3: 1 minute measurement at each attenuation), 1 minute calibration (step 1 and 2), 30 minutes controllable noise source going down (step 3: again 1 minute measurement at each step) etc. The ambient temperature is kept stable (within 0.2°C) at all times.

**3. Noise Injection Mode**

If the CNS had an effect on the measurement in the previous routine, this measurement will be repeated twice (CNS off and CNS on). In case there is no effect, only the measurement without the CNS is needed. This measurement routine is exactly the same as Routine 2, but now NIR is operated in the noise injection mode.

In the following measurements the CNS is kept off if it didn't have an effect on these two measurements. If the CNS did have an effect in the measurements, it is kept on in every routine if not otherwise instructed.

## 3.7 Measurement D: Correlation Coefficient

In this configuration different amount of noise is injected to the H- and V-channels with alternating phase difference (Figure 3-6). When both magnitude and phase of the received noise is known the correlation coefficient can be both measured and calculated.

*Table 3-5. Radiometer properties solve using Measurement Configuration D*

| | A | B | C | D | E | F | G |
|---|---|---|---|---|---|---|---|
| System Noise Temperature | | X | | | | | |
| Sensitivity | | X | | | X | | |
| Linearity | | | X | | | | |
| Polarimetric Properties | X | X | | X | | | X |
| Stability | | X | | | X | | |
| Calibration Accuracy | X | X | X | X | X | X | X |
| Absolute Accuracy | X | X | X | X | X | X | X |

The idea is to have the same amount of noise coming to both attenuators. If the attenuation is e.g. equal in the channels then both channels receive the same amount of noise yielding a well-defined correlation coefficient, assuming of course that also the phase difference is known (Section 4.4.6).

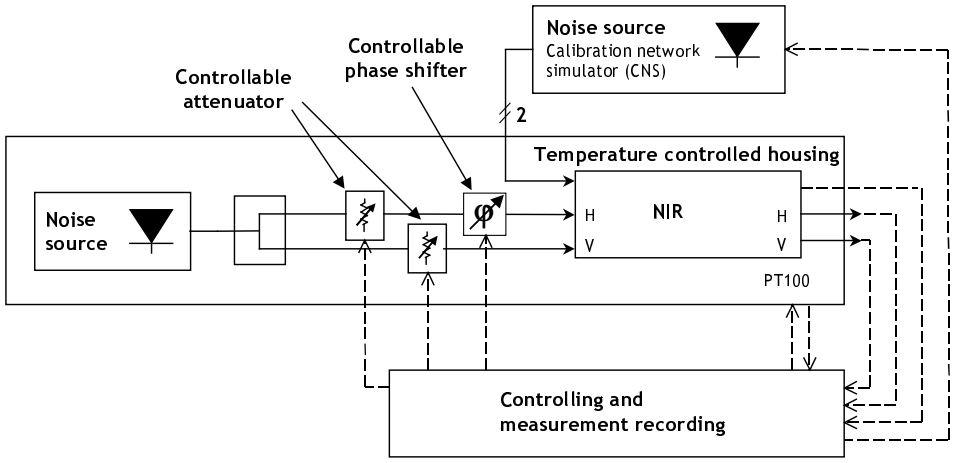


*Figure 3-6. Measurement Configuration D is used for solving the polarimetric properties of NIR. The polarimetric input is created using a noise source, controllable attenuator and a phase shifter. Arbitrary polarimetric input for the receivers can then be selected.*

The routes of the signal from the noise source to the NIR, with all the possible attenuations, will be measured using a VNA so that the accurate attenuation of the noise signal is known (see the first measurement routine). The data set produced is then used for analysis.

**Configuration**

The measurement configuration consists of the following parts (see Figure 3-5):

- NIR and the measurement chain in temperature controllable housing
- Noise source
- Two electronically controllable attenuators
- Electronically controllable phase shifter
- Power divider
- CNS
- Equipment to control the attenuators and to record the results i.e. NIR and test equipment data.

See Appendix D for selection of the components and devices. The configuration produces data including standard NIR data, NIR ambient temperature, attenuation of both attenuators and attenuator temperatures. Data handling and storing is considered in more detail in Section 3.2.

**1. VNA Measurement of the Connecting Network**

The connecting network has to be measured using a VNA in order to know the accurate attenuation for every attenuator state. The following measurement procedure is performed:

The VNA is connected to the input of the power divider and to the H- and V-channel output, in turn, of the connecting network. Full S-parameter measurement is performed with every possible attenuator state.

The temperature of the components is kept stable during the measurement (within 0.2°C) somewhere between 23°C and 26°C [9] e.g. using the NIR temperature controlled housing.

**2. Measurement of Correlation Coefficient in Both Modes**

First the correlation coefficient is examined in the total power mode. The measurement procedure consists of the following steps:

1. Measurement through minimum attenuation in both channels and zero phase shift
2. Minimum attenuation in H-channel and changing attenuation in V-channel
3. Measurement through minimum attenuation in both channels and zero phase shift
4. Minimum attenuation in V-channel and changing attenuation in H-channel
5. Measurement through minimum attenuation in both channels and zero phase shift
6. Minimum attenuation in both channels and changing phase in H-channel
7. Measurement through minimum attenuation in both channels and zero phase shift

At steps 2 and 4 the attenuation in the other channel is raised and lowered twice so that with each amount of attenuation the measurement time is 30 seconds with both modes i.e. 30 seconds total power mode, 30 seconds noise injection mode, change of attenuation, 30 seconds total power mode, 30 seconds noise injection mode, change of attenuation and so on. This means about four hours of measurement time.

At step 6 the phase in channel H is changed from 0 to 90 degrees and back twice in 5-degree steps, so that every step is measured 30 seconds time in both modes. This means a total measurement time of about one and half an hour.

For steps 1, 3, 5 and 7 the correlation is measured using three delays, namely $\tau$ = 0, $\tau$ = +T and $\tau$ = -T, for the fringe-washing function measurement. See Section 2.8.4 for details.

The ambient temperature of the measurement configuration is all the time kept stable (within 0.2°C) somewhere between 23°C and 26°C [9].

In the analysis phase the correlation coefficients measured in noise injection mode and in total power mode are compared (among other things) and the performance of the so-called blind correlation (Section 2.8.2) can be evaluated.

## 3.8 Measurement E: Antenna Loads

In this measurement configuration the radiometer is tested with the antenna attached. Two targets are needed for these measurements. They will be constructed from absorber material for 1.4 GHz and will have different physical temperatures (Appendix B).

*Table 3-6. Radiometer properties solved using Measurement Configuration E*

| | A | B | C | D | E | F | G |
|---|---|---|---|---|---|---|---|
| System Noise Temperature | | X | | | | | |
| Sensitivity | | X | | | X | | |
| Linearity | | | X | | | | |
| Polarimetric Properties | X | X | | X | | | X |
| Stability | | X | | | X | | |
| Calibration Accuracy | X | X | X | X | X | X | X |
| Absolute Accuracy | X | X | X | X | X | X | X |

It is difficult to perform the measurements of different targets at the same time like in the measurements with matched terminations. The targets have to be manually changed and, therefore, the continuous time of measurement is limited. The temperature-controlled housing should have a window for the NIR antenna, constructed e.g. from polyethylene-foam (Appendix D), so that the physical temperature of the NIR and its antenna can be controlled separately from the load.

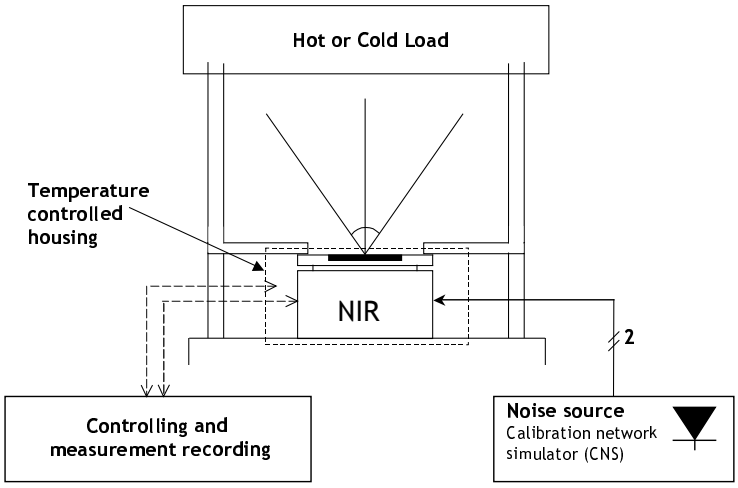


*Figure 3-7. Measurement configuration for measurements with antenna loads (see Appendix B). NIR has to be inside a temperature controllable housing that has a window for the antenna, since also the physical temperature of the antenna has to be changed.*

**Configuration**

The biggest problem with these measurements is the construction and analysis of the targets. This is very dependable on the type of targets used. The measurement analysis presented in Chapter 4 is based on the targets introduced in the Appendix B. The measurement configuration consists of the following items (Figure 3-7):

- NIR in temperature controllable housing
- Cold measurement target (absorber with liquid nitrogen), see Appendix B
- Hot measurement target (absorber in ambient temperature, temperature measured), see Appendix B
- CNS
- Equipment to record the results.

See Appendix D for selection of the components and devices. The configuration produces the following data: standard NIR data, NIR ambient temperature and temperature of the load (in the case of the hot load). Data handling and storing is considered in more detail in Section 3.2.

**1. Basic Measurement Routines With Hot Load**

The normal noise injection operation is used and the hot load is measured three times for three-hour periods. The ambient temperature of the NIR is kept stable i.e. within 0.2°C somewhere between 23°C and 26°C [9].

**2. Basic Measurement Routine With Cold Load**

The normal noise injection operation is used. The minimum temperature of the cold load is measured 10 times because of the uncertainties of the cold load. See

Appendix B for details about measurements of the cold load. The NIR ambient temperature is kept stable i.e. within 0.2°C somewhere between 23°C and 26°C.

**3. Measurement in Varying Ambient Temperature**

The normal noise injection operation is used and two kinds of measurements are performed:

First the ambient temperature is varied from 23°C to 26°C (this is the range of the predicted temperature for the final NIR [9]) in one-degree steps so that at every temperature the measurement time is about 10 minutes. The temperature is raised and lowered 2 times (i.e. 23-26-23-26-23). The point is that also the temperature of the antenna changes.

Second the ambient temperature is also changed between 5°C and 50°C in five-degree steps so that every step is measured 5 minutes. The temperature is raised and lowered 2 times (sequence defined as above).

## 3.9 Measurement F: Sky

Sky measurements are made to test the low brightness temperature response of the NIR in case a sky calibration method is needed. Table 3-7 below shows the properties of the NIR that concern this configuration.

*Table 3-7. Radiometer properties solved using Measurement Configuration F*

| | A | B | C | D | E | F | G |
|---|---|---|---|---|---|---|---|
| System Noise Temperature | | X | | | | | |
| Sensitivity | | X | | | X | | |
| Linearity | | | X | | | | |
| Polarimetric Properties | X | X | | X | | | X |
| Stability | | X | | | X | | |
| Calibration Accuracy | X | X | X | X | X | X | X |
| Absolute Accuracy | X | X | X | X | X | X | X |

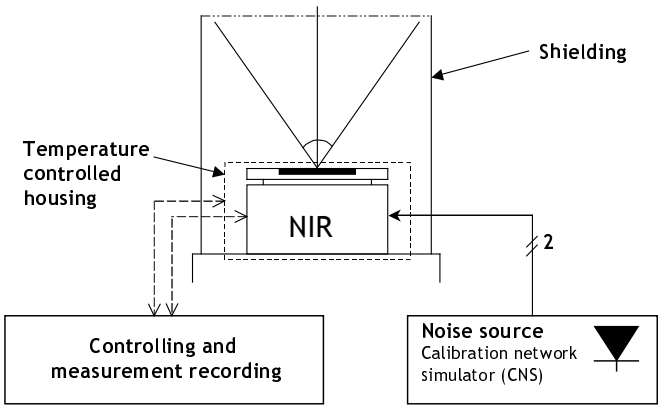


*Figure 3-8. Sky measurements are carried out by pointing the NIR straight to the sky and protecting it from the disturbances with a shielding structure. The total brightness temperature seen by NIR is about 6.5K [20].*

Clear sky conditions are required even though the operating frequency is only 1.4 GHz in order to have a well defined brightness temperature. The received radiation consists of 2.7K of the cosmic background and some radiation from astronomical sources, from the sun and from the atmosphere summing up as a brightness temperature of about 6.5K [20].

**Configuration**

The measurement will be done outdoors. The NIR is sealed inside a temperature-controlled housing. Same kind of housing as in the Measurement Configuration E can be used. Equipment needed for the sky measurements are the following:

- NIR in temperature controllable housing
- Calibration Network Simulator
- Power meter
- Equipment to record the results.

See Appendix D for selection of the components and devices. The configuration produces the following pieces of data: standard NIR data, ambient temperature of the NIR and noise power from the CNS. Data handling and storing is considered in more detail in section 3.2.

**Plain Sky Measurement**

Normal noise injection operation is used here and the measurement is carried out in the following steps:

Calibration with the hot and cold absorber load, measurement of the sky followed by another calibration.

The measurement is done four times. The absorber loads are used to verify the NIR operation. The NIR ambient temperature is kept stable (within 0.2°C) somewhere between 23°C and 26°C [9].

## 3.10 Measurement G: Polarimetric

In this configuration an active polarimetric load is measured through the antenna. The active load is a transmitter antenna, whose Stokes parameters are known and controllable (Figure 3-9). The measurements are to be carried out in an anechoic chamber.

*Table 3-8. Radiometer properties solved using Measurement Configuration G*

| | A | B | C | D | E | F | G |
|---|---|---|---|---|---|---|---|
| System Noise Temperature | | X | | | | | |
| Sensitivity | | X | | | X | | |
| Linearity | | | X | | | | |
| Polarimetric Properties | X | X | | X | | | X |
| Stability | | X | | | X | | |
| Calibration Accuracy | X | X | X | X | X | X | X |
| Absolute Accuracy | X | X | X | X | X | X | X |

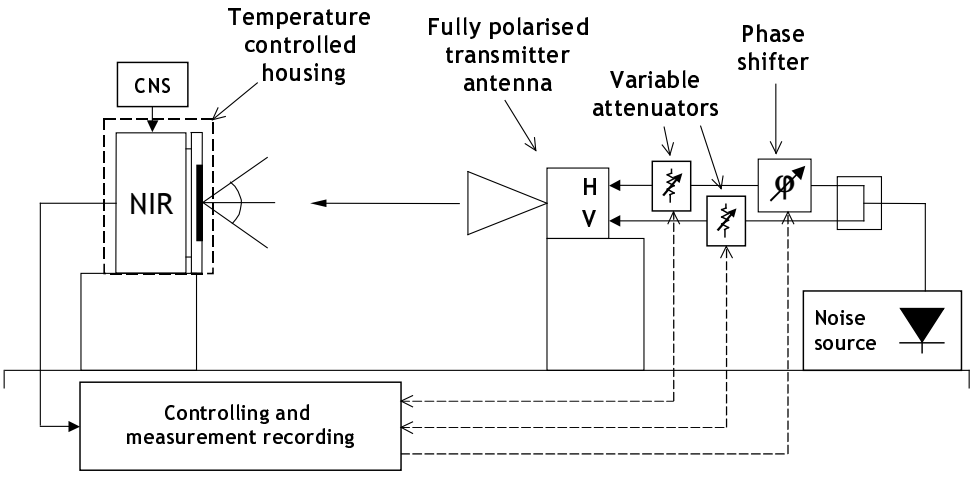


*Figure 3-9. Schematic diagram of the active load method for polarimetric measurements with the antenna. NIR is sealed inside a temperature controllable housing as in the antenna loads measurement. The polarisation state of the transmitter antenna can be arbitrarily selected.*

**Configuration**

The connection to the antenna is the same as the connection to the receivers in Measurement Configuration D (see Figure 3-6). If the same components and cables are used, the same VNA measurements as in Routine 1 in Measurement Configuration D can be used. The Stokes parameters and their uncertainties of the target, as seen by NIR, are analysed in Appendix C. The following equipment are needed for the measurements:

- NIR in temperature controllable housing
- CNS
- Equipment to record the results
- Fully polarised antenna
- Two electronically controllable attenuators
- Electronically controllable phase shifter
- Power divider
- Noise source.

See Appendix D for selection of the components and devices. Data produced by the configuration includes standard NIR data, NIR ambient temperature, attenuation of both attenuators and the attenuator temperatures. Data handling and storing is considered in more detail in Section 3.2.

**1. Third Stokes Parameter Measurement**

The idea of this routine is based on the fact that the measured third Stokes parameter depends only on the power of the horizontal and vertical polarisations, while phase difference is zero and thus fourth Stokes parameter is zero all the time. The normal noise-injection operation is used and the CNS is on all the time. The subsequent steps are followed:

1. The phase difference is set to 0 degrees and the attenuation in both channels are set as the same (1 minute)
2. The attenuation in the H-channel is increased to a certain level (15 minutes)
3. The attenuation in the V-channel is increased to the same level as in the H-channel (15 minutes)
4. Measurement of the same attenuation (1 minutes)

The measurement is repeated three times and the ambient temperature of the NIR is kept stable (within 0.2°C) somewhere between 23°C and 26°C.

**2. Fourth Stokes Parameter Measurement**

The idea of this routine is that the measured fourth Stokes parameter depends only on the power of the horizontal and vertical polarisations, while phase difference is 90 degrees and thus third Stokes parameter is zero all the time. The normal noise-injection operation is used and the CNS is on all the time. The subsequent steps are followed:

1. The attenuation in both channels are set as the same and the phase difference is set 90 degrees (1 minute)
2. The attenuation in the H-channel is increased to a certain level (15 minute)
3. The attenuation in the V-channel is increased to the same level as in the H-channel (15 minute)
4. Measurement of the same attenuation (1 minute)

The measurement is repeated three times and the ambient temperature of the NIR is kept stable (within 0.2°C) somewhere between 23°C and 26°C.

**3. Both Stokes Parameters Measurement**

The idea of this routine is to change all the energy from the third Stokes parameter to the fourth and back without changing the power levels of the horizontal and vertical polarisations. The normal noise-injection operation is used and the CNS is on all the time. The subsequent steps are followed:

1. The phase difference is set to 0 degrees and the attenuation in both channels are set as the same (1 minute)
2. The phase difference is increased to 90 degrees (15 minute)
3. The phase difference is decreased to 0 degrees (15 minute)
4. Measurement of the same attenuation and 0 degrees phase difference (1 minute)

The measurement is repeated three times and the ambient temperature of the NIR is kept stable (within 0.2°C) somewhere between 23°C and 26°C.

# 4 ANALYSIS

This chapter introduces the analyses of the measurements so that proper conclusions about the measurement results can be made and the correct operation of the NIR can be evaluated. Throughout the chapter the same table as in the previous chapter will be followed indicating which measurements concern a particular NIR property.

## 4.1 System Noise Temperature

An essential part of the tests is the determination of the NIR system noise temperature is. It has to be solved for both channels separately. Principles are introduced in 2.3. Routine 1 of the Measurement Configuration B provides the required data.

*Table 4-1. Measurements required for the determination of system noise temperature*

| | A | B | C | D | E | F | G |
|---|---|---|---|---|---|---|---|
| System Noise Temperature | | X | | | | | |
| Sensitivity | | X | | | X | | |
| Linearity | | | X | | | | |
| Polarimetric Properties | X | X | | X | | | X |
| Stability | | X | | | X | | |
| Calibration Accuracy | X | X | X | X | X | X | X |
| Absolute Accuracy | X | X | X | X | X | X | X |

### 4.1.1 Using Y-Factor Method

As introduced in Section 2.3 the receiver noise temperature can be solved using the so-called Y-factor method:

$$T_e = \frac{T_1 - YT_2}{Y - 1}, \tag{4-1}$$

where $T_1$ is the noise temperature of the hot load and $T_2$ is that of the cold load. However, in the connection of Measurement Configuration B the receiver is connected to the load through a switch and a power divider. The losses of the chain including the cables are to be measured with a vector network analyser for all the routes of the signal. The noise temperature of the chain reduced to its input can be determined as follows (e.g. [3]):

$$T_{chain}^{H/V,1/2} = \left(L_{chain}^{H/V,1/2} - 1\right) T_{chain}^{phys}, \tag{4-2}$$

where $T_{chain}^{H/V,1/2}$ is the noise temperature of the chain that goes through that channel of power divider that is connected to the horizontal or vertical channel of the NIR and through the switch in position 1 or 2; $L_{chain}^{H/V,1/2}$ is the attenuation of the connecting chain (sub- and superscripts as before) and $T_{chain}^{phys}$ is the physical temperature of the connecting chain.

The noise temperature for the whole system after the antenna connection ([3]) is defined as

$$T_e^{H/V,1/2} = T_{chain}^{H/V,1/2} + L_{chain}^{H/V,1/2} T_{rec}^{H/V}, \tag{4-3}$$

where $T_{rec}^{H/V}$ is the receiver noise temperature of the H- or V-channel and $L_{chain}^{H/V,1/2}$ is the measured total attenuation of the connecting chain. The Equation (2-21) can be written as

$$Y^{H/V} = \frac{T_1 + T_{chain}^{H/V,1} + L_{chain}^{H/V,1} T_{rec}^{H/V}}{T_2 + T_{chain}^{H/V,2} + L_{chain}^{H/V,2} T_{rec}^{H/V}}, \tag{4-4}$$

which yields

$$T_{rec}^{H/V} = \frac{T_1 - Y^{H/V} T_2 + T_{chain}^{H/V,1} - Y^{H/V} T_{chain}^{H/V,2}}{Y^{H/V} L_{chain}^{H/V,2} - L_{chain}^{H/V,1}}, \tag{4-5}$$

and when Equation (4-2) is applied, the formula for the receiver noise temperature is finally achieved:

$$T_{rec}^{H/V} = \frac{T_1 - Y^{H/V} T_2 + \left(L_{chain}^{H/V,1} - 1 - Y^{H/V}\left(L_{chain}^{H/V,2} + 1\right)\right) T_{chain}^{phys}}{Y^{H/V} L_{chain}^{H/V,2} - L_{chain}^{H/V,1}}. \tag{4-6}$$

**Uncertainty**

The uncertainty using the standard propagation of error (see Section 2.9) is determined for the system noise temperature as follows:

$$\begin{aligned}
\Delta T_{rec}^{H/V} = & \left(\frac{1}{Y^{H/V} L_{chain}^{H/V,2} - L_{chain}^{H/V,1}}\right)^2 \left(\left(\Delta T_1\right)^2 + \left(Y^{H/V} \Delta T_2\right)^2\right) \\
& + \left(\frac{L_{chain}^{H/V,1} - 1 - Y^{H/V}\left(L_{chain}^{H/V,2} + 1\right)}{Y^{H/V} L_{chain}^{H/V,2} - L_{chain}^{H/V,1}} \Delta T_{chain}^{phys}\right)^2 \\
& + \left(\left(\frac{\left(1 - Y^{H/V}\right) T_{chain}^{phys}}{Y^{H/V} L_{chain}^{H/V,2} - L_{chain}^{H/V,1}} - \frac{T_1 - YT_2 + \left(L_{chain}^{H/V,1} - 1 - Y^{H/V}\left(L_{chain}^{H/V,2} + 1\right)\right) T_{chain}^{phys}}{\left(Y^{H/V} L_{chain}^{H/V,2} - L_{chain}^{H/V,1}\right)^2} (Y - 1)\right) \Delta L_{chain}\right)^2 \\
& + \left(\left(\frac{-T_2 - \left(L_{chain}^{H/V,2} + 1\right) T_{chain}^{phys}}{Y^{H/V} L_{chain}^{H/V,2} - L_{chain}^{H/V,1}} - \frac{T_1 - YT_2 + \left(L_{chain}^{H/V,1} - 1 - Y^{H/V}\left(L_{chain}^{H/V,2} + 1\right)\right) T_{chain}^{phys}}{\left(Y^{H/V} L_{chain}^{H/V,2} - L_{chain}^{H/V,1}\right)^2} L_{chain}^{H/V,2}\right) \Delta Y\right)^2\Bigg]^{\frac{1}{2}}
\end{aligned} \tag{4-7}$$

where

$$\Delta Y = \sqrt{\left(\frac{1}{P_2}\Delta P_1\right)^2 + \left(\frac{P_1}{P_2^2}\Delta P_2\right)^2}\ ,\ \Delta P_1 = \Delta P_2 = \Delta P,$$
$$\Delta Y = \sqrt{\left(\frac{1+P_1^2}{P_2^2}\right)(\Delta P)^2} \qquad (4\text{-}8)$$

in which $\Delta P$ is the PMS uncertainty of the LICEF-receiver. Sample calculation of the receiver noise temperature uncertainty can be found in Appendix E.

### 4.1.2 Calculation of Receiver Noise Temperature

The calculation is performed using data produced by routine 1 of Measurement Configuration B (total power mode). That means that one pair of averaged power values will be produced for both channels every 40 seconds. The output of the PMS is used.

Measured powers are marked as $P_H[n]$ and $P_V[n]$ where H stands for the horizontal and V for vertical channel measured from LICEF output. The noise temperature of the hot load is marked as $T_1[n]$, which is measured and noise temperature of the cold load is marked as $T_2[n]$, which is determined as introduced in Appendix A. In this case $n$ is increased every 20 seconds. The quantities are averaged to the 20-second periods. The status of the switch will be used to determine whether the hot or cold load was measured.

The receiver noise temperature can now be determined by averaging system noise temperatures calculated every 40 seconds:

$$T_{rec}^{H/V}[i] = \frac{T_1[n] - Y^{H/V}[m]T_2[n+1] + \left(L_{chain}^{H/V,1} - 1 - Y^{H/V}[m]\left(L_{chain}^{H/V,2} + 1\right)\right)T_{chain}^{phys}[n]}{Y^{H/V}[m]L_{chain}^{H/V,2} - L_{chain}^{H/V,1}}, \qquad (4\text{-}9)$$

$$n=1,3,5,...N \quad \text{and} \quad m=(n+1)/2,$$

where $i$ increases by one for every $n$, $N$ is the amount of measurements of both loads altogether, $T_{amb}$ is the measured ambient temperature of the NIR and

$$Y^{H/V}[n] = \frac{P_1^{H/V}[n]}{P_2^{H/V}[n+1]}. \qquad (4\text{-}10)$$

Note that factor $Y$ is calculated only once per two measurement values of $P$ (namely $P_1$ and $P_2$) and thus in Equation (4-9) the index of $Y$ cannot be increased as the index of $T_1$ and $T_2$.

The final result for $T_{rec}$ is achieved by averaging the elements of $T_{rec}$ that are measured at the same temperature. The reliability of the determined receiver noise temperature, Equation (4-9), can be evaluated by calculating its standard deviation as introduced in Section 2.9, which can be interpreted as its confidence interval.

### 4.1.3 Measurement of System Noise Temperature Using Sensitivity

In the next section the sensitivity will be determined. It can also be used to determine the system noise temperature when the antenna target is known to stay constant. NIR has to be calibrated with a standard one-point calibration procedure as presented in Section 2.7.2. Based on the Equations (4-15) and (4-18) in the next section the following can be written:

$$\begin{aligned}\Delta T_{NI} &= \frac{2T_{sys}}{\sqrt{B\tau}} = \frac{2\left(T_{rec}+T_{ant}\right)}{\sqrt{B\tau}} = \frac{2\left(T_{rec}+T_{ref}\right)}{\sqrt{B\tau}} \\ &= \Delta T_{\sigma} = \sqrt{\frac{1}{N-1}\sum_{k=1}^{N}\left(T_k-\overline{T}\right)^2} = \sqrt{\frac{1}{N-1}\sum_{k=1}^{N}\left(T_k-T_{ref}\right)^2} = \Delta T_{\sigma}\end{aligned} \tag{4-11}$$

from which it can be seen that when the standard deviation of the radiometer output is known the receiver noise temperature can be solved as follows:

$$T_{rec} = \frac{1}{2}\left[\Delta T_{\sigma}\right]\sqrt{B\tau} - T_{ref}\ . \tag{4-12}$$

This way the receiver noise temperature can be calculated without the effect of the detector offset, which is a problem in the Y-factor method.

## 4.2 Sensitivity

In this section the solving of radiometric resolution of the first two Stokes parameters ($T_v$ and $T_h$) of the NIR is introduced. The sensitivity for the third and fourth Stokes parameter is handled later, since they are more complicated to measure and involve e.g. uncertainty of the correlation coefficients.

Two methods are here presented: a theoretical one, which is based on the system noise temperature determined in Section 4.1 and a practical one, which is based on the standard deviation of the NIR measurements.

*Table 4-2. Measurements required for the determination of sensitivity*

| | A | B | C | D | E | F | G |
|---|---|---|---|---|---|---|---|
| System Noise Temperature | | X | | | | | |
| Sensitivity | | X | | | X | | |
| Linearity | | | X | | | | |
| Polarimetric Properties | X | X | | X | | | X |
| Stability | | X | | | X | | |
| Calibration Accuracy | X | X | X | X | X | X | X |
| Absolute Accuracy | X | X | X | X | X | X | X |

As the table above indicates the results from the Measurement Configurations A and D are needed.

### 4.2.1 Theoretical Sensitivity

The system noise temperature is defined in Equation (2-18) where $T_{ant,max}$=296K at the maximum [9] and the value of $T_{rec}$ is determined in Section 4.1. Thus, the system noise temperature:

$$T_{sys} = T_{ant,max} + T_{rec}, \tag{4-13}$$

Now the sensitivity for the both channels of NIR can be determined in total power mode (Section 2.2.1):

$$\Delta T_{TP}^{H/V} = \frac{T_{ant,max} + T_{rec}}{\sqrt{B\tau}}, \tag{4-14}$$

and in noise-injection mode by replacing the antenna temperature with reference noise temperature (Section 2.2.3):

$$\Delta T_{NI}^{H/V} = \frac{2\left(T_{ref} + T_{rec}\right)}{\sqrt{B\tau}}. \tag{4-15}$$

**Uncertainty**

Uncertainty for the theoretical sensitivity is obtained with the standard propagation of error (Section 2.9.2) from Equation (4-14):

$$\begin{aligned}\Delta T_{TP}^{error} = \Bigg[ & \left(\frac{1}{\sqrt{B\tau}}\right)^2 \left( \left(\Delta T_{ant,\max}\right)^2 + \left(\Delta T_{rec}\right)^2 \right) \\ & + \left(\frac{\tau\left(T_{ant,\max} + T_{rec}\right)}{\left(B\tau\right)^{3/2}}\right)^2 \left(\Delta B\right)^2 + \left(\frac{B\left(T_{ant,\max} + T_{rec}\right)}{\left(B\tau\right)^{3/2}}\right)^2 \left(\Delta\tau\right)^2 \Bigg]^{1/2},\end{aligned} \tag{4-16}$$

where in the right-hand side Δ denotes the error of the variable. The uncertainty for the Dicke, or noise-injection, mode is clearly given by:

$$\Delta T_{NI}^{error} = 2\Delta T_{TP}^{error}, \tag{4-17}$$

when $T_{ant,max}$ is replaced by $T_{ref}$. Appendix E contains a sample calculation of the theoretical sensitivity uncertainty as a function of the receiver noise temperature uncertainty demonstrating the connection of their uncertainties.

### 4.2.2 Sensitivity Based on Measurements

The practical sensitivity is determined for both channels in two cases: when the matched load is attached and when the loads are seen through the antenna, because the antenna can have an increasing effect to the sensitivity. Additionally

both total power and noise-injection operation are used to determine the sensitivity of the receiver itself.

In practice, the sensitivity of a radiometer is the standard deviation of the measurement results of a stable target (see Section 2.4). When the target of a measurement is stable all the variations of the noise temperature in the output of a radiometer are due to the noise of the receiver itself (and, of course, to random variations of the noise-like signal of the target). This way the smallest observable change in a target can be determined.

$$\Delta T_\sigma = \sqrt{\frac{1}{N-1}\sum_{k=1}^{N}\left(T_k - \overline{T}\right)^2} \tag{4-18}$$

where $N$ is the amount of the samples, $T_k$ is one sample of brightness temperature and $\overline{T}$ is the average of the samples.

**Matched Load in Total Power Mode**

Data from Measurement Configuration B Routine 1 is used. The calibration coefficients are calculated from every hot-cold measurement pair by averaging and from standard deviations of the single calibrated measurements the sensitivity is determined.

In total power mode NIR has to be calibrated as presented in Section 2.7. NIR sees the calibration loads $T_1$ and $T_2$ as

$$\begin{aligned} T_1' &= \left(1 - \frac{1}{L_{chain,therm}^{H/V,1}}\right) T_{chain}^{phys} + \frac{T_1}{L_{chain}^{H/V,1}} \\ T_2' &= \left(1 - \frac{1}{L_{chain,therm}^{H/V,2}}\right) T_{chain}^{phys} + \frac{T_2}{L_{chain}^{H/V,2}} \end{aligned} \tag{4-19}$$

where $L_{chain}^{H/V,1/2}$ is the attenuation of the chain connecting the load (1 or 2) to the receiver (H or V) and $L_{chain,therm}^{H/V,1/2}$ is the attenuation causing the additional thermal noise.

Now the brightness temperature of a measurement $P_x$ can be written as (Section 2.7):

$$T_x = AP_x + B, \tag{4-20}$$

where $A$ and $B$ are the calibration coefficients. This way the brightness temperatures are retrieved from the data produced by the total power mode of NIR.

Routine 1 of Measurement Configuration B measures 20 seconds hot load then 20 seconds cold load then again hot and so on. The data is handled in steps and on

every step calibration coefficient is calculated by averaging the hot and cold load measurements (every 40 seconds). Then every single measurement is transferred to the brightness temperatures, Equation (4-20). Notice that in this process the switch and power divider do not cause any extra work since they are calibrated out.

When the data is converted to the brightness temperatures the standard deviation is calculated from the hot and cold measurements separately. The physical temperature deviations of the hot load from its average can be compensated by changing the measured brightness temperature the amount of the deviation in the temperature of the hot load. This can be done since the brightness temperature emitted by a matched load is the same as its physical temperature.

**Matched Load in Noise-injection Mode**

In the noise-injection mode NIR needs only one reference load and no cold load is needed (Section 2.7.2). Only the knowledge of the temperature of the measured load has to be known. Thus results from Measurement Configuration B Routine 5 are used.

As above the variations of the physical temperature of the matched load can be compensated by changing the measured brightness temperatures the same amount, if the changes are in order of some degrees.

**Antenna Load in Noise-injection Mode**

The sensitivity is also determined when the measurement is made through the antenna looking to the absorber load in room temperature. Of course the cold load could be used but that would be more complicated. The brightness temperature of the target has to be accurately known (see Appendix B) and also this time its variations can be compensated in the measured data. Data from Measurement Configuration E Routine 1 is used.

**Uncertainty of Practical Sensitivity**

From Equation (4-18) it can be seen that uncertainty of the practical sensitivity is the same as is the overall measurement uncertainty of the NIR determined in Section 4.7.

## 4.3 Linearity

The behaviour of NIR detection is supposed to be linear. However, the detector is not ideal and thus the uncertainty caused by its nonlinearity must be tested. Data from the Measurement Configuration C is utilised. Linearity is determined for both the total power mode and the noise-injection mode.

*Table 4-3. Measurements required for the determination of linearity*

| | A | B | C | D | E | F | G |
|---|---|---|---|---|---|---|---|
| System Noise Temperature | | X | | | | | |
| Sensitivity | | X | | | X | | |
| Linearity | | | X | | | | |
| Polarimetric Properties | X | X | | X | | | X |
| Stability | | X | | | X | | |
| Calibration Accuracy | X | X | X | X | X | X | X |
| Absolute Accuracy | X | X | X | X | X | X | X |

First the controllable noise source is investigated and then the measurement analysis is performed.

### 4.3.1 Controllable Noise Source

The controllable noise source is based on the stable noise source and a digitally controlled attenuator. The attenuation of the attenuator has to be measured in its every position. Also every route the signal goes in the connecting network (switch, attenuator, power divider) has to be measured. That yields a variable $L(x_{sw})_{change}^{H/V,1/2}$, where H/V indicates which route of the power divider is used, 1/2 indicates which switch position is used and $x_{sw}$ tells how much attenuation is selected. Additionally $L(x_{sw})_{change,therm}^{H/V,1/2}$ is determined, from which the division of the power divider is reduced in order to find out the attenuation causing thermal noise. Now the noise temperature seen by the NIR can be calculated from the following

$$T_{in,calc} = \left(1 - \frac{1}{L(x_{sw})_{change,therm}^{H/V,1/2}}\right) T_{change}^{phys} + \frac{T_{load}}{L(x_{sw})_{change}^{H/V,1/2}} \tag{4-21}$$

where $T_{load}$ is the noise temperature of the noise source ($T_{noise}$) or the cold load ($T_{cold}$) and $T_{change}^{phys}$ is the physical temperature of the controllable noise source connecting network, which is supposed to be the same as the ambient temperature of NIR. Thus the incoming power can be determined and the response of the radiometer can be analysed. The output of the controllable noise source is simulated in Appendix E.

### 4.3.2 Analysis of Measurement of Controllable Noise Source

In this Section is presented how the linearity is retrieved from the data of the Measurement Configuration C.

**Total Power Mode**

First the configuration is calibrated. A well-defined hot target is realised by turning the noise source off (seen as matched load) and by adjusting the maximum attenuation to the digital attenuator. Now the chain works like a matched load with the noise temperature equal to its physical temperature. For a well-defined cold load the attenuation is turned to minimum and the switch is turned to the cold

load. With these measurements the calibration line and calibration coefficients (see Section 2.7) are determined.

The noise temperature for the hot load, when noise is off, is practically the same as the physical temperature of the chain when the maximum attenuation is selected:

$$T_{in,calc}^{hot} \approx T_{change}^{phys} \tag{4-22}$$

and for the cold load the noise temperature seen by the receiver is:

$$T_{in,calc}^{cold} = \left(1 - \frac{1}{L(1)_{change,therm}^{H/V,2}}\right) T_{change}^{phys} + \frac{T_{cold}}{L(1)_{change}^{H/V,2}}, \tag{4-23}$$

where $L(1)_{change}^{H/V,2}$ and $L(1)_{change,therm}^{H/V,2}$ are the attenuations of the connecting chain when the switch is turned to the cold load and the attenuation is at minimum. For the measured power $P_{detect}$ (PMS measurement) the calibration line, of the noise temperature, can be written as

$$T_{in,meas} = AP_{detect} + B \tag{4-24}$$

where the calibration coefficients $A$ and $B$ are

$$A = \frac{P^{hot} - P^{cold}}{T_{in,calc}^{hot} - T_{in,calc}^{cold}} = \frac{P^{hot} - P^{cold}}{\frac{T_{change}^{phys}}{L(1)_{change,therm}^{H/V,2}} - \frac{T_{cold}}{L(1)_{change}^{H/V,2}}} \tag{4-25}$$

$$\begin{aligned} B &= \frac{P^{cold} T_{in,calc}^{hot} - P^{hot} T_{in,calc}^{cold}}{T_{in,calc}^{hot} - T_{in,calc}^{cold}} \\ &= \frac{P^{cold} T_{change}^{phys} - \left(1 - \frac{1}{L(1)_{change,therm}^{H/V,2}}\right) T_{change}^{phys} P^{hot} - \frac{T_{cold} P^{hot}}{L(1)_{change}^{H/V,2}}}{\frac{T_{change}^{phys}}{L(1)_{change,therm}^{H/V,2}} - \frac{T_{cold}}{L(1)_{change}^{H/V,2}}} \end{aligned} \tag{4-26}$$

where the $P^{hot}$ and $P^{cold}$ are responses of the NIR in total power mode (PMS signal) during hot and cold load measurements respectively.

The final $A$ and $B$ are retrieved from the average of the begin and end calibrations, since the change in response of the receiver is assumed to be linear. They could also be calculated as a function of time but this is not needed when the measurement time is short.

Now, when $T_{in}$ is changed with the attenuator the detected power $P_{detect}$ changes. Because $T_{in}$ can be both calculated (Equation (4-21)) and measured (Equation (4-24)) the linearity can be determined from the deviation of these two.

So, when the $P_{detect}$ is measured as a function of the attenuation of the digital attenuator (in practice, this means that the attenuator position is saved with the power measurement data), the following can be retrieved:

$$\begin{aligned}\Delta T_{lin} &= T_{in,meas} - T_{in,calc} \\ &= AP_{detect} - B - \left(1 - \frac{1}{L(x_{sw})^{H/V,1/2}_{change,therm}}\right) T^{phys}_{change} - \frac{T_{load}}{L(x_{sw})^{H/V,1/2}_{change}}\end{aligned} \tag{4-25}$$

**Uncertainty for Total Power Mode**

The uncertainties have been calculated using the standard propagation of errors (see Section 2.9). For the linearity calculation:

$$\Delta T^{error}_{lin} = \sqrt{\left(\Delta T_{in,meas}\right)^2 + \left(\Delta T_{in,calc}\right)^2}\,, \tag{4-26}$$

in which the uncertainty for the measured brightness temperature is as follows:

$$\Delta T_{in,meas} = \sqrt{A^2(\Delta P)^2 + P^2(\Delta A)^2 + \left(\Delta B^2\right)}, \tag{4-27}$$

where $\Delta P$ is the estimated uncertainty of the detection. Notice that this produces a bit of a dilemma here since the error of detection is in fact the property we are trying to find out. However giving the $\Delta P$ the PMS measurement error here enables the possibility to investigate the *linearity* of the detection.

The uncertainty for the calculated incoming brightness temperature using again the standard propagation of errors (see Section 2.9) is:

$$\begin{aligned}\Delta T_{in,calc} = \Bigg[&\left(1 + \frac{1}{L(x_{sw})^{H/V,1/2}_{change,therm}}\right)^2 \left(\Delta T^{phys}_{change}\right)^2 + \left(\frac{1}{L(x_{sw})^{H/V,1/2}_{change}}\right)^2 \left(\Delta T_{load}\right)^2 \\ &+ \left(\frac{T^{phys}_{change}}{\left(L(x_{sw})^{H/V,1/2}_{change,therm}\right)^2} - \frac{T_{load}}{\left(L(x_{sw})^{H/V,1/2}_{change}\right)^2}\right)^2 \left(\Delta L_{change}\right)^2\Bigg]^{\frac{1}{2}},\end{aligned} \tag{4-28}$$

where $\Delta T_{load}$ is the uncertainty of the noise source ($\Delta T_{noise}$) or that of the cold load ($\Delta T_{cold}$) and $\Delta L_{change}$ is the uncertainty of the attenuation of the controllable noise source. The uncertainty of the controllable noise source output is simulated in Appendix E. The uncertainties of the calibration positions are:

$$\Delta T^{hot}_{in,calc} = \Delta T^{phys}_{change} \tag{4-29}$$

$$\Delta T_{in,calc}^{cold} = \left[ \left( 1 + \frac{1}{L(1)_{change,therm}^{H/V,2}} \right)^2 \left( \Delta T_{change}^{phys} \right)^2 + \left( \frac{1}{L(1)_{change}^{H/V,2}} \right)^2 \left( \Delta T_{cold} \right)^2 + \left( \frac{T_{change}^{phys}}{\left( L(1)_{change,therm}^{H/V,2} \right)^2} - \frac{T_{cold}}{\left( L(1)_{change}^{H/V,2} \right)^2} \right)^2 \left( \Delta L_{change} \right)^2 \right]^{\frac{1}{2}} \quad (4\text{-}30)$$

The uncertainties for parameters A and B can be written as follows since $\Delta P^{hot}=\Delta P^{cold}=\Delta P$:

$$\Delta A = \left[ \left( \frac{2}{T_{in,calc}^{hot} - T_{in,calc}^{cold}} \right)^2 \Delta P^2 + \left( \frac{P^{hot} - P^{cold}}{\left( T_{in,calc}^{hot} - T_{in,calc}^{cold} \right)^2} \right)^2 \left( \Delta T_{in,calc}^{hot} \right)^2 + \left( \frac{P^{hot} - P^{cold}}{\left( T_{in,calc}^{hot} - T_{in,calc}^{cold} \right)^2} \right) \left( \Delta T_{in,calc}^{cold} \right)^2 \right]^{1/2} \quad (4\text{-}31)$$

$$\Delta B = \left[ \left( \left( \frac{T_{in,calc}^{hot} - P^{hot} T_{in,calc}^{cold}}{T_{in,calc}^{hot} - T_{in,calc}^{cold}} \right)^2 + \left( \frac{P^{cold} T_{in,calc}^{hot} - T_{in,calc}^{cold}}{T_{in,calc}^{hot} - T_{in,calc}^{cold}} \right)^2 \right) (\Delta P)^2 + \left( \frac{P^{cold} - P^{hot} T_{in,calc}^{cold}}{T_{in,calc}^{hot} - T_{in,calc}^{cold}} + \frac{P^{cold} T_{in,calc}^{hot} - P^{hot} T_{in,calc}^{cold}}{\left( T_{in,calc}^{hot} - T_{in,calc}^{cold} \right)^2} \right)^2 \left( \Delta T_{in,calc}^{hot} \right)^2 + \left( \frac{P^{cold} T_{in,calc}^{hot} - P^{hot}}{T_{in,calc}^{hot} - T_{in,calc}^{cold}} + \frac{P^{cold} T_{in,calc}^{hot} - P^{hot} T_{in,calc}^{cold}}{\left( T_{in,calc}^{hot} - T_{in,calc}^{cold} \right)^2} \right)^2 \left( \Delta T_{in,calc}^{cold} \right)^2 \right]^{1/2} \quad (4\text{-}32)$$

**Noise-injection Mode**

In the noise-injection mode the determination of the linearity is very similar to that in the case of the total power mode. Two-point calibration is used in order to retrieve the line for comparison. The $P_{detect}$ is now got from the NIR output, obviously, and not from PMS.

# 4.4 Polarimetric Properties

The polarimetric properties of the NIR are solved using VNA measurement (Measurement Configuration A), correlation measurements (Measurement Configuration D) and polarimetric measurements (Measurement Configuration G). 3-delay method measurements for the fringe-washing factor are done in Measurement Configuration B.

*Table 4-4. Measurements required for the determination of polarimetric properties*

| | A | B | C | D | E | F | G |
|---|---|---|---|---|---|---|---|
| System Noise Temperature | | X | | | | | |
| Sensitivity | | X | | | X | | |
| Linearity | | | X | | | | |
| Polarimetric Properties | X | X | | X | | | X |
| Stability | | X | | | X | | |
| Calibration Accuracy | X | X | X | X | X | X | X |
| Absolute Accuracy | X | X | X | X | X | X | X |

### 4.4.1 Noise Temperatures in Measurement Configuration D

In Measurement Configuration D the receivers see the noise source through attenuators and power divider. Additionally in the connecting network of channel H there is a phase shifter. All the signal paths are measured with a VNA as introduced in Measurement Routine D/1 and the attenuations of the paths form variables $L_{chain}^{H/V}(x_{att})$ and $L_{chain,therm}^{H/V}(x_{att})$ for attenuation, where $x_{att}$ is the attenuator position of the channel in question (H/V) and $\varphi(x_{ph})$ for phase difference of the inputs, where $x_{ph}$ is the phase shifter position. Hence the noise temperatures seen by the receivers can be written as:

$$T_{in}^{H/V} = \left(1 - \frac{1}{L_{chain,therm}^{H/V}(x_{att})}\right) T_{chain}^{phys} + \frac{T_{noise}}{L_{chain}^{H/V}(x_{att})}, \tag{4-33}$$

where $T_{noise}$ is the noise temperature of the noise source and $T_{chain}^{phys}$ is the physical temperature of the connecting network.

### 4.4.2 Frequency and Phase Responses and Bandwidths

The frequency and phase responses and bandwidths of the receivers are measured in Measurement Configuration A, resulting the functions $H_H(f)$ and $H_V(f)$ for the frequency responses of the H and V receiver, respectively; $\phi_{Hi}(f)$, $\phi_{Hq}(f)$, $\phi_{Vi}(f)$ and $\phi_{Vq}(f)$ for the phase responses of the H and V receiver, respectively and $B_H$ and $B_V$ for the bandwidths of the H and V receivers, respectively.

Using these functions the in-phase and quadrature errors can be straightforwardly calculated and the fringe-washing function can be determined as introduced in Section 2.8.3. In-phase errors are retrieved from:

$$\begin{aligned} \theta_i^{inph} &= \phi_{Vi}(f) - \phi_{Hi}(f) \\ \theta_q^{inph} &= \phi_{Vq}(f) - \phi_{Hq}(f) \end{aligned}, \tag{4-34}$$

and quadrature errors form:

$$\begin{aligned} \theta_H^{quad} &= 90° - \left[\phi_{Hi}(f) - \phi_{Hq}(f)\right] \\ \theta_V^{quad} &= 90° - \left[\phi_{Vi}(f) - \phi_{Vq}(f)\right] \end{aligned}. \tag{4-35}$$

For the fringe-washing function calculation the normalised frequency responses are needed. For H-channel it is determined as follows:

$$H_{n,H}(f) = \frac{H_H(f)}{\max(H_H)} \tag{4-36}$$

and analogously for V-channel.

### 4.4.3 In-phase and Quadrature Error Measurement

In-phase errors can be calculated from the phase responses of the receivers, as told in the previous paragraph, but they can also be measured with correlator along with quadrature errors. Quadrature errors of the H and V channels are (see Section 2.8.5)

$$\begin{aligned} \theta_V^{quad} &= -\sin^{-1}(\mu_{ViVq}) \\ \theta_H^{quad} &= -\sin^{-1}(\mu_{HiHq}) \end{aligned} \tag{4-37}$$

where $\mu_{ViVq}$ and $\mu_{HiHq}$ is the correlation between I- and Q-output of V- and H-channel, respectively. Correlator works so that it calculates these correlations all the time as default. Data from e.g. Measurement Configuration D can be used.

The in-phase errors can be reduced from the phase of the complex correlation as follows (this is the method proposed in calibration procedure introduced in Section 2.8.5):

$$\begin{bmatrix} \mu_{HiVi} \\ \mu_{HqVi} \end{bmatrix}_{new} = \mathbf{Q}^{-1} \begin{bmatrix} \mu_{HiVi} \\ \mu_{HqVi} \end{bmatrix}_{old} \quad \text{and} \quad \begin{bmatrix} \mu_{HqVq} \\ \mu_{HiVq} \end{bmatrix}_{new} = \mathbf{Q}^{-1} \begin{bmatrix} \mu_{HqVq} \\ \mu_{HiVq} \end{bmatrix}_{old}, \tag{4-38}$$

where

$$\mathbf{Q}^{-1} = \frac{1}{\cos(\theta_V^{quad})} \begin{bmatrix} \cos\left(\frac{1}{2}\theta_H^{quad} + \frac{1}{2}\theta_V^{quad}\right) & -\sin\left(\frac{1}{2}\theta_H^{quad} - \frac{1}{2}\theta_V^{quad}\right) \\ \sin\left(\frac{1}{2}\theta_H^{quad} + \frac{1}{2}\theta_V^{quad}\right) & \cos\left(\frac{1}{2}\theta_H^{quad} - \frac{1}{2}\theta_V^{quad}\right) \end{bmatrix} \tag{4-39}$$

since

$$\mathbf{Q} = \begin{bmatrix} \cos\left(\frac{1}{2}\theta_H^{quad} - \frac{1}{2}\theta_V^{quad}\right) & \sin\left(\frac{1}{2}\theta_H^{quad} - \frac{1}{2}\theta_V^{quad}\right) \\ -\sin\left(\frac{1}{2}\theta_H^{quad} + \frac{1}{2}\theta_V^{quad}\right) & \cos\left(\frac{1}{2}\theta_H^{quad} + \frac{1}{2}\theta_V^{quad}\right) \end{bmatrix} \tag{4-40}$$

and

$$\det(\mathbf{Q}) = \left| \cos\left(\frac{1}{2}\theta_H^{quad} - \frac{1}{2}\theta_V^{quad}\right)\cos\left(\frac{1}{2}\theta_H^{quad} + \frac{1}{2}\theta_V^{quad}\right) + \sin\left(\frac{1}{2}\theta_H^{quad} - \frac{1}{2}\theta_V^{quad}\right)\sin\left(\frac{1}{2}\theta_H^{quad} + \frac{1}{2}\theta_V^{quad}\right)\right| \quad (4\text{-}41)$$
$$= \cos\left(\frac{1}{2}\theta_H^{quad} + \frac{1}{2}\theta_V^{quad} - \frac{1}{2}\theta_H^{quad} + \frac{1}{2}\theta_V^{quad}\right) = \cos\left(\theta_V^{quad}\right).$$

Now we can apply $\theta_H^{quad}$ and $\theta_V^{quad}$ from Equation (4-35) or Equation (4-37) to the Equation (4-39) and so compare the resulted correlation coefficients.

### 4.4.4 Fringe-Washing Function

The fringe-washing function can be calculated as described in Sections 2.8.3 and 4.4.2 or it can be measured with the so-called 3-delay method introduced in Section 2.8.4. Measurements required for carrying out the 3-delay method are performed in Measurement Configuration D.

First the three values for fringe-washing factor are calculated from the correlation measurements with three different delays, as described in Measurement Configuration D, using Equation (2-53). Then coefficients *A*, *B* and *C* of Equation (2-54) are solved numerically in order to get an approximation for the amplitude of the fringe-washing function. Then the linear system of the Equation (2-56) is solved to get an approximation for the phase of the fringe-washing function, introduced in Equation (2-55).

### 4.4.5 Modulus Terms

With the Measurement Configuration D the modulus terms $\tilde{g}$ for TP-mode and $\tilde{g}_2$, $\tilde{g}_3$ and $\tilde{g}_4$ for NI-mode can be calculated using the measured correlation coefficient and simulating the ideal correlation coefficient (e.g. Equation (2-35)), or using the radiometer properties and known loads, when the fringe-washing function $g_{FW}$ is known (e.g. Equation (2-36)). With a known load the correlation coefficient can be known and thus the modulus terms can be verified.

**Total Power Mode**

The modulus term for the TP-mode can be determined straight from its definition, introduced in Equation (2-36), or by measuring correlation coefficient from the loads, whose ideal correlation coefficient can be calculated (Measurement Configuration D). Derived from Equation (2-35):

$$\tilde{g}_{meas} = \frac{\mu_{TP}}{\mu_0}, \quad (4\text{-}42)$$

where $\mu_{TP}$ is the measured correlation coefficient in TP-mode and $\mu_0$ is the calculated correlation coefficient. The noise is created in one source and is then

divided into the both channels, thus when the noise temperatures coming to the detectors and their phase difference are known, the ideal correlation coefficient can be calculated e.g. by simulation.

The difference of the modulus terms determined using (1) the measured correlations and (2) the measured receiver properties the following:

$$\tilde{g}_{diff} = \tilde{g}_{meas} - \tilde{g} = \frac{\mu}{\mu_0(T_{ant})} - \tilde{g}(T_{ant}, T_{rec}, g_{FW}), \tag{4-43}$$

Obviously $\tilde{g}_{diff}$ should be zero within the uncertainties of $\tilde{g}_{meas}$ and $\tilde{g}$. The determination of the uncertainty of the simulated correlation coefficient has to be done statistically by repeating the simulation several times and the uncertainty of the measured correlation coefficient is considered in Section 4.4.6.

The uncertainty for the modulus term of TP-mode (Equation (2-36)) using the standard propagation of error (Section 2.9.2) is:

$$\begin{aligned}
\Delta\tilde{g} = \Bigg( & \frac{T_{Vant}T_{Hant}}{(T_{Vant}+T_{Vrec})(T_{Hant}+T_{Hrec})}(\Delta g_{FW})^2 \\
& + \left( \frac{g_{FW}\sqrt{T_{Vant}T_{Hant}}}{2(T_{Vant}+T_{Vrec})^{3/2}\sqrt{T_{Hant}+T_{Hrec}}} \right)^2 (\Delta T_{Vrec})^2 \\
& + \left( \frac{g_{FW}\sqrt{T_{Vant}T_{Hant}}}{2\sqrt{T_{Vant}+T_{Vrec}}(T_{Hant}+T_{Hrec})^{3/2}} \right)^2 (\Delta T_{Hrec})^2 \\
& + \left( \frac{\sqrt{T_{Hant}}}{2\sqrt{(T_{Vant}+T_{Vrec})(T_{Hant}+T_{Hrec})}} \left( \frac{1}{\sqrt{T_{Vant}}} - \frac{\sqrt{T_{Vant}}}{(T_{Vant}+T_{Vrec})} \right) \right)^2 (\Delta T_{Vant})^2 \\
& + \left( \frac{\sqrt{T_{Vant}}}{2\sqrt{(T_{Vant}+T_{Vrec})(T_{Hant}+T_{Hrec})}} \left( \frac{1}{\sqrt{T_{Hant}}} - \frac{\sqrt{T_{Hant}}}{(T_{Hant}+T_{Hrec})} \right) \right)^2 (\Delta T_{Hant})^2 \Bigg)^{\frac{1}{2}}.
\end{aligned} \tag{4-44}$$

For the measured modulus term the uncertainty is:

$$\Delta\tilde{g}_{meas} = \sqrt{\left( \frac{1}{\mu_0}\Delta\mu_{TP} \right)^2 + \left( \frac{\mu_{TP}}{\mu_0^2}\Delta\mu_0 \right)^2}. \tag{4-45}$$

See Section 4.4.6 for the uncertainty of correlation coefficient $\Delta\mu_{TP}$.

**Noise-injection Mode**

The evaluation of the three modulus terms of the blind correlation mode of the noise-injection mode is much more complicated issue than that of the TP-mode

since the relation between ideal and measured correlation coefficient is more complex.

Solving the relation of the correlation coefficients from the approximation Equation (4-56) yields:

$$\tilde{g}_2 N_2 + \tilde{g}_3 N_3 + \tilde{g}_4 N_4 = \frac{\mu_B}{\mu_{0,appr}} N \,, \tag{4-46}$$

where $\mu_B$ is in blind mode measured correlation coefficient and $\mu_{0,appr}$ is the simulated ideal correlation coefficient (see Section 4.4.6). The number of samples $N$ and number of samples used at each step of the noise-injection procedure $N_2$, $N_3$ and $N_4$ are known. The right side can now be calculated and its correspondence to the separately calculated modulus terms can be evaluated.

The uncertainties for the calculated modulus terms of the noise-injection mode, introduced in Equations (2-41) - (2-43) when the noise injection is longer in the V-channel, using the standard propagation of error (Section 2.9.2) are:

$$\begin{aligned}
\Delta\tilde{g}_2 = \Bigg( & \frac{T_{Vant} T_{Hant}}{(T_{Vant} + T_{Vrec} + T_{VN})(T_{Hant} + T_{Hrec} + T_{HN})} \Delta g_{FW}{}^2 \\
& + \left( \frac{g_{FW} \sqrt{T_{Vant} T_{Hant}}}{2(T_{Vant} + T_{Vrec} + T_{VN})^{3/2} \sqrt{T_{Hant} + T_{Hrec} + T_{HN}}} \right)^2 \left( \Delta T_{Vrec}{}^2 + \Delta T_{VN}{}^2 \right) \\
& + \left( \frac{g_{FW} \sqrt{T_{Vant} T_{Hant}}}{2\sqrt{T_{Vant} + T_{Vrec} + T_{VN}} (T_{Hant} + T_{Hrec} + T_{HN})^{3/2}} \right)^2 \left( \Delta T_{Hrec}{}^2 + \Delta T_{HN}{}^2 \right) \\
& + \left( \frac{\sqrt{T_{Hant}}}{2\sqrt{(T_{Vant} + T_{Vrec} + T_{VN})(T_{Hant} + T_{Hrec} + T_{HN})}} \left( \frac{1}{\sqrt{T_{Vant}}} - \frac{\sqrt{T_{Vant}}}{(T_{Vant} + T_{Vrec} + T_{VN})} \right) \right)^2 \Delta T_{Vant}{}^2 \\
& + \left( \frac{\sqrt{T_{Vant}}}{2\sqrt{(T_{Vant} + T_{Vrec} + T_{VN})(T_{Hant} + T_{Hrec} + T_{HN})}} \left( \frac{1}{\sqrt{T_{Hant}}} - \frac{\sqrt{T_{Hant}}}{(T_{Hant} + T_{Hrec} + T_{HN})} \right) \right)^2 \Delta T_{Hant}{}^2 \Bigg)^{\frac{1}{2}}
\end{aligned} \tag{4-47}$$

$$\Delta\tilde{g}_3 = \left( \frac{T_{Vant} T_{Hant}}{(T_{Vant} + T_{Vrec} + T_{VN})(T_{Hant} + T_{Hrec})} \Delta g_{FW}{}^2 \right.$$
$$+ \left( \frac{g_{FW} \sqrt{T_{Vant} T_{Hant}}}{2(T_{Vant} + T_{Vrec} + T_{VN})^{3/2} \sqrt{T_{Hant} + T_{Hrec}}} \right)^2 \left( \Delta T_{Vrec}{}^2 + \Delta T_{VN}{}^2 \right)$$
$$+ \left( \frac{g_{FW} \sqrt{T_{Vant} T_{Hant}}}{2\sqrt{T_{Vant} + T_{Vrec} + T_{VN}} (T_{Hant} + T_{Hrec})^{3/2}} \right)^2 \Delta T_{Hrec}{}^2 \qquad (4\text{-}48)$$
$$+ \left( \frac{\sqrt{T_{Hant}}}{2\sqrt{(T_{Vant} + T_{Vrec} + T_{VN})(T_{Hant} + T_{Hrec})}} \left( \frac{1}{\sqrt{T_{Vant}}} - \frac{\sqrt{T_{Vant}}}{(T_{Vant} + T_{Vrec} + T_{VN})} \right) \right)^2 \Delta T_{Vant}{}^2$$
$$\left. + \left( \frac{\sqrt{T_{Vant}}}{2\sqrt{(T_{Vant} + T_{Vrec} + T_{VN})(T_{Hant} + T_{Hrec})}} \left( \frac{1}{\sqrt{T_{Hant}}} - \frac{\sqrt{T_{Hant}}}{(T_{Hant} + T_{Hrec})} \right) \right)^2 \Delta T_{Hant}{}^2 \right)^{\frac{1}{2}}$$

and

$$\Delta\tilde{g}_4 = \Delta\tilde{g}\,, \qquad (4\text{-}49)$$

since the subscript 4 denotes the noise injection phase in which the noise is injected to neither of the channels. If the noise injection is longer in the H-channel the determination of the uncertainties is analogous. The uncertainties of the modulus terms are simulated in Appendix E.

### 4.4.6 Correlation Coefficient

**Total Power Mode**

From Equation (2-35) the ideal correlation coefficient $\mu_0$ can be calculated from the correlation coefficient measured in the total power mode $\mu_{TP}$ as follows:

$$\mu_0 = \frac{\mu_{TP}}{\tilde{g}} = \frac{\mu_{TP}}{g_{FW} \sqrt{T_{Vant} T_{Hant}}} \sqrt{(T_{Vant} + T_{Vrec})(T_{Hant} + T_{Hrec})}\,, \qquad (4\text{-}50)$$

If the uncertainty of the modulus term is known, the uncertainty for the ideal correlation coefficient can be written as:

$$\Delta\mu_0 = \sqrt{\left( \frac{1}{\tilde{g}} \right)^2 (\Delta\mu_{TP})^2 + \left( \frac{\mu_{TP}}{\tilde{g}^2} \right)^2 (\Delta\tilde{g})^2}\,, \qquad (4\text{-}51)$$

For the modulus term the accuracy of the antenna temperature depends on the uncertainties of the noise source and connecting network of the Measurement Configuration D, see Equation (4-44).

**Noise-injection Mode: Blind Correlation**

Equation (2-44) can be formulated to the following from, which is easier to evaluate:

$$\sin^{-1}(\tilde{g}_2\mu_0)\frac{N_2}{N}+\sin^{-1}(\tilde{g}_3\mu_0)\frac{N_3}{N}+\sin^{-1}(\tilde{g}_4\mu_0)\frac{N_4}{N}-\sin^{-1}(\mu_k)=0 \qquad (4\text{-}52)$$

Since the measured correlation coefficient $\mu_k$ is in practice small the following approximation may be used [9]:

$$Z_k=\frac{2}{\pi}\sin^{-1}(\mu_k)\cong\frac{2}{\pi}\mu_k\,, \qquad (4\text{-}53)$$

from this it follows that:

$$\mu_B\cong\tilde{g}_2\mu_{0,appr}\frac{N_2}{N}+\tilde{g}_3\mu_{0,appr}\frac{N_3}{N}+\tilde{g}_4\mu_{0,appr}\frac{N_4}{N} \qquad (4\text{-}54)$$

where $\mu_B$ is in the blind mode measured correlation coefficient and the ideal correlation coefficient can now be analytically solved:

$$\mu_{0,appr}\cong\frac{\mu_B N}{\tilde{g}_2N_2+\tilde{g}_3N_3+\tilde{g}_4N_4} \qquad (4\text{-}56)$$

For the blind correlation can now be written

$$\mu_{0,appr}=\frac{\mu_B}{g_{FW}\sqrt{T_{Vant}T_{Hant}}}\frac{N}{\left(N_2\sqrt{\frac{1}{T_{v,all}T_{h,all}}}+N_3\sqrt{\frac{1}{T_{v,all}T_{h,sys}}}+N_4\sqrt{\frac{1}{T_{v,sys}T_{h,sys}}}\right)} \qquad (4\text{-}57)$$

where $\mu_B$ is with the blind mode measured correlation coefficient and

$$\begin{aligned}T_{v,all}&=T_{Vant}+T_{Vrec}+T_{VN}\\T_{v,sys}&=T_{Vant}+T_{Vrec}\end{aligned}\quad\text{and}\quad\begin{aligned}T_{h,all}&=T_{Hant}+T_{Hrec}+T_{HN}\\T_{h,sys}&=T_{Hant}+T_{Hrec}\end{aligned} \qquad (4\text{-}58)$$

The error for the ideal correlation coefficient approximation has the maximum value when the total power coming to the antenna is big and both horizontally and vertically polarised and the fringe-washing factor is one. The error in the case of $T_v$ = 140 *K*, $T_h$ = 150 *K* and $g_{FW}$ = 1 is plotted in Figure 4-1 (noise injection longer in the V-channel as in the preceding analysis).

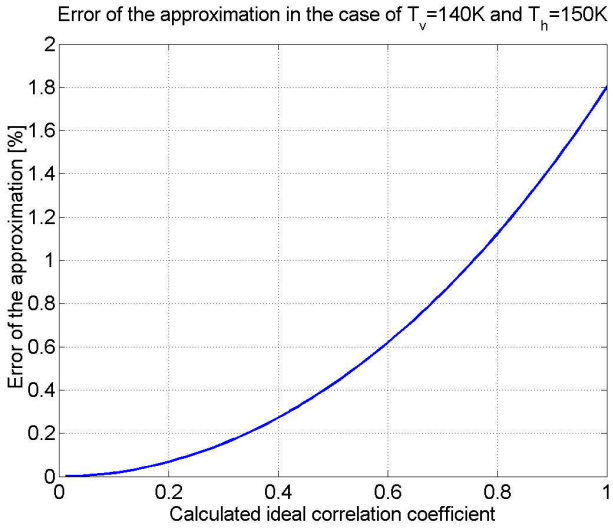


*Figure 4-1. Error of the correlation coefficient approximation of Equation (4-57) when compared to the true value giving Equation (4-52). Vertical antenna brightness temperature is $T_{v,ant}$ = 140K, horizontal is $T_{h,ant}$ = 150K and fringe-washing factor is $g_{FW}$ = 1 yielding the maximum error. Error can be stated to be $(\mu_{0,appr} - \mu_0)/\mu_0 \cdot 100\% < 2\%$.*

The maximum error of the approximation can be stated to be smaller than 2%. When the total uncertainty of the ideal correlation coefficient is calculated, also the maximum error of approximation is included as follows:

$$\Delta\mu_{0,appr} = \left[\left(\frac{N}{\tilde{g}_2 N_2 + \tilde{g}_3 N_3 + \tilde{g}_4 N_4}\right)^2 \Delta\mu^2 + \right.$$
$$\left. + \left(\frac{N}{(\tilde{g}_2 N_2 + \tilde{g}_3 N_3 + \tilde{g}_4 N_4)^2}\right)^2 \left((N_2\Delta\tilde{g}_2)^2 + (N_3\Delta\tilde{g}_3)^2 + (N_4\Delta\tilde{g}_4)^2\right)\right]^{\frac{1}{2}} \cdot 1.02 \quad (4\text{-}60)$$

The uncertainties of the modulus terms are calculated in the previous paragraph.

**Comparison Between Total Power Mode and Noise-injection Mode**

Since the correlation coefficients $\mu_{TP}$ and $\mu_B$ are measured effectively at the same time in the Measurement Configuration D, the antenna brightness temperatures and receiver noise temperatures are identical in Equations (4-50) and (4-57). Thus the following may be written:

$$\Delta\mu_0^{TP-B} = \mu_{0,TP} - \mu_{0,appr,B} = \frac{1}{g_{FW}\sqrt{T_{Vant}T_{Hant}}}$$
$$\cdot \left( \mu_{TP}\sqrt{T_{v,sys}T_{h,sys}} - \frac{\mu_B N}{\left( N_2\sqrt{\frac{1}{T_{v,all}T_{h,all}}} + N_3\sqrt{\frac{1}{T_{v,all}T_{h,sys}}} + N_4\sqrt{\frac{1}{T_{v,sys}T_{h,sys}}} \right)} \right) \quad (4\text{-}61)$$

and it reduces to:

$$\Delta\mu_0^{TP-B} = \frac{\sqrt{T_{v,sys}T_{h,sys}}}{g_{FW}\sqrt{T_{Vant}T_{Hant}}} \cdot \left( \mu_{TP} - \mu_B \frac{N}{\left( N_2 \sqrt{\frac{T_{v,sys}T_{h,sys}}{T_{v,all}T_{h,all}}} + N_3 \sqrt{\frac{T_{v,sys}}{T_{v,all}}} + N_4 \right)} \right), \quad (4\text{-}62)$$

with which the blind mode correlation can be evaluated.

# 4.5 Stability

The stability of the response of the NIR is determined, with and without antenna, in two main cases: (1) nominal case, when the ambient temperature does not change and (2) exceptional case when the temperature changes radically. As a definition of stability the deviation from the average, difference between minimum and maximum values and Allan variance (Section 2.6.1) are used.

*Table 4-5. Measurements required for the determination of stability*

| | A | B | C | D | E | F | G |
|---|---|---|---|---|---|---|---|
| System Noise Temperature | | X | | | | | |
| Sensitivity | | X | | | X | | |
| Linearity | | | X | | | | |
| Polarimetric Properties | X | X | | X | | | X |
| Stability | | X | | | X | | |
| Calibration Accuracy | X | X | X | X | X | X | X |
| Absolute Accuracy | X | X | X | X | X | X | X |

## 4.5.1 Total Power Mode

For the determination of the total power mode stability of the NIR the Measurement Configurations B and E are used. First the stability without the antenna is investigated and then the case where the antenna is attached.

**Constant Temperature**

The stability is calculated for both antenna and centralised noise source measurements using the measurement routines B/1 and B/4. The following methods can be applied for the data of the both measurements.

It is very practical to determine the stability from the calibration coefficients *A* and *B*, introduced in Section 2.7, when two known loads are measured like in the measurement routines at hand. In principle the gain instabilities can be deduced from the variations of *A* and the offset instabilities from the variations of *B*.

The calibration coefficients *A* and *B* are defined as follows when each hot and cold load measurement step is integrated as one value so that they form a vector *P* in which hot and cold load measurements alternate:

$$A^{H/V}[i] = \frac{P_{hot}^{H/V}[n] - P_{cold}^{H/V}[n+1]}{T_{hot}^{H/V}[n] - T_{cold}^{H/V}[n+1]}, \quad n=1,3,5\ldots \tag{4-63}$$

$$B^{H/V}[i] = \frac{P_{cold}^{H/V}[n+1]T_{hot}[n] - P_{hot}^{H/V}[n]T_{cold}[n+1]}{T_{hot}^{H/V}[n] - T_{cold}^{H/V}[n+1]}, \quad n=1,3,5\ldots \tag{4-64}$$

in which *i* increases by one for each *n* and the measurement targets are seen by the receivers as follows

$$T_{hot}^{H/V} = \left(1 - \frac{1}{L_{chain,therm}^{H/V,1}}\right)T_{amb} + \frac{T_{hot}^{phys}}{L_{chain}^{H/V,1}} \tag{4-65}$$

$$T_{cold}^{H/V} = \left(1 - \frac{1}{L_{chain,therm}^{H/V,2}}\right)T_{amb} + \frac{T_{cold}^{phys}}{L_{chain}^{H/V,2}} \tag{4-66}$$

where $L_{chain}^{H/V,1/2}$ and $L_{chain,therm}^{H/V,1/2}$ are the attenuations of the connecting network between the loads and the receivers, in which *H/V* indicates the receiver and 1/2 indicates the switch position (1 being the hot load) and subscript *term* indicates the amount of attenuation that causes additional thermal noise; $T_{hot}^{phys}$ is the physical temperature of the hot load and $T_{cold}^{phys}$ is the noise temperature emitted by the cold load as introduced in Appendix A. $T_{hot}^{phys}$ and $T_{cold}^{phys}$ are determined for every *P* so that when they are applied to the Equations (4-63) and (4-64) they are temporally synchronised with *P*.

As already presented the calibration coefficients define the so-called calibration line with which the measured brightness temperature can be defined from the measured voltage:

$$T[i] = A[i]P + B[i], \quad i=1,2,3\ldots \tag{4-67}$$

Now, when the previously calculated calibration coefficients are applied to a constant figure of voltage *P* the real variations in the NIR response can be determined from the resulting vector *T*. The value of *P* used here should be the observed maximum in order to find out the biggest possible error in the measurement. Thus the stability in total power mode without the antenna can be written as follows:

$$\Delta T_{TP} = \max(T) - \min(T) \tag{4-68}$$

**Allan variance in Total Power Mode**

Measurement routine B/3 is used for calculating the Allan variance (Section 2.6) of the both receivers. There is an optimal integration time after which observing

efficiency is lost due to the drift and this integration time is determined using the Allan variance:

$$\sigma_A^2(m) \cong \frac{1}{m}\sum_{k=1}^{m}\frac{\left(\overline{P}_{k+1}-\overline{P}_k\right)^2}{2} \tag{4-69}$$

where $\overline{P}_k$ is one averaged period and $m$ is the amount of averaged periods. Calculation of $\overline{P}_k$ from real measurement data can be done as follows:

$$\overline{P}_k = \frac{1}{n}\sum_{i=(k-1)n+1}^{kn} P_i \tag{4-70}$$

where $k$ is the number of averaged period, $n$ is the amount of samples in one averaged period, $i$ is the number of a sample and $P_i$ is one measurement sample.

When this is calculated from the measurement data of Measurement Routine B/3 the optimum integration time can be determined.

**Varying Temperature**

For the determination of the effects of varying ambient temperature on NIR the calibration coefficients are calculated as before from the data produced by Measurement Routine B/2. Equation (4-67) is once more calculated and the total power mode response of the NIR in varying temperature can be determined with Equation (4-68).

Since the temperature information is stored with the all the other measurements, the response as function of temperature is also easily determined.

### 4.5.2 Noise-injection Mode

For the determination of the noise-injection mode stability of the NIR the Measurement Configurations B and E are used. First the stability without the antenna is investigated and then the case where the antenna is attached.

**Constant Temperature without Antenna**

The stability of NIR in constant temperature is solved using the Measurement Routines B/5 and B/8. The method is the same used in the “Constant Temperature without Antenna” in Section 4.5.1.

For Allan variance the Measurement Routines B/7 is used and it is analysed the same way as in the previous paragraph.

**Varying Temperature without Antenna**

In varying temperature the noise-injection mode stability is analysed using the data from Measurement Routine B/6. See the “Varying Temperature without Antenna” in Section 4.5.1 for the analysis.

**Constant Temperature with Antenna**

The antenna measurements are done so that first the data is calibrated using the hot load (Measurement routine E/1) then the cold load is measured (Measurement routine E/2) using this value. The measurement is also calibrated using the cold load measurement and then the hot load is measured with this value.

For both cases almost the same methodology as introduced in "Constant Temperature without Antenna" in Section 4.5.1 can be used with the exception that the Equation (4-67) is written now

$$T[i] = T_{ref}[i] - T_N \eta[i], \quad i=1,2,3\ldots \tag{4-71}$$

where $T_{ref}$ is the reference noise temperature, $T_N$ is the calibrated noise temperature of the noise-injection and $\eta$ is the measured power, which is in this case the pulse length of the noise injection (see Section 2.7.2).

**Varying Temperature with Antenna**

The stability with varying temperature is done as above using the Measurement Routine E/3 for measurement data and Measurement routine E/2 for calibration data.

# 4.6 Calibration Accuracy

The calibration of NIR is a very critical issue. The two purposes of the NIR should be brought back to mind: measurement of the calibration network of the MIRAS and polarimetric measurement of the brightness temperature. The latter involves the calibration of the third and fourth Stokes parameter introduced in Section 2.8. All the related analyses and error analyses are handled in this section.

*Table 4-6. Measurements required for the determination of calibration accuracy*

| | A | B | C | D | E | F | G |
|---|---|---|---|---|---|---|---|
| System Noise Temperature | | X | | | | | |
| Sensitivity | | X | | | X | | |
| Linearity | | | X | | | | |
| Polarimetric Properties | X | X | | X | | | X |
| Stability | | X | | | X | | |
| Calibration Accuracy | X | X | X | X | X | X | X |
| Absolute Accuracy | X | X | X | X | X | X | X |

The proposed NIR calibration procedure is introduced in Section 2.8.5 and the analyses presented here are based on the assumption that the calibration is carried out according to it.

## 4.6.1 Calibration of Horizontal and Vertical Polarisation

In this paragraph the calibration methods of the power measurement of the horizontal and vertical polarisation are analysed.

**Noise-injection Mode**

The NIR noise-injection mode is calibrated according to Section 2.8.5, where the noise injection temperatures are obtained as follows:

$$T_{VN,HN} = \frac{T_{ref} - T_{Vant,Hant}^{calib}}{\eta_{V,H}}, \tag{4-72}$$

in which here $T_{ref}$ is the Dicke-reference temperature, $\eta_{V,H}$ is the noise injection duty cycle in the channels V and H and $T_{Vant,Hant}^{calib}$ is the antenna temperature in channels V and H when the calibration target is looked at.

The uncertainty of the noise injection temperature, using the standard propagation of error, is

$$\Delta T_{VN,HN} = \sqrt{\left(\frac{1}{\eta_{V,H}}\right)^2 \left[\left(\Delta T_{ref}\right)^2 + \left(\Delta T_{Vant,Hant}^{calib}\right)^2\right] + \left(\frac{T_{ref} - T_{Vant,Hant}^{calib}}{\left(\eta_{V,H}\right)^2} \Delta\eta_{V,H}\right)^2} \tag{4-73}$$

Notice that larger the noise injection duty cycle, $\eta_{V,H}$, smaller the uncertainty i.e. colder the calibration target more accurate calibration result. This obviously favours the use of the sky as the calibration target as is also demonstrated in Appendix E. Measured antenna temperature can be written

$$T_{Vant,Hant} = T_{ref} - \eta_{V,H} T_{VN,HN} \tag{4-74}$$

And the uncertainty for this, which can be defined as the calibration uncertainty of the measurements of the horizontal and vertical polarisations in the noise-injection mode, with the standard propagation of error is

$$\Delta T_{Vant,Hant} = \Delta T_{Calib}^{NI} = \sqrt{\left(\Delta T_{ref}\right)^2 + \left(T_{VN,HN}\right)^2 \left(\Delta\eta_{V,H}\right)^2 + \left(\eta_{V,H}\right)^2 \left(\Delta T_{VN,HN}\right)^2}, \tag{4-75}$$

from which it can be seen that the smaller the noise injection duty cycle, $\eta_{V,H}$, better the antenna temperature measurement accuracy i.e. when the antenna temperature is close to the noise temperature of the reference load $T_{ref}$ the accuracy would be at the best.

Now the noise injection temperatures are obtained using known loads as e.g. in Measurement Configuration E and then another known loads are measured and the differences in the results are examined. The first load can be e.g. the liquid nitrogen load and then the hot load and sky could be measured giving more targets for comparison.

**Total Power Mode**

NIR total power mode is calibrated using two calibration targets as introduced in Section 2.7. The relation between the detected power, $P_x$, and noise temperature of the antenna, $T_x$, can be written as

$$T_x = AP_x + B\,. \tag{4-76}$$

The uncertainty for this and for the so-called calibration coefficients, $A$ and $B$, are presented in Section 4.3.2. Uncertainty of the calibration coefficients depends on the accuracy of the calibration targets and the linearity of the detection. Thus, the calibration uncertainty for the horizontal and vertical polarisation of the total power mode is here defined as:

$$\Delta T_{Calib}^{TP} = \sqrt{P(\Delta A)^2 + A(\Delta P)^2 + (\Delta B)^2}\,, \tag{4-77}$$

where $\Delta A$ is the same as presented in Equation (4-31), $\Delta B$ is the same as presented in Equation (4-32) and detecting error $\Delta P$ is evaluated in Section 4.3.

## 4.6.2 Calibration of 3rd and 4th Stokes Parameter

The third and fourth Stokes parameters are calibrated in NIR by carrying out the calibration steps A through F in Section 2.8.5 using Measurement Configurations D. Since the Stokes parameters of the load in Measurement Configurations D and G are known the calibration measurement results can be compared to the real values.

The uncertainty of the Stokes parameter measurement depends on the horizontal and vertical channel calibration uncertainty (see Section 4.6.1), modulus term uncertainties (see Section 4.4.5) and correlation coefficient uncertainties (see Section 4.4.6). Uncertainties of each of these form the total calibration uncertainty of the third and fourth Stokes parameter.

**Noise-injection Mode**

In the noise-injection mode the calibration uncertainties can be further divided down to the following things:

1. Horizontal and vertical channel measurement calibration (Section 4.6.1 above)
2. Quantizer offset voltage correction for correlation coefficient (Section 2.8.5)
3. In-phase and quadrature error correction for correlation coefficient (Section 4.4.3)
4. Receiver noise temperatures for modulus terms (Y-factor method with antenna measurement and calibration network measurement, below)
5. Noise injection temperatures for modulus terms (Section 4.6.1 above)
6. Fringe-washing function with 3-delay method for modulus terms (Section 4.4.4)

The Y-factor method of the fourth point is handled in detail already in Sections 2.3 and 4.1. However during the operational calibration of NIR the references are found in the following manner: (1) first NIR is calibrated using a known antenna load e.g. sky, then measurement of (2) calibration network and (3) antenna are carried out normally.

Now, when the calibration network is measured, the PMS output of NIR is balanced to the calibration network noise temperature, which is of course known from the noise-injection measurement. Similarly, when the antenna is measured, the PMS output is balanced to the reference noise temperature, which is known. The equations introduced in Section 4.1 can now be applied and the receiver noise temperature calculated and uncertainty determined, using uncertainty of the calibration network measurement uncertainty (Section 4.7.2) and reference load uncertainty.

**Total Power Mode**

Also in the total power mode the calibration uncertainties can be further divided down to the following things:

1. Horizontal and vertical channel measurement calibration (Section 4.6.1 above)
2. Quantizer offset voltage correction for correlation coefficient (Section 2.8.5)
3. In-phase and quadrature error correction for correlation coefficient (Section 4.4.3)
4. Receiver noise temperatures for modulus term (Y-factor method with antenna measurement and calibration network measurement, below)
5. Fringe-washing function with 3-delay method for modulus terms (Section 4.4.4)

As the receivers are calibrated (see Section 4.6.1) also the receiver noise temperatures can be determined with the two loads as introduced in Section 4.1.2.

# 4.7 Absolute Accuracy

In this section the analysis of the absolute accuracy of the NIR is carried out. This is the property that in the end defines how well the NIR can perform its tasks given in the Chapter 1.

*Table 4-7. Measurements required for the determination of absolute accuracy*

| | A | B | C | D | E | F | G |
|---|---|---|---|---|---|---|---|
| System Noise Temperature | | X | | | | | |
| Sensitivity | | X | | | X | | |
| Linearity | | | X | | | | |
| Polarimetric Properties | X | X | | X | | | X |
| Stability | | X | | | X | | |
| Calibration Accuracy | X | X | X | X | X | X | X |
| Absolute Accuracy | X | X | X | X | X | X | X |

Results from all the measurements are analysed and final calculations are done in this section. Separate figures are given for the brightness temperature measurement of the antenna and for the centralised noise source measurement. These performance figures are essential when the functionality of the whole MIRAS Demonstrator is estimated.

### 4.7.1 Antenna Measurement Accuracy

This paragraph introduces determination of the accuracy with which NIR can measure the four Stokes parameters from a brightness temperature scene.

**Noise-injection Mode: Horizontal and Vertical Polarisation**

The absolute accuracy of the horizontal and vertical polarisation measurements in noise-injection mode depends on the following items:

1. Sensitivity, the measured standard deviation, $\Delta T_\sigma$
2. Calibration accuracy of one point calibration (target accuracy), $\Delta T_{Calib}^{NI}$
3. Linearity meaning how well the calibration applies with larger and smaller input powers, $\Delta T_{lin}^{NI}$

The accuracy can be calculated in a straightforward manner by taking the quadratic sum over the uncertainties above:

$$\Delta T_{H,V}^{NI} = \sqrt{\Delta T_\sigma{}^2 + \Delta T_{Calib}^{NI}{}^2 + \Delta T_{lin}^{NI\,2}} \,. \tag{4-78}$$

**Noise-injection Mode: Third and Fourth Stokes Parameter**

The absolute accuracy of the third and fourth Stokes parameters measurement in noise-injection mode depends on the following items:

1. Accuracy of the horizontal and vertical polarisation from above, $\Delta T_{H,V}^{NI}$
2. Modulus term uncertainties $\Delta\tilde{g}_2$, $\Delta\tilde{g}_3$ and $\Delta\tilde{g}_4$
3. Correlation coefficient uncertainties $\Delta\mu_{ii}$ and $\Delta\mu_{qi}$

The uncertainty for the third Stokes parameter can be written by applying the standard propagation of errors method to Equation (2-63):

$$\Delta T_3 = \left[ \left( \frac{\mu_{ii}}{\sqrt{T_{Vant} T_{Hant}} \left( \tilde{g}_2 \frac{N_2}{N} + \tilde{g}_3 \frac{N_3}{N} + \tilde{g}_4 \frac{N_4}{N} \right)} \right)^2 \left( T_{Hant}{}^2 \Delta T_V^{NI\,2} + T_{Vant}{}^2 \Delta T_H^{NI\,2} \right) \right. \tag{4-79}$$

$$+\left(\frac{2\sqrt{T_{Vant}T_{Hant}}}{\left(\tilde{g}_2\frac{N_2}{N}+\tilde{g}_3\frac{N_3}{N}+\tilde{g}_4\frac{N_4}{N}\right)}\right)^2\Delta\mu_{ii}{}^2$$

$$+\left(\frac{2\sqrt{T_{Vant}T_{Hant}}\,\mu_{ii}}{\left(\tilde{g}_2\frac{N_2}{N}+\tilde{g}_3\frac{N_3}{N}+\tilde{g}_4\frac{N_4}{N}\right)^2}\right)^2\left[\left(\frac{N_2}{N}\Delta\tilde{g}_2\right)^2+\left(\frac{N_3}{N}\Delta\tilde{g}_3\right)^2+\left(\frac{N_4}{N}\Delta\tilde{g}_4\right)^2\right]^{\frac{1}{2}}$$

Uncertainty for the fourth Stokes parameter, $\Delta T_4$, is retrieved by replacing $\mu_{ii}$ by $\mu_{qi}$. The noise-injection periods $N_2/N$, $N_3/N$ and $N_4/N$ are determined from the output of NIR. Some simulations of the third and fourth Stokes parameters uncertainties as the function of modulus term uncertainties and correlation coefficient uncertainties are presented in Appendix E.

**Total Power Mode: Horizontal and Vertical Polarisation**

The absolute accuracy of the horizontal and vertical polarisation measurements in noise-injection mode depends on the following items:

1. Sensitivity, the measured standard deviation, $\Delta T_\sigma$
2. Calibration accuracy of the two point calibration (target accuracy), $\Delta T_{Calib}^{TP}$
3. Linearity meaning how well the calibration applies between the calibration input powers, $\Delta T_{lin}^{TP}$

The accuracy can be straightforwardly calculated by taking the quadratic sum over the uncertainties mentioned above:

$$\Delta T_{H,V}^{TP}=\sqrt{\Delta T_\sigma{}^2+\Delta T_{Calib}^{TP}{}^2+\Delta T_{lin}^{TP\,2}}\ . \tag{4-80}$$

**Total Power Mode: Third and Fourth Stokes Parameter**

The absolute accuracy of the third and fourth Stokes parameters measurement in total power mode depends on the following items:

1. Accuracy of the horizontal and vertical polarisation from above, $\Delta T_{H,V}^{TP}$
2. Modulus term uncertainty $\Delta\tilde{g}$
3. Correlation coefficient uncertainties $\Delta\mu_{ii}$ and $\Delta\mu_{qi}$

$$\Delta T_3=\left[\left(\frac{\mu_{ii}}{\sqrt{T_{Vant}T_{Hant}}\,\tilde{g}}\right)^2\left(T_{Hant}{}^2\Delta T_V^{TP\,2}+T_{Vant}{}^2\Delta T_H^{TP\,2}\right)\right. \tag{4-81}$$

$$+\left(\frac{2\sqrt{T_{Vant}T_{Hant}}}{\tilde{g}}\right)^2\Delta\mu_{ii}{}^2+\left(\frac{2\sqrt{T_{Vant}T_{Hant}}\,\mu_{ii}}{\tilde{g}^2}\right)^2\Delta\tilde{g}^2\Bigg]^{\frac{1}{2}}$$

Uncertainty for the fourth Stokes parameter, $\Delta T_4$, is retrieved by replacing $\mu_{ii}$ with $\mu_{qi}$.

### 4.7.2 Calibration Network Noise Measurement Accuracy

The other main purpose of NIR is to measure the noise temperature of the centralised noise source of the MIRAS. This paragraph introduces the accuracy of this measurement. The calibration network noise temperature is determined from the following:

$$T_C=\eta T_{ref,inj}+(1-\eta)T_{ref}\,, \tag{4-82}$$

where $\eta$ is the noise injection duty-cycle, $T_{ref,inj}$ and $T_{ref}$ are the reference branch noise temperatures coming to the receiver when noise injection is on and off, respectively. Uncertainty for this can be written using the standard propagation of errors (see Section 2.9.2) as:

$$\Delta T_C=\sqrt{\eta^2\Delta T_{ref,inj}{}^2+(1-\eta)^2\Delta T_{ref}{}^2+\left(T_{ref,inj}-T_{ref}\right)^2\Delta\eta^2} \tag{4-83}$$

In principle it can be assumed that noise injection duty-cycle is known without uncertainty since it is the output of NIR and length of the duty-cycle is very well defined i.e. duty-cycle is always “right” but knowledge of the reference noise temperatures going into the receiver might be “wrong”, thus

$$\Delta T_C=\sqrt{\eta^2\Delta T_{ref,inj}{}^2+(1-\eta)^2\Delta T_{ref}{}^2}\,. \tag{4-84}$$

Reference noise temperature, when additional noise is injected $T_{ref,inj}$, is determined by measuring known load in antenna measurement mode, that is, with the normal noise-injection calibration introduced in Section 2.7.2. Now from the noise injection temperature going into the antenna branch the noise going to the reference branch is determined, see Figure 2-10. During the calibration the noise temperature coming into the receiver is defined as:

$$T'_{ant}=T_{ant}^{calib}+T_N=T_{ant}^{calib}+\frac{T_{inj}-T_{ant}^{calib}}{F_{NC}}\,, \tag{4-85}$$

where $T_{ant}^{calib}$ is the calibration target noise temperature coming to the directional coupler, $T_{inj}$ is the noise-injection noise temperature coming to the directional coupler and $F_{NC}$ is the coupling of the directional coupler. Now it can be written:

$$T_{inj}=T_N F_{NC}+T_{ant}^{calib}\,, \tag{4-86}$$

and also

$$T_{inj} = T_{noise} L_{NA} + \left(1 - \frac{1}{L_{NA}}\right) T_{L_{NA}}^{phys}, \tag{4-87}$$

where $T_{noise}$ is the noise temperature coming from the noise-injection switch, $L_{NA}$ is the attenuator between the switch and the directional coupler and $T_{L_{NA}}^{phys}$ is the physical temperature of the attenuator. For the reference branch, when the noise is injected, the noise temperature is defined as

$$T_{ref,inj} = T_{noise} L_{Nref} + \left(1 - \frac{1}{L_{Nref}}\right) T_{L_{Nref}}^{phys}, \tag{4-88}$$

where $L_{Nref}$ is the attenuation of the attenuator between the noise-injection switch and $T_{L_{Nref}}^{phys}$ is its physical temperature. Notice that it is assumed that the noise temperature leaving the switch is assumed to be the same for the both antenna and reference branch. Using the above equations the reference noise temperature during noise injection can now be written as:

$$T_{ref,inj} = \frac{1}{L_{NA}} \left[ T_N F_{NC} + T_{ant}^{calib} - \left(1 - \frac{1}{L_{NA}}\right) T_{L_{NA}}^{phys} \right] L_{Nref} + \left(1 - \frac{1}{L_{Nref}}\right) T_{L_{Nref}}^{phys} \tag{4-89}$$

Using the standard propagation for error (see Section 2.9.2) the uncertainty for this can be written as

$$\begin{aligned} \Delta T_{ref,inj} = \Bigg[ & \left( \frac{F_{NC} L_{Nref}}{L_{NA}} \Delta T_N \right)^2 + \left( \frac{T_N L_{Nref}}{L_{NA}} \Delta F_{NC} \right)^2 + \\ & + \left( \frac{1}{L_{NA}} \left( T_N F_{NC} + T_{ant}^{calib} - \left(1 - \frac{1}{L_{NA}}\right) T_{L_{NA}}^{phys} \right) + \frac{T_{L_{Nref}}^{phys}}{{L_{NA}}^2} \right)^2 \Delta {L_{Nref}}^2 + \\ & + \left( \frac{L_{Nref}}{{L_{NA}}^2} \left( T_{L_{NA}}^{phys} - T_N F_{NC} - T_{ant}^{calib} + \frac{2 T_{L_{NA}}^{phys}}{L_{NA}} \right) \Delta L_{NA} \right)^2 + \\ & + \left( \frac{L_{Nref}}{L_{NA}} \left(1 - \frac{1}{L_{NA}}\right) \Delta T_{L_{NA}}^{phys} \right)^2 + \left(1 - \frac{1}{L_{Nref}}\right)^2 \Delta {T_{L_{Nref}}^{phys}}^2 \Bigg]^{\frac{1}{2}} \end{aligned} \tag{4-90}$$

where $\Delta T_N$ is determined during the antenna calibration handled in Section 4.6.1 and the rest of the uncertainties are determined from specifications and measurements during manufacturing. Physical temperature measurement accuracy is at least 0.1°C as introduced in Appendix D.

Reference branch noise temperature, when noise injection is off, is defined as:

$$T_{ref} = T_{leak} L_{Nref} + \left(1 - \frac{1}{L_{Nref}}\right) T_{L_{Nref}}^{phys}, \tag{4-91}$$

in which $T_{leak}$ is through the noise-injection switch leaked noise temperature, when the switch is turned to the matched termination. It is determined during the manufacturing phase of NIR. Uncertainty can be written as:

$$\Delta T_{ref} = \sqrt{L_{Nref}{}^2 \Delta T_{leak}{}^2 + \left(1 - \frac{1}{L_{Nref}}\right)^2 \Delta T_{L_{Nref}}^{phys\,2} + \left(T_{leak} + \frac{T_{L_{Nref}}^{phys}}{L_{Nref}{}^2}\right)^2 \Delta L_{Nref}{}^2}\,. \tag{4-92}$$

Also $\Delta T_{leak}$ is determined during manufacturing by measuring the isolation of the switch in different temperatures etc. Now it can be stated that the accuracy of the calibration network measurement depends on three main uncertainties, namely:

1. Noise injection calibration uncertainty, $\Delta T_N$
2. Reference branch noise temperature uncertainty when noise is injected, $\Delta T_{ref,inj}$
3. Reference branch noise temperature uncertainty when noise is not injected, $\Delta T_{ref}$

Using the equations presented and mentioned above the absolute accuracy of the calibration network noise measurement can be determined.

# 5 CONCLUSIONS

Detailed description of the test plan of MDPP-2 NIR was given. First the measurement arrangements were described and then the analyses leading to the solving of the NIR properties were introduced.

The goal is to test the ability of NIR to perform its main purposes, which are polarimetric measurement of brightness temperature scene and total power measurement of the noise temperature of the centralised noise source.

With sample calculations it was verified that the goal is met and all the critical parameters for the proper operation of the NIR instrument can be tested using the configurations and procedures described in this work.

# REFERENCES


[1] Ulaby, F.T., Moore, R. K., Fung, A. K., "Microwave Remote Sensing Active and Passive, Volume 1, Fundamentals and Radiometry", 1981, Addison-Wesley Publishing Company, 456 pp.

[2] Skou, Neils, "Microwave Radiometer Systems: Design and Analysis", 1989, Artech House, Inc.

[3] Pozar, David M., "Microwave Engineering", 2nd Edition, 1998, John Wiley & Sons, Inc.

[4] Walls, F. L., Allan, D. W., "Measurements of Frequency Stability"

[5] Barnes, J. A. et al., "Characterization of Frequency Stability", IEEE Trans. Instrument. Meas., vol. IM-20, No.2, May 1971, pp.105-120

[6] Schieder, R., Rau, G., Vowinkel, B., "Characterization and Measurement of Radiometer Stability", Proc. 14th European Microwave Conference, pp. 248-253, 1984

[7] Ishimaru, A., "Wave Propagation and Scattering in Random Media, Volume 1, Single Scattering and Transport Theory", 1978, Academic Press, 250 pp.

[8] Bevington, Philip R., Robinson, Keith D., "Data Reduction and Error Analysis for the Physical Sciences", 2nd Edition, 1992, McGraw-Hill, Inc.

[9] Tauriainen S., Lahtinen J., Colliander A., Uusitalo J., Toikka M., "MDPP-2 / CAS-2: PDR: NIR Preliminary Design Report", Helsinki University of Technology 2002

[10] Martín-Neira M., Martín-Polegre A., Ribó S. "Introduction to Two-dimensional Aperture Synthesis Microwave Radiometry for Earth Observation: Polarimetric Formulation of The Visibility Function", Internal ESTEC Working Paper No 2130, 2001

[11] Kong, J. A., "Electromagnetic Wave Theory", John Wiley & Sons, Inc., 1986

[12] Tauriainen S., Colliander A., Uusitalo J., Toikka M., "MDPP-2 / CAS-2: CDR: NIR Critical Design Report", Helsinki University of Technology, 2002

[13] Han, Y., Westwater, E. R., "Analysis and Improvement of Tipping Calibration for Ground-Based Microwave Radiometer", IEEE Transactions on Geoscience and Remote Sensing, Vol. 38, 2000

[14] Butora, R., Martín-Neira, M., Rivada, Angel-Luis, "Fringe-Washing Function Calibration in Aperture Synthesis Microwave Radiometry", Submitted 2002

[15] Stelzried, C. T., "Temperature Calibration of Microwave Thermal Noise Sources", IEEE Transactions on Microwave Theory and Techniques, January 1965

[16] Alonso, M., Finn, E. J., "Fundamental University Physics, Volume One: Mechanics and Thermodynamics, 2nd Edition", Addison-Wesley, 1980

[17] Korn, G. A., Korn, T. M., "Mathematical Handbook for Scientists and Engineers: Definitions, Theorems and Formulas for Reference and Review", Dover Publications Inc., 2000

[18] Uusitalo, J., "NIR Calibration Procedure", Ylinen Electronics Ltd., 20/5/2002

[19] Colliander, A., "Note on NIR Noise Module Tests", Helsinki University of Technology, 4/6/2002

[20] Delahye, J-Y., Golé, P., Waldteufel, P., "Calibration error of L-band sky-looking ground-based radiometers", Radio Science, Vol. 37, No. 1, 2002

[21] Sagués, L., "LICEF-2B/2C Test Report", Mier Communicaciones, Issue 1, 8/8/2002

# APPENDIX A: MATCHED COLD LOAD

In this appendix a setup where a matched load is sunk in liquid nitrogen is investigated. A schematic diagram of the setup is shown in Figure A-1. The purpose is to define the noise temperature *T'* at the output.

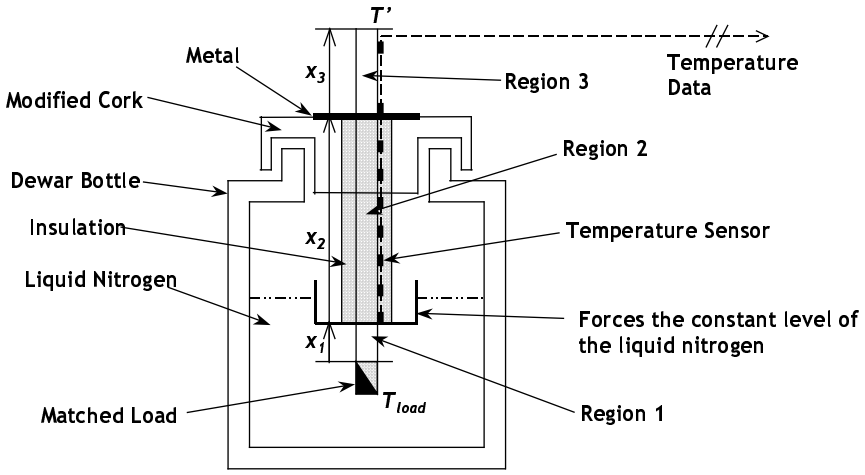


*Figure A-1. Realisation of a cold load. Matched load is sunk in liquid nitrogen in a Dewar bottle having the temperature of about 77K. In region 1of the transmission line the temperature is assumed to be that of the liquid nitrogen, in region 2 the temperature has a distribution and in region 3 the temperature is assumed to be constant and that of the setup ambient.*

In Figure A-1 the transmission line is divided into three sections. The first is in the liquid nitrogen and has a constant temperature of about 77K. The second spans from the surface of the liquid nitrogen to a metal plate. The metal plate is assumed to be large enough to maintain its temperature as the same as the temperature of the setup ambient. Temperature is spread between these two points and characterisation of this distribution and its effect on the output noise temperature *T'* is the main focus of this appendix. The third region is assumed to be once again constant and having the temperature of the setup ambient.

In the following it is proposed to add insulation around region 2 of the cable, as presented in Figure A-1, in order to force the temperature distribution in this region linear. Analysis in the case of the linear temperature distribution with constant and non-constant attenuation is carried out.

## A.1 Temperature Distribution in the Cable

Let's consider the configuration of Figure A-1 without the insulation. The differential equation for a travelling wave of power $P$ toward positive $x$ in a transmission line with attenuation coefficient $\alpha(x)$ and temperature $T(x)$ is [15]:

$$\frac{dP}{dx} = -2\alpha(x)P + 2\alpha(x)kT(x)B \qquad \text{(A-1)}$$

From Nyquist's theorem [3] it is known that $P=kT_xB$ and by dividing the resulted equation by $kB$, the differential equation in terms of equivalent noise temperature $T_x$ is

$$\frac{dT_x}{dx} + 2\alpha(x)T_x = 2\alpha(x)T(x) \tag{A-2}$$

This linear first-order differential equation has the following solution [15]:

$$T' = \frac{T_{load} + \int_0^l 2\alpha(x)T(x)e^{\int_0^x 2\alpha(x)dx}dx}{e^{\int_0^x 2\alpha(x)dx}\Big|_{x=l}} \tag{A-3}$$

For the configuration in Figure A-1 the length $l$ can be divided in three sections yielding:

$$\begin{aligned} T' = \frac{1}{e^{\int_0^x 2\alpha(x)dx}\Big|_{x=l}} \Bigg( & T_{load} + \int_0^{x_1} 2\alpha_1(x)T_1(x)e^{\int_0^x 2\alpha(x)dx}dx \\ & + \int_{x_1}^{x_2} 2\alpha_2(x)T_2(x)e^{\int_{x_1}^x 2\alpha(x)dx}dx + \int_{x_2}^{x_3} 2\alpha_3(x)T_3(x)e^{\int_{x_2}^x 2\alpha(x)dx}dx \Bigg) \end{aligned} \tag{A-4}$$

in which each section has the attenuation determined as follows:

$$e^{\int_{x_{i-1}}^x 2\alpha(x)dx} = L_i(x) = \int_{x_{i-1}}^x l(T_i(x))dx, \quad x_0=0 \tag{A-5}$$

where $l(T(x))$ is the attenuation of the transmission line per unit length as function of its physical temperature which, in turn, is function of the location. The total attenuation of the line is now:

$$\begin{aligned} e^{\int_0^x 2\alpha(x)dx}\Big|_{x=l} &= L_{tot} = \int_0^l l(T(x))dx \\ &= \int_0^{x_1} l(T_1(x))dx + \int_{x_1}^{x_2} l(T_2(x))dx + \int_{x_2}^{x_3} l(T_3(x))dx \end{aligned} \tag{A-6}$$

The Equation (A-4) can now be written:

$$T' = \frac{1}{L_{tot}} \Bigg( T_{load} + \int_0^{x_1} 2\alpha_1(x)T_1(x)l(x)dx \tag{A-7}$$

$$+\int_{x_1}^{x_2} 2\alpha_2(x)T_2(x)l(x)dx+\int_{x_2}^{x_3} 2\alpha_3(x)T_3(x)l(x)dx\Bigg)$$

Since the temperature is assumed to be constant in regions 1 and 3, the above equation may be formulated as:

$$T'=\frac{1}{L_{tot}}\left[T_{load}+2T_{load}L_1\alpha_1x_1+\int_{x_1}^{x_2}2\alpha_2(x)T_2(x)\left(\int_{x_1}^{x}l(x)dx\right)dx+2T_{amb}L_3\alpha_3(x_3-x_2)\right] \quad \text{(A-8)}$$

Because the attenuation and the attenuation coefficient have the relation of

$$e^{2\alpha x}=L \Leftrightarrow \alpha=\frac{\ln L}{2x}, \quad \text{(A-9)}$$

the noise temperature at the output may be written

$$T'=\frac{1}{L_{tot}}\left(T_{load}+T_{load}L_1\ln L_1+\int_{x_1}^{x_2}T_2(x)l(x)\frac{\ln(l(x))}{x}dx+T_{amb}L_3\ln L_3\right) \quad \text{(A-10)}$$

The total attenuation of the transmission line can also be simplified due to the constant temperatures of the regions 1 and 3:

$$L_{tot}=l(T_{load})x_1+\int_{x_1}^{x_2}l(T_2(x))dx+l(T_{amb})(x_3-x_2) \quad \text{(A-11)}$$

Now the attenuation of the transmission line per unit length as function of its physical temperature has to be determined and of course the temperature distribution in the region 2 of the transmission line has to be measured. For both variables a function may be fitted to the measured data and it is possible that analytical solutions can be found. Of course the equations may also be solved numerically.

## A.2 Effect of the Insulation

When insulation is added to the region 2 the temperature distribution in this region should became linear according to basic thermodynamic principles (e.g. [16]). The upper end of the transmission line in region 2 is connected to a metal plate having the same temperature as that of the setup ambient. Thus the upper end has the temperature of $T_{amb}$ and the lower end the temperature of $T_{load}$.

The temperature distribution $T_2$ of Equation (A-8) is now described with the following function (e.g. [17]):

$$T_2(x)=ax+b, \quad \text{(A-12)}$$

where

$$a = \frac{T_{amb} - T_{load}}{x_2 - x_1} \tag{A-13}$$

and

$$b = \frac{x_2 T_{load} - x_1 T_{amb}}{x_2 - x_1}. \tag{A-14}$$

This yields a function for the temperature distribution in region 2:

$$T_2(x) = \frac{(T_{amb} - T_{load})x + x_2 T_{load} - x_1 T_{amb}}{x_2 - x_1}, \tag{A-15}$$

which can be applied to Equation (A-10).

**Non-constant Attenuation with Linear Temperature Distribution**

The temperature distribution in region 2 is now linear as stated in Equation (A-15) and if the relation between the attenuation of the transmission line and the temperature of the transmission line is assumed linear, also the attenuation in region 2 can be assumed linear. This yields for the $l(x)$ following equation (analogously to Equation (A-15)):

$$l(x) = \frac{(l_2 - l_1)x + x_2 l_1 - x_1 l_2}{x_2 - x_1} \tag{A-16}$$

where $l_1 = l(T_{load})$ and $l_2 = l(T_{amb})$. This can now be inserted, with (A-15), into the Equation (A-10) and the integral may be numerically solved.

**Constant Attenuation with Linear Temperature Distribution**

If the attenuation of the transmission line is assumed independent from its temperature i.e. constant, the middle term of Equation (A-8) can be written, with Equation (A-12), as follows

$$\begin{aligned} &\int_{x_1}^{x_2} 2\alpha_2(x) T_2(x) L_2(x) dx \Rightarrow \int_{x_1}^{x_2} 2T_2(x)\alpha_2 L_2 dx \Rightarrow \int_{x_1}^{x_2} 2(ax+b)\alpha_2 L_2 dx \\ &= 2\alpha_2 L_2 \Big|_{x_1}^{x_2} \left( \frac{1}{2} a x^2 + bx \right) = 2\alpha_2 L_2 \left( \frac{1}{2} a \left( {x_2}^2 - {x_1}^2 \right) + b(x_2 - x_1) \right) \\ &= \alpha_2 L_2 \left( (x_2 - x_1) T_{amb} + (x_2 + x_1) T_{load} \right) \end{aligned} \tag{A-17}$$

Now Equation (A-8) can be formulated to be

$$\begin{aligned} T' = \frac{1}{L_{tot}} \big[ & T_{load} + 2T_{load} L_1 \alpha_1 x_1 + \alpha_2 L_2 \left( (x_2 - x_1) T_{amb} + (x_2 + x_1) T_{load} \right) \\ & + 2T_{amb} L_3 \alpha_3 (x_3 - x_2) \big] \end{aligned} \tag{A-18}$$

and when the Equation (A-9) is taken into account it becomes

$$T' = \frac{1}{L_{tot}}\left( T_{load} + 2T_{load} L_1 \ln L_1 + \frac{L_2 \ln L_2}{2}\left( T_{amb} + \frac{(x_2 + x_1)}{(x_2 - x_1)} T_{load} \right) + 2T_{amb} L_3 \ln L_3 \right) \quad \text{(A-19)}$$

where

$$L_{tot} = L_1 + L_2 + L_3 \quad \text{(A-20)}$$

in which

$$\begin{aligned} L_1 &= l_{nom} x_1 \\ L_2 &= l_{nom}(x_2 - x_1), \\ L_3 &= l_{nom}(x_3 - x_2) \end{aligned} \quad \text{(A-21)}$$

where $l_{nom}$ is the nominal attenuation per length unit of the transmission line.

## A.3 Conclusions

Equations for determining the output noise temperature of the cold load assembly of Figure A-1 were presented. Linear temperature distribution with constant and non-constant attenuation was also analysed.

Measurements of the system will demonstrate whether the linear temperature distribution could be applied. If this were possible within acceptable uncertainty limits (depending on the measurement), it would significantly simplify a construction of a well-defined cold load.

# APPENDIX B: ANTENNA LOADS

In this appendix some of the properties of the antenna loads, used in the tests, are described.

## B.1 Hot Load

The hot load is realised with an absorber, whose temperature is measured. Multi-point measurement is needed in order to assure accurate temperature distribution of the temperature in the antenna lobe. The minimum size of the absorber is determined using 5*dB* beamwidth, far-field condition and physical restrictions.

For the antenna of NIR the 5dB beamwidth is about 40 degrees. 5*dB* beamwidth, instead of 3*dB*, is used in order to improve the accuracy of the target brightness temperature determination.

The far-field condition is satisfied when [3]

$$r \geq \frac{2D^2}{\lambda}, \tag{B-1}$$

where $r$ is the distance from the antenna, $D$ is the diameter of the antenna and $\lambda$ is the wavelength. Now, for the antenna of the NIR $r$=0.1$m$. In the following $r$=0.25$m$ is used in order to simplify the construction and to be on the safe side.

Figure B-1 presents a possible configuration for the hot load. The minimum radius of the absorber is calculated to be 0.21$m$ for the 5dB beamwidth.

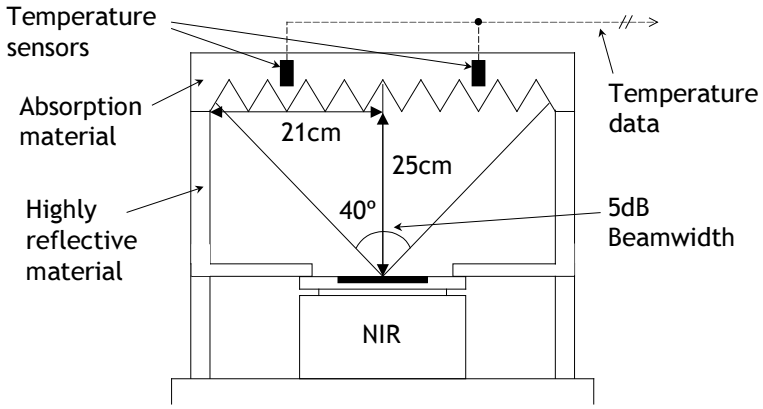


*Figure B-1. Hot load realised with an absorber.*

However, commercially available absorbers are for instance of size 0.61$m$ x 0.61$m$. It would be futile to cut this to the size of 0.42$m$ x 0.42$m$ but using the original size makes it possible to have 15*dB* beamwidth pointing at the absorber.

This would increase the accuracy significantly since then only a small amount of radiation of the walls adds to the measurement of the load.

Temperature distribution of the absorber is determined from the multi-point measurements using interpolation. When the temperature map of the absorber is known the brightness temperature received by NIR can be calculated using the measured antenna pattern of NIR antenna. The antenna temperature is defined as [1]

$$T_A = \frac{\iint_{4\pi} T_B(\theta,\phi) F_n(\theta,\phi) d\Omega}{\iint_{4\pi} F_n(\theta,\phi) d\Omega}, \tag{B-2}$$

where $T_B$ is the brightness temperature i.e. in this case the physical temperature of the target and $F_n$ is the normalised antenna pattern of the NIR antenna. The above equation can be numerically solved when the temperature distribution of the absorber is determined and the antenna pattern is known (can be retrieved e.g. from [21]).

When highly reflective material (e.g. aluminium) is used in the walls of the structure its brightness temperature causes minimal error. The emissivity of the walls should be known from specifications and the brightness temperature calculated using Equation (2-6).

## B.2 Cold Load

The cold load can be constructed from an absorber (which can be sunk into liquid nitrogen), Styrofoam, highly reflective material (e.g. Aluminium) and a container (see Figure B-2). The same calculations as in the preceding section concerning the dimensions can be applied here. The temperature of the absorber is assumed to be that of the liquid nitrogen i.e. 77.4K, but the assumed antenna temperature have to be manipulated because of the effect of the Styrofoam.

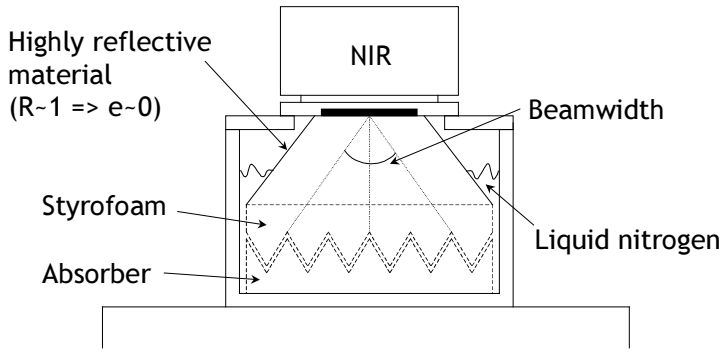


*Figure B-2. Possible setup for the cold load realised with absorber and liquid nitrogen*

The critical component in this configuration is the reflection coefficient between the Styrofoam and air: it should be as close to zero as possible in order to have

accurate results. This means that the relative permittivity of the Styrofoam has to be close to one since the reflection coefficient of power is defined as [1]

$$R = \left| \frac{\eta_2 - \eta_1}{\eta_2 + \eta_1} \right|^2 = \left| \frac{\varepsilon_1 - \varepsilon_2}{\varepsilon_1 + \varepsilon_2} \right|^2, \tag{B-3}$$

where $\eta_1$ and $\eta_2$ are the wave impedances of the air and Styrofoam, respectively and $\varepsilon_1$ and $\varepsilon_2$ are the permittivities of the air and Styrofoam, respectively.

Now the power of the radiation coming through the Styrofoam and reflecting from it at the upper side can be determined when the permittivity of it is known.

# APPENDIX C: POLARIMETRIC ANTENNA MEASUREMENTS

## C.1 Active Load Method

A realisation of an active polarimetric load is presented for the testing of NIR. Schematic diagram of the measurement arrangement is introduced in Figure C-1.

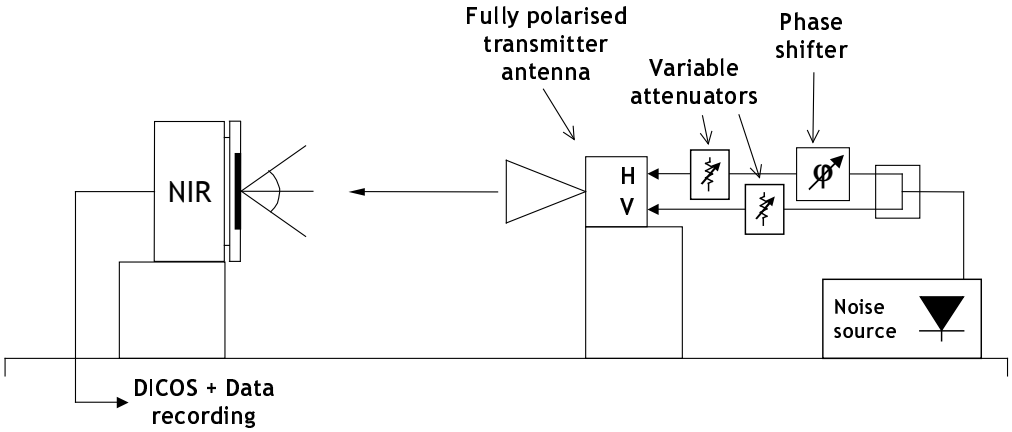


*Figure C-1. Schematic diagram about the active load method for polarimetric measurements with the antenna.*

The received Stokes parameters, and their uncertainties, are calculated in the case of ideal environment i.e. there are no reflections from the measurement equipment or its surroundings. Modified Stokes parameters are defined as [7]

$$T_B = \begin{bmatrix} T_V \\ T_H \\ T_3 \\ T_4 \end{bmatrix} = \frac{\lambda^2}{k_B \eta} \begin{bmatrix} \left\langle |E_V|^2 \right\rangle \\ \left\langle |E_V|^2 \right\rangle \\ 2\Re\left\{ E_V E_H^{\,*} \right\rangle \\ 2\Im\left\{ E_V E_H^{\,*} \right\rangle \end{bmatrix}, \tag{C-1}$$

where the brackets < > are defined as

$$\left\langle x(t) \right\rangle = \frac{1}{T} \int_0^T x(t) dt \,. \tag{C-2}$$

The electromagnetic wave is defined as follows [11]

$$\overline{E}(t,x) = \overline{E}_V(t,x) + \overline{E}_H(t,x) = E_{V0} e^{i(\omega t - \beta x)} \overline{u}_V + E_{H0} e^{i(\omega t - \phi - \beta x)} \overline{u}_H \,, \tag{C-3}$$

where $E_{V0}$ and $E_{H0}$ are the amplitudes of the vertical and horizontal polarisations, respectively; $\omega$ is the angular velocity of the wave; $t$ is time; $\beta$ is the propagation

coefficient; $x$ is the place of the wave and $\phi$ is the phase difference of the polarisations.

The first and second parameter of Equation (C-1) can be calculated as follows

$$\left\langle \left|E_V\right|^2 \right\rangle = \left\langle E_V {E_V}^* \right\rangle = \frac{1}{T}\int_0^T E_{V0} e^{i(\omega t-\beta x)} E_{V0} e^{-i(\omega t-\beta x)} dt = \\ = \frac{{E_{V0}}^2}{T}\int_0^T e^{i(\omega t-\beta x)-i(\omega t-\beta x)} dt = {E_{V0}}^2 \tag{C-4}$$

The third parameter is solved as below

$$2\Re\left\{\left\langle E_V {E_H}^* \right\rangle\right\} = 2\Re\left\{\frac{1}{T}\int_0^T E_{V0} e^{i(\omega t-\beta x)} E_{H0} e^{-i(\omega t-\phi-\beta x)} dt\right\} = \\ = \frac{2E_{V0}E_{H0}}{T}\Re\left\{\int_0^T e^{i(\omega t-\beta x)-i(\omega t-\phi-\beta x)} dt\right\} = \\ = \frac{2E_{V0}E_{H0}}{T}\Re\left\{\int_0^T e^{i\phi} dt\right\} = \\ = 2E_{V0}E_{H0}\Re\{(\cos\phi + i\sin\phi)\} = \\ = 2E_{V0}E_{H0}\cos\phi \tag{C-5}$$

and thus the fourth can be solved analogously to be

$$2\Im\left\{\left\langle E_V {E_H}^* \right\rangle\right\} = 2E_{V0}E_{H0}\sin\phi\,. \tag{C-6}$$

From Equation (C-1) the following can be solved

$$T_V = \frac{\lambda^2}{k_B\eta}\left\langle \left|E_V\right|^2 \right\rangle = \frac{\lambda^2}{k_B\eta}{E_{V0}}^2 \\ \Leftrightarrow E_{V0} = \sqrt{\frac{k_B\eta}{\lambda^2}T_V} \tag{C-7}$$

and

$$E_{H0} = \sqrt{\frac{k_B\eta}{\lambda^2}T_H}\,. \tag{C-8}$$

Thus the third parameter can be written as

$$T_3 = \frac{\lambda^2}{k_B\eta}2\Re\left\{\left\langle E_V {E_H}^* \right\rangle\right\} = \frac{\lambda^2}{k_B\eta}2E_{V0}E_{H0}\cos\phi = \\ = 2\sqrt{T_V T_H}\cos\phi \tag{C-9}$$

and analogously the fourth

$$T_4 = 2\sqrt{T_V T_H}\,\sin\phi\,. \tag{C-10}$$

Finally the modified Stokes parameters can be written as

$$T_B = \begin{bmatrix} T_V \\ T_H \\ T_3 \\ T_4 \end{bmatrix} = \begin{bmatrix} T_V \\ T_H \\ 2\sqrt{T_V T_H}\cos\phi \\ 2\sqrt{T_V T_H}\sin\phi \end{bmatrix} \tag{C-11}$$

The noise temperature at the input of the transmitter antenna for the both polarisations is defined as

$$\begin{aligned} T_V &= \left(1 - \frac{1}{L_V(x_{Vatt})}\right) T_{phys} + \frac{T_N}{L_V(x_{Vatt})} \\ T_H &= \left(1 - \frac{1}{L_H(x_{Hatt})}\right) T_{phys} + \frac{T_N}{L_H(x_{Hatt})} \end{aligned} \tag{C-12}$$

where $T_N$ is the noise temperature of the noise module coming out of the power divider (assumed to be same for both channels); Tphys is the physical temperature of the connecting network and $L_V(x_{Vatt})$ and $L_H(x_{Hatt})$ are the attenuations in the channels going to the V- and H-input of the antenna, respectively, $x_{Vatt}$ and $x_{Hatt}$ being the positions of the controllable attenuators in the V- and H-channel, respectively. Phase difference in the transmitter antenna is defined as follows

$$\phi = \varphi_H(x_{shift}) - \varphi_V \tag{C-13}$$

Free space attenuation is determined as [3]

$$L_s = \left(\frac{\lambda}{4\pi r}\right)^2 \tag{C-14}$$

where $\lambda$ is the wavelength and $r$ is distance between the antennas. Now the received power at both polarisations can be written as

$$\begin{aligned} T_V' &= T_V \left(\frac{\lambda}{4\pi r}\right)^2 G_{Vt} G_{Vr} \\ &= \left[\left(1 - \frac{1}{L_V(x_{Vatt})}\right) T_{phys} + \frac{T_N}{L_V(x_{Vatt})}\right] \left(\frac{\lambda}{4\pi r}\right)^2 G_{Vt} G_{Vr} \end{aligned} \tag{C-15}$$

$$
\begin{aligned}
T_H' &= T_H \left(\frac{\lambda}{4\pi r}\right)^2 G_{Ht} G_{Hr} \\
&= \left[\left(1 - \frac{1}{L_H(x_{Hatt})}\right) T_{phys} + \frac{T_N}{L_H(x_{Hatt})}\right] \left(\frac{\lambda}{4\pi r}\right)^2 G_{Ht} G_{Hr}
\end{aligned}
\tag{C-16}
$$

where $G_{Vt}$ and $G_{Ht}$ are the transmitter antenna gains in V and H polarisation, respectively and $G_{Vr}$ and $G_{Hr}$ are the receiver antenna gains in V and H polarisation, respectively.

The received third and fourth Stokes parameters are now written as

$$
T_3 = 2\left(\frac{\lambda}{4\pi r}\right)^2 \sqrt{T_V T_H G_{Vt} G_{Vr} G_{Ht} G_{Hr}} \cos\phi \tag{C-17}
$$

$$
T_4 = 2\left(\frac{\lambda}{4\pi r}\right)^2 \sqrt{T_V T_H G_{Vt} G_{Vr} G_{Ht} G_{Hr}} \sin\phi \tag{C-18}
$$

and their uncertainties are calculated as follows using the standard propagation of error [8]

$$
\begin{aligned}
\Delta T_3 = \Bigg[ & \left( \frac{4\lambda}{(4\pi r)^2} \sqrt{T_V T_H G_{Vt} G_{Vr} G_{Ht} G_{Hr}} \cos\phi \Delta\lambda \right)^2 + \\
& + \left( -4\left(\frac{\lambda}{4\pi}\right)^2 \frac{1}{r^3} \sqrt{T_V T_H G_{Vt} G_{Vr} G_{Ht} G_{Hr}} \cos\phi \Delta r \right)^2 \\
& + \left( 2\left(\frac{\lambda}{4\pi r}\right)^2 \frac{T_H G_{Vt} G_{Vr} G_{Ht} G_{Hr}}{\sqrt{T_V T_H G_{Vt} G_{Vr} G_{Ht} G_{Hr}}} \cos\phi \Delta T_V \right)^2 \\
& + \left( 2\left(\frac{\lambda}{4\pi r}\right)^2 \frac{T_V G_{Vt} G_{Vr} G_{Ht} G_{Hr}}{\sqrt{T_V T_H G_{Vt} G_{Vr} G_{Ht} G_{Hr}}} \cos\phi \Delta T_H \right)^2 \\
& + \left( 2\left(\frac{\lambda}{4\pi r}\right)^2 \frac{T_V T_H G_{Vr} G_{Ht} G_{Hr}}{\sqrt{T_V T_H G_{Vt} G_{Vr} G_{Ht} G_{Hr}}} \cos\phi \Delta G_{Vt} \right)^2 \\
& + \left( 2\left(\frac{\lambda}{4\pi r}\right)^2 \frac{T_V T_H G_{Vt} G_{Ht} G_{Hr}}{\sqrt{T_V T_H G_{Vt} G_{Vr} G_{Ht} G_{Hr}}} \cos\phi \Delta G_{Vr} \right)^2 \\
& + \left( 2\left(\frac{\lambda}{4\pi r}\right)^2 \frac{T_V T_H G_{Ht} G_{Vr} G_{Hr}}{\sqrt{T_V T_H G_{Vt} G_{Vr} G_{Ht} G_{Hr}}} \cos\phi \Delta G_{Ht} \right)^2
\end{aligned}
\tag{C-19}
$$

$$+\left(2\left(\frac{\lambda}{4\pi r}\right)^2\frac{T_V T_H G_{Ht} G_{Vr} G_{Ht}}{\sqrt{T_V T_H G_{Vt} G_{Vr} G_{Ht} G_{Hr}}}\cos\phi\Delta G_{Hr}\right)^2$$

$$+\left(-2\left(\frac{\lambda}{4\pi r}\right)^2\sqrt{T_V T_H G_{Vt} G_{Vr} G_{Ht} G_{Hr}}\sin\phi\Delta\phi\right)^2\Bigg]^{\frac{1}{2}}$$

Fourth parameter is determined analogously. The uncertainties of the horizontal and vertical polarisations going to the transmitter antenna are determined as follows:

$$\Delta T_V = \left[\left(\left(1-\frac{1}{L_V\left(x_{Vatt}\right)}\right)\Delta T_{phys}\right)^2+\left(\frac{1}{L_V\left(x_{Vatt}\right)}\Delta T_N\right)^2+\frac{T_{phys}-T_N}{L_V\left(x_{Vatt}\right)^2}\Delta L\right] \qquad \text{(C-20)}$$

$$\Delta T_H = \left[\left(\left(1-\frac{1}{L_H\left(x_{Hatt}\right)}\right)\Delta T_{phys}\right)^2+\left(\frac{1}{L_H\left(x_{Hatt}\right)}\Delta T_N\right)^2+\left(\frac{T_{phys}-T_N}{L_H\left(x_{Hatt}\right)^2}\Delta L\right)^2\right] \qquad \text{(C-21)}$$

The uncertainty of the received vertical polarisation may be written as:

$$\begin{aligned}\Delta T_V{}' = \Bigg[&\left(\left(\frac{\lambda}{4\pi r}\right)^2 G_{Vt} G_{Vr}\Delta T_V\right)^2+\left(T_V\frac{2\lambda}{(4\pi r)^2}G_{Vt}G_{Vr}\Delta\lambda\right)^2\\ &+\left(-T_V 2\left(\frac{\lambda}{4\pi}\right)^2\frac{1}{r^3}G_{Vt}G_{Vr}\Delta r\right)^2+\left(T_V\left(\frac{\lambda}{4\pi r}\right)^2 G_{Vr}\Delta G_{Vt}\right)^2\\ &+\left(T_V\left(\frac{\lambda}{4\pi r}\right)^2 G_{Vt}\Delta G_{Vr}\right)^2\Bigg]^{\frac{1}{2}}\end{aligned} \qquad \text{(C-22)}$$

and the uncertainty of the horizontal polarisation can be determined analogously.

## C.2 Conclusions

The analysis of an active polarimetric load in ideal surroundings was presented. In a more accurate analysis also the reflections of the environment and the equipment itself has to be taken into account. The idea here was just to address the measurement situation from the electromagnetic point of view so that it easy to deepen the analysis.

# APPENDIX D: MEASUREMENT EQUIPMENT

In this appendix the key pieces of measurement equipment are briefly introduced. The required items are listed below:

- Temperature-controlled housing (see Section D.3)
- CNS (see Section D.2)
- Matched cold load (Appendix A)
- Antenna loads (Appendix B)
- Polarimetric antenna load (Appendix C)
- Noise source
- Two digitally controlled attenuators
- Digitally controlled switch
- Power divider
- Directional coupler
- Temperature sensors
- High-quality cables.

In the following the components, the CNS and the temperature-controlled housing are separately discussed.

## D.1 Measurement Components

In this section an overview on the proposed components of the measurement equipment is made. The properties of the devices are introduced as stated in data sheets and for some test results are presented. Notice that these are only possible components that can be used in order to make the test successful but also equivalent devices may be used. Details and suggestions of the some of the required components are listed below.

**Noise source e.g. Noise Com Inc. NC503/12**

The noise module is the same as used in NIR noise-injection. In the tests it will be used as CNS and a measurement source. The manufacturer given specifications are listed below:

Manufacturer: Noise Com Inc.
Type: NC503 / 12
Frequency range: 0,2-5000 MHz
Output: White Gaussian noise
Minimum output ENR @ 50 ohm: 31 dB
Output flatness: ± 1,5 dB
Temperature coefficient: 0,01 dB/C
Supply sensitivity: 0,1dB / %ΔV (0,001dB/1,2mV)
Operating temperature: -55C to +85C
Supply voltage +12 V
Supply current: 0,2 to 5mA

Packaging: Drop-in (TO-8)
Space qualified: On request (MIL-E-5400T)

The performance of the noise module is also measured and below is a short summary of the results. In [19] the measurements are described in detail.

Output ENR @ 50 ohm: 30,6 dB
Output flatness: No ripple identified
Output matching: power on return loss 8dB (TBC, not reliable due to the noise), power off return loss 2dB
Temperature coefficient: 0,01 dB/°C
Supply sensitivity: 0,00102dB/mV
Supply current: 4mA @ 12V
Long term stability: 0.010dB

**Digitally controlled attenuator e.g. Hittite HMC307QS16G**

1dB steps
Range 31dB
Insertion loss: 2dB
Return loss: min. 11dB

**Digitally controlled switch e.g. Hittite HMC241QS16**

Insertion loss ~1dB
Isolation >40dB
Switching time negligible in these tests

**Power divider e.g. Mini-circuits BP2G**

Insertion losses: 3.60dB & 3.70dB
Isolation 23dB
VSWR: in 1.11, out1: 1.04, out2 1.08

**Directional coupler e.g. Mini-circuits D19G**

Coupling: 18.2±1.2
Mainline loss: 0.3dB
Directivity: 15dB
VSWR: 1.2

**Temperature sensor e.g. PT100**

Accuracy 0.1K
Relative accuracy 0.02K

Additionally some high quality cables are needed. The most important property is the attenuation, which should be as low as possible in order to reduce the uncertainties.

## D.2 Realising Calibration Network Simulator

Throughout the measurements the so-called Calibration Network Simulator (CNS) is used. Its purpose is to make the measurement situation as realistic as possible by introducing the same amount of noise as in the case where the real calibration network is connected to the NIR. The CNS can then be used for testing the measurement of the centralised noise source and as an error-causing factor due to finite isolation of the Dicke switch [9] and possible reflections in the connecting network.

In fact the CNS is simply a stable noise source. The same module used in NIR (NC503/12, see Section D.1) can be used here. It has to be temperature (within 1K) and voltage/current stabilised to ensure stable power level and the power has to be attenuated to the level of the real calibration network ($T_C$=3000K [9]).

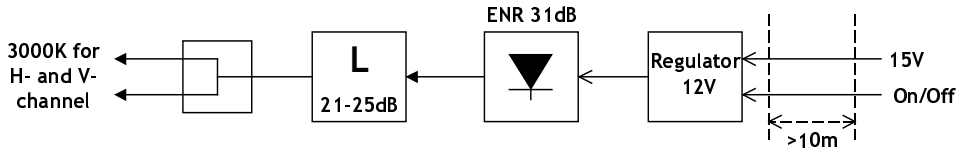


*Figure D-1. Schematic diagram of the Calibration Network Simulator*

Electromagnetic shielding is needed and power supply and power switch cables have to be at least 10 meters long as are the rest of the NIR cables (see Section 3.2.1).

## D.3 Temperature-controlled Housing

A temperature-controlled housing is being constructed in HUT LST, which can be used for the NIR tests. Figure D-2 presents the schematic diagram of the housing.

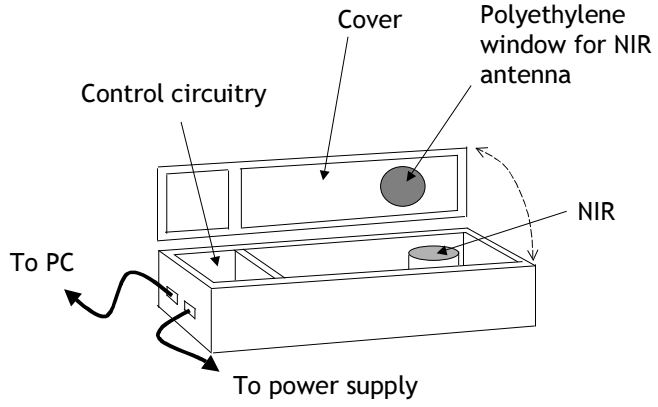


*Figure D-2. Schematic diagram of the temperature-controlled housing.*

The temperature of the housing is controlled with a PC. Possibly the NIR Control Unit may also be used to control the housing. For the measurements involving antenna there is a polyethylene window in the cover of the housing and rest of the housing includes electromagnetic shielding.

# APPENDIX E: UNCERTAINTY SIMULATIONS

In this appendix some calculations of the equations presented in the text are carried out using estimated realistic values.

## E.1 Receiver Noise Temperature

Section 4.1 contains an analysis on how the receiver noise temperature of NIR can be determined. In this section the calculations are carried out with some reasonable estimations for the variables.

| | |
|---|---|
| $L_1=L_2=1dB$ | Attenuation of the connecting chain for both loads |
| $\Delta L_{chain}=x\ dB$ | Uncertainty of the attenuation measurement |
| $T_1=295K$ | Hot load temperature |
| $\Delta T_1=0.1K$ | Uncertainty of the hot load |
| $T_2=80K$ | Cold load temperature |
| $\Delta T_2=0.3K$ | Uncertainty of the cold load |
| $T_{phys}=295K$ | Physical temperature of the connecting chain |
| $\Delta T_{phys}=0.1K$ | Uncertainty of the connecting chain temperature |
| $V_1=0.1V$ | NIR PMS1 hot load response |
| $V_2=0.059V$ | NIR PMS1 cold load response |
| $\Delta V=10^{-4}V$ | Uncertainty of the PMS1 (estimated) |

These values yield:

| | |
|---|---|
| $Y=1.49$ | Y-factor from $V_1$ and $V_2$: Equation (2-21) |
| $\Delta Y=7.6\cdot10^{-4}$ | Uncertainty of the above Y-factor: Equation (4-8) |
| $T_{rec}=222.5K$ | Receiver noise temperature: Equation (4-6) |

The uncertainty of the above procedure is presented in Figure E-1 as a function of the attenuation uncertainty of the connecting chain. It can be seen that accuracy of the attenuation measurement is very critical issue. As a result an accuracy better than $\Delta L_{chain} = 0.05\ dB$ is stated as a requirement for the attenuation measurements.

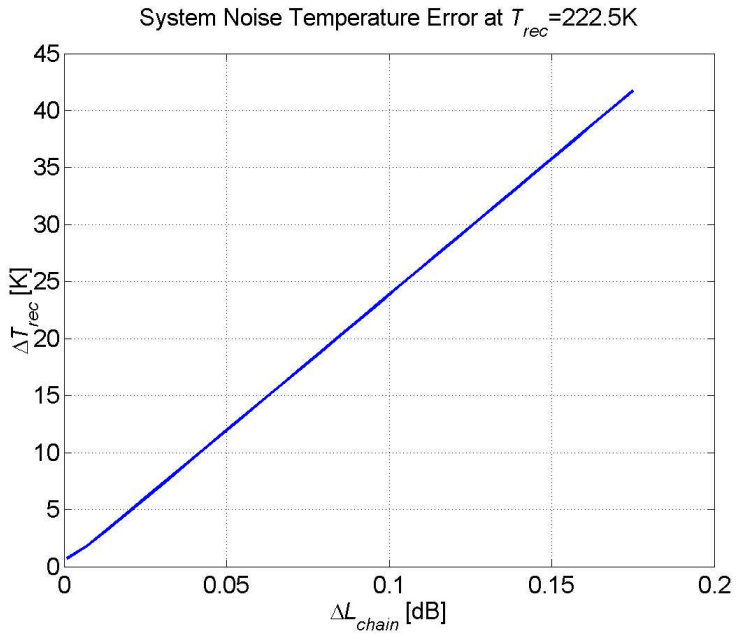


*Figure E-1. Uncertainty of the receiver noise temperature as function of the attenuation measurement uncertainty. As can be seen the procedure is very sensitive to the uncertainty of the attenuation measurement.*

## E.2 Sensitivity

In this section is analysed the effect of the receiver noise temperature uncertainty on the theoretical sensitivity calculation presented in Section 4.2.1.

| | |
|---|---|
| $T_{rec} = 225\ K$ | Receiver noise temperature |
| $\Delta T_{rec} = x\ K$ | Uncertainty of the receiver noise temperature |
| $B = 19\ MHz$ | Bandwidth |
| $\Delta B = 1\ MHz$ | Uncertainty of the bandwidth |
| $\tau = 1.2\ s$ | Integration time |
| $\Delta\tau = 0\ s$ | Uncertainty of the integration time |
| $T_{ref} = 296\ K$ | Reference noise temperature |
| $\Delta T_{ref} = 0.2\ K$ | Uncertainty of the reference noise temperature |

The above values yield:

$\Delta T_{NI} = 0.22\ K$ Sensitivity in noise-injection mode: Equation (4-15)

and Figure E-2 presents the uncertainty of the sensitivity above sensitivity as function of the receiver noise temperature uncertainty. It can be seen that the determined sensitivity is not strongly affected by the uncertainty of the receiver noise temperature and thus the calculation can be estimated to be fairly accurate.

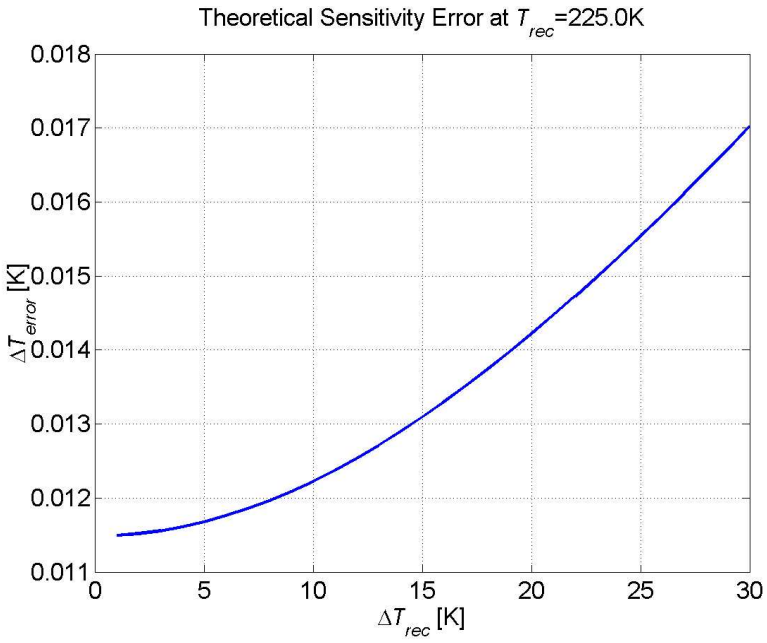


*Figure E-2. Theoretical sensitivity uncertainty as a function of receiver noise temperature uncertainty.*

## E.3 Linearity

In this section the linearity measurement procedure is evaluated. The noise temperature emitted by of the controllable noise source is calculated and its uncertainties evaluated with different attenuation uncertainty values.

| | |
|---|---|
| $T_{cold} = 85\ K$ | Cold load output noise temperature |
| $\Delta T_{cold} = 1\ K$ | Cold load uncertainty |
| $T_{noise} = 10^4\ K$ | Noise source output noise temperature |
| $\Delta T_{noise} = 5\ K$ | Noise source uncertainty |
| $T_{phys} = 295\ K$ | Physical temperature of the connecting chain |
| $\Delta T_{phys} = 0.2\ K$ | Uncertainty of the physical temperature |
| $L$= 5-34 $dB$ | Attenuation of the connecting chain in all the attenuator states (same for both channels and both switch states) |
| $L_{therm}$ = 2-31 $dB$ | Attenuation causing thermal noise |
| $\Delta L = 0.02 dB$ | Uncertainty of the attenuation |

Now the above values yield noise temperatures at radiometer input presented in Figure E-3 in both of the switch states i.e. when connected to the cold load and when connected to the noise source.

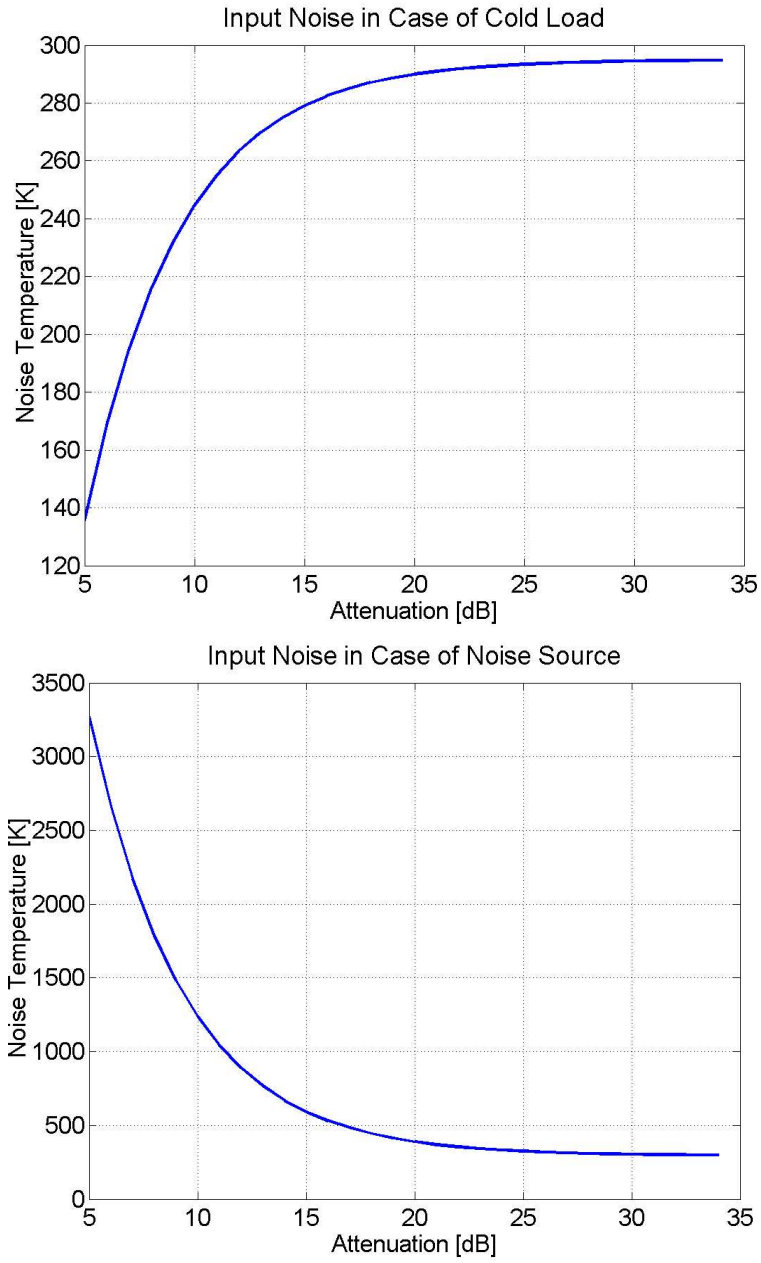


*Figure E-3. Noise coming from the controllable noise source and going into the receivers.*

Figure E-4 presents the uncertainty of the input noise temperature as a function of attenuation measurement uncertainty in the most sensitive cases (see Figure E-5). It can be see that the attenuation measurement accuracy has a very strong effect on the noise temperature uncertainty.

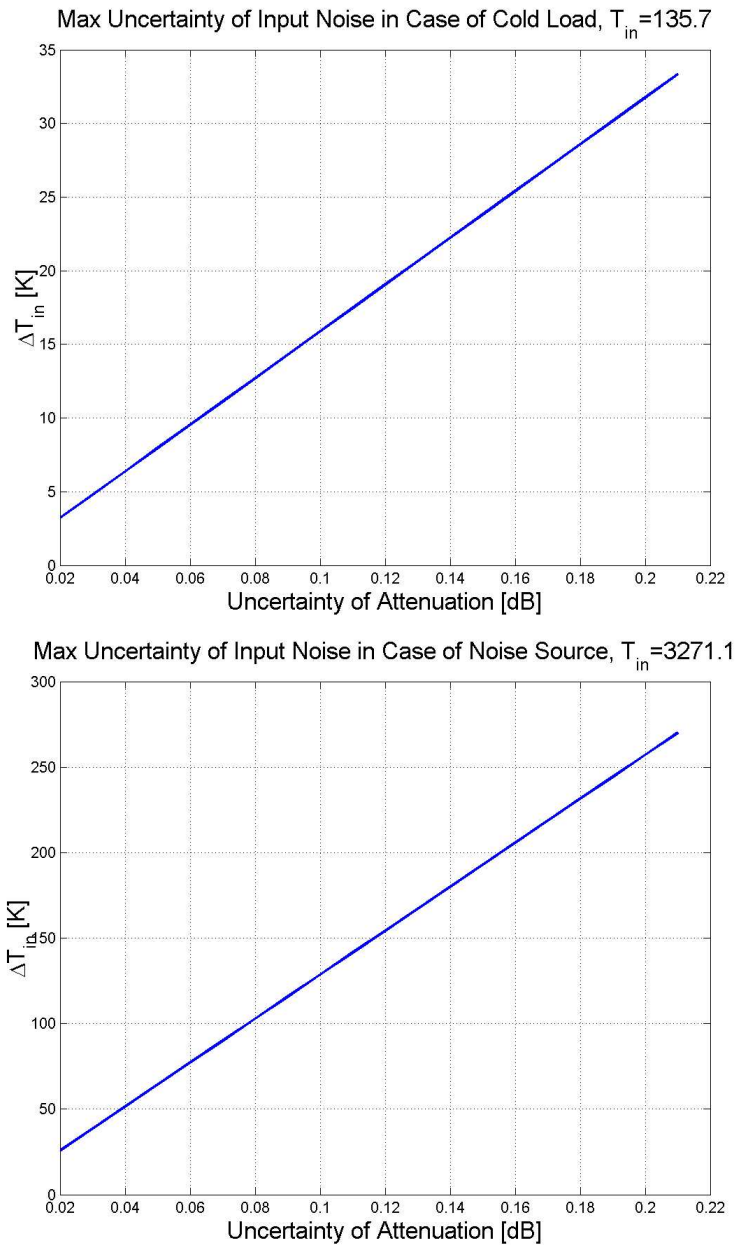


*Figure E-4. Uncertainty of the input noise temperature as a function of attenuation uncertainty.*

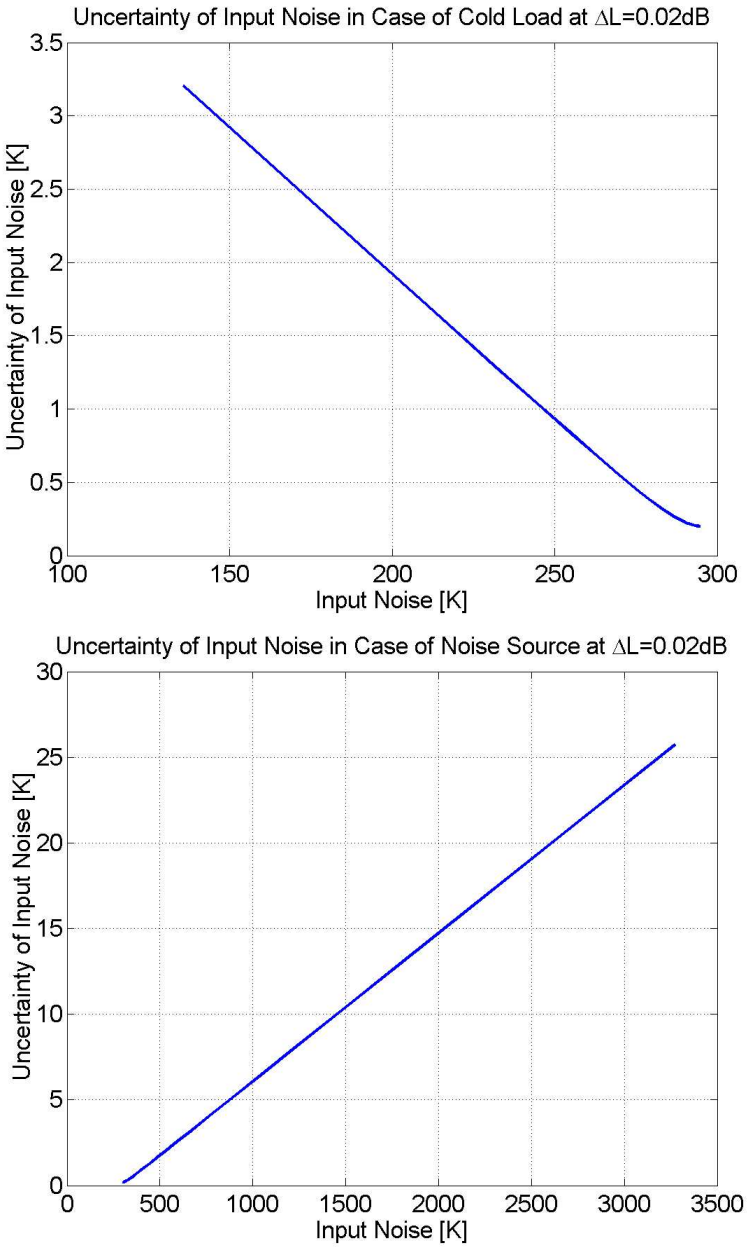


*Figure E-5. Uncertainty of the input noise temperature as a function of input noise temperature magnitude.*

## E.4 Calibration of Antenna Measurement

In this section the calibration uncertainty of NIR is shortly evaluated. Antenna temperature uncertainty is evaluated in three cases in which the calibration target brightness temperature is assumed to be different.

$T_{ref}$ = 296 $K$ Reference noise temperature
$\Delta T_{ref}$ = 0.2 $K$ Uncertainty of the reference noise temperature
$T_N$ = 400 $K$ Noise-injection noise temperature

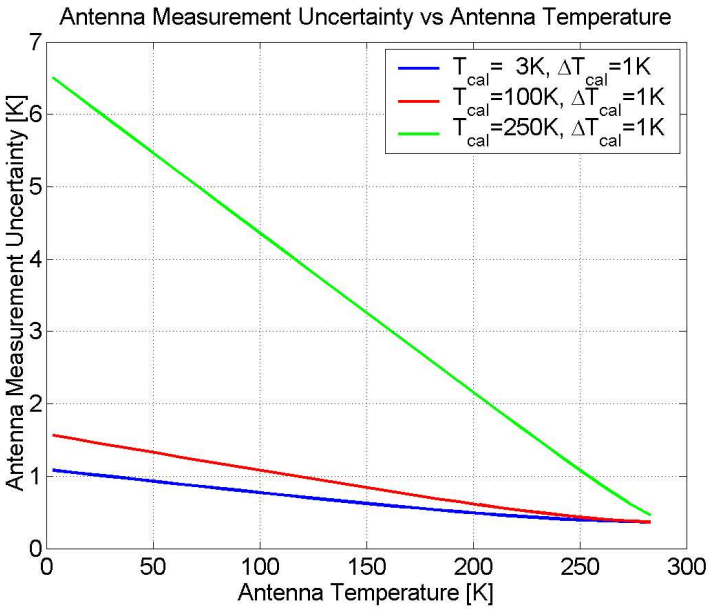


*Figure E-6. Antenna measurement uncertainty as a function of antenna temperature with different calibration targets.*

Figure E-6 presents the three cases where the radiometer is first calibrated with a target having a certain brightness temperature and then a target with varying brightness temperature is measured. Effect of the calibration on this measurement is plotted in Figure E-6. The uncertainty is calculated using Equation (4-78) (linearity error is ignored and sensitivity is assumed to be 0.3 *K*). It can be seen that lower the calibration target brightness temperature better the calibration result as Equation (4-73) already suggested.

This result is a very strong motivation for calibrating NIR with a sky measurement, since it has low brightness temperature and it is very well defined (better than the 1 *K* used here).

## E.5 Modulus Terms

In this section the uncertainties of the modulus terms of NIR noise-injection mode are evaluated as function of the receiver noise temperature. The following values were used for the calculation:

| | |
|---|---|
| $T_{Vant}^{calib} = T_{Hant}^{calib} = 3\ K$ | Calibration target (sky) brightness temperature |
| $\Delta T_{Vant}^{calib} = \Delta T_{Hant}^{calib} = 0.3\ K$ | Calibration target uncertainty |
| $\Delta T_{\sigma} = 0.3\ K$ | Sensitivity |
| $\Delta T_{lin} = 0.7\ K$ | Uncertainty caused by linearity error |
| $T_{Hant} = 120\ K$ | Horizontal polarisation antenna temperature |
| $T_{Vant} = 80\ K$ | Vertical polarisation antenna temperature |
| $T_{ref} = 296\ K$ | Reference noise temperature |
| $\Delta T_{ref} = 0.2\ K$ | Uncertainty of the reference noise temperature |
| $T_N = 400\ K$ | Noise-injection noise temperature |
| $g_{FW} = 1$ | Fringe-washing factor |

| | |
|---|---|
| $\Delta g_{FW} = 0$ | Uncertainty of the fringe-washing factor |
| $T_{Vrec} = 225\ K$ | Receiver noise temperature |
| $T_{Hrec} = 225\ K$ | Receiver noise temperature |
| $\Delta T_{Vrec} = \Delta T_{Hrec} = x\ K$ | Uncertainties of the receiver noise temperatures |

These values yield the following:

| | |
|---|---|
| $\Delta T_N = 1.00\ K$ | Uncertainty of noise-injection noise: Equation (4-73) |
| $\Delta T_{Hcalib} = 0.30\ K$ | Horizontal calibration uncertainty: Equation (4-75) |
| $\Delta T_{Vcalib} = 0.33\ K$ | Vertical calibration uncertainty: Equation (4-75) |
| $\Delta T_H = 0.82\ K$ | Horizontal polarisation uncertainty: Equation (4-78) |
| $\Delta T_V = 0.83\ K$ | Vertical polarisation uncertainty: Equation (4-78) |

Figure E-7 presents the relative uncertainty of all the modulus terms of the noise-injection mode as function of the receiver noise temperature uncertainty.

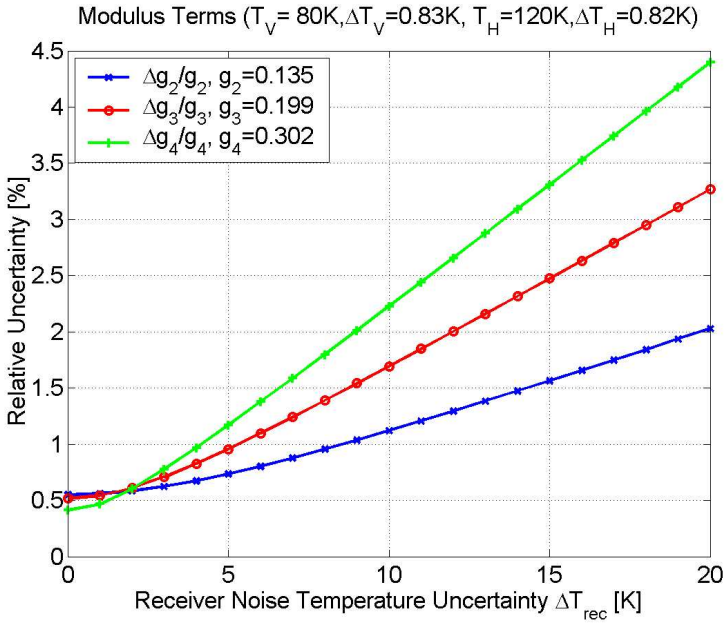


*Figure E-7. Relative modulus term uncertainties as a function of receiver noise temperature uncertainty when antenna temperature is for the vertical channel $T_V = 80$ K and for the horizontal channel $T_H = 120$ K.*

It can be seen from the plots of Figure E-7 that the relative errors increase significantly after receiver noise uncertainty is above three Kelvins.

## E.6 Third and Fourth Stokes Parameters Accuracy

In this section the third and fourth Stokes parameter accuracy is evaluated in two cases: as function of receiver noise temperature and as function of correlation coefficient. The basic values used in these calculations are the same as in the previous section.

Figure E-8 presents the case where receiver noise temperature uncertainty changes and the correlation coefficient uncertainty is assumed zero. The modulus terms used for calculating the third and fourth Stokes parameters are the same as plotted in Figure E-7.

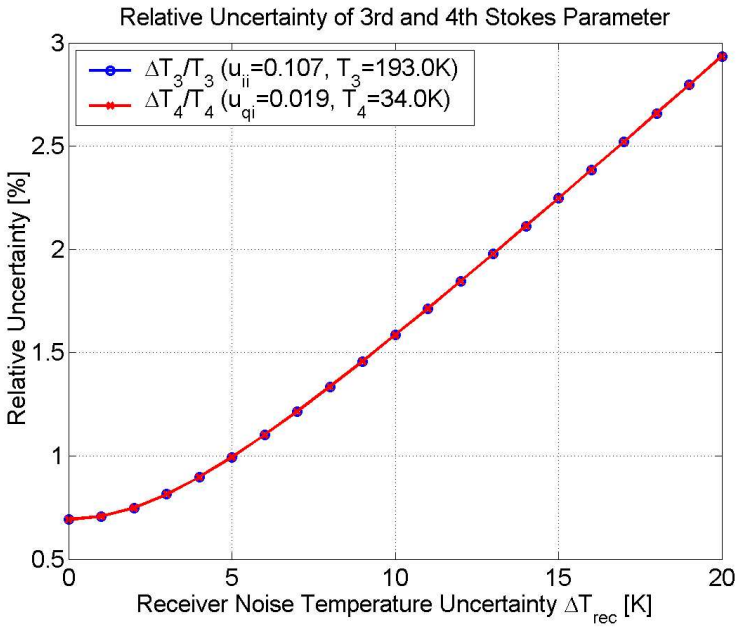


*Figure E-8. Uncertainty of the third and fourth Stokes parameter as function of receiver noise temperature. The correlation coefficient uncertainty is zero. This is the same situation as presented in Figure E-7. The plots indicate that the relative uncertainty is the same for the both third and fourth Stokes parameter.*

As can be seen the receiver noise temperature uncertainty starts to affect the Stokes parameter uncertainty strongly after 3 *K*, as is the case with modulus terms i.e. the uncertainty of the modulus term is the affecting factor.

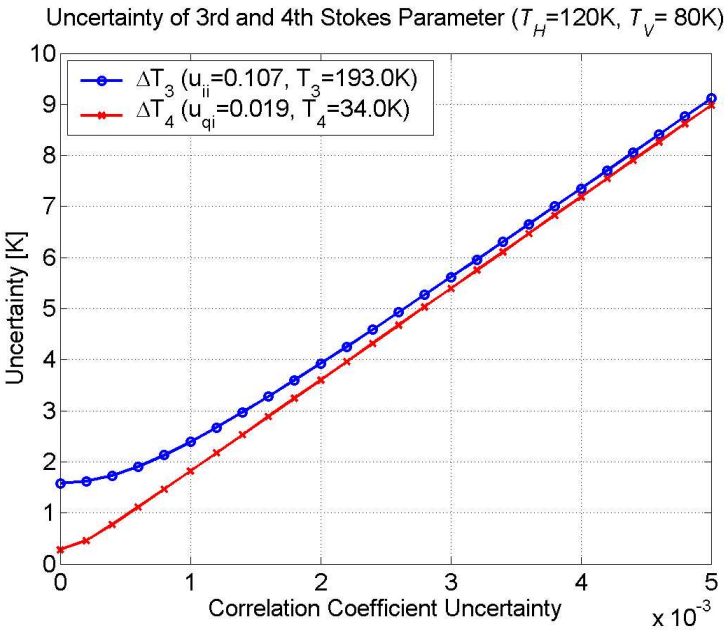


*Figure E-9. Uncertainty of third and fourth Stokes parameters as a function of correlation coefficient uncertainty.*

Figure E-9 presents the case where the correlation coefficient changes and receiver noise temperature uncertainties $\Delta T_{Hrec} = \Delta T_{Vrec} = 3\ K$. From the curves in Figure E-9 it can be seen that the correlation coefficient uncertainty, $\Delta\mu$, must be at least less than $10^{-3}$.